

Fabrication of Copper Phthalocyanine/Molybdenum Disulfide Nanosensors for Electrochemical Detection of Dopamine



by

Rukhsar Rasool

(Registration No: 00000403018)

A thesis submitted to the National University of Sciences and Technology, Islamabad,
in partial fulfillment of the requirements for the degree of

Master of Science in Chemistry

Supervisor: Dr. Habib Nasir

Department of Chemistry, School of Natural Sciences
National University of Sciences & Technology (NUST)

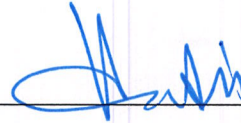
Islamabad, Pakistan

(2024)

THESIS ACCEPTANCE CERTIFICATE

Certified that final copy of MS thesis written by **Rukhsar Rasool** (Registration No. **00000403018**), of **School of Natural Sciences** has been vetted by undersigned, found complete in all respects as per NUST statutes/regulations, is free of plagiarism, errors, and mistakes and is accepted as partial fulfillment for award of MS/M.Phil degree. It is further certified that necessary amendments as pointed out by GEC members and external examiner of the scholar have also been incorporated in the said thesis.

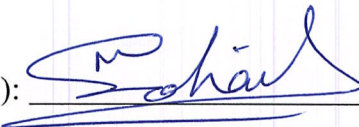
Signature: _____



Name of Supervisor: Prof. Habib Nasir

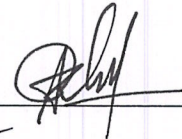
Date: _____

Signature (HoD): _____



Date: 07/01/2025

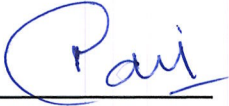
Signature ^{A/} (Dean/Principal): _____



Date: 0-1-2025

National University of Sciences & Technology**MS THESIS WORK**

We hereby recommend that the dissertation prepared under our supervision by: Rukhsar Rasool, Regn No. 00000403018 Titled Fabrication of Copper Phthalocyanine/Molybdenum-Disulfide Nanosensor for Electrochemical Detection of Dopamine be Accepted in partial fulfillment of the requirements for the award of MS degree.

Examination Committee Members1. Name: Dr. MUHAMMAD ADIL MANSOORSignature: 2. Name: DR. KHADIJA MUNAWARSignature: Supervisor's Name PROF. HABIB NASIRSignature: 


Head of Department

07/01/2025
Date

COUNTERSIGNEDDate: 01-2025


A/Dean/Principal

Dedication

This thesis is dedicated to my cherished parents, the indefatigable architects of my aspirations, whose boundless affection, profound sacrifices, and unwavering fortitude have constituted the cornerstone of my every triumph, illuminating my path through the labyrinth of trials and uncertainties with their steadfast faith.

Acknowledgments

First and foremost, I am deeply obliged to **ALLAH ALMIGHTY**, the most beneficent and merciful. I obey ALLAH, who granted me the best health and opportunity to be a student at NUST and work with such an enthusiastic and dedicated teacher. All of this was possible by the **Holy Prophet MUHAMMAD (S.A.W)**, whose principles educate us at every stage of life.

I want to acknowledge my warmest gratitude to my worthy supervisor, **Dr. Habib Nasir**, whose inspirational personality, thoughtful guidance, and advice made me complete this work with great passion. His support and motivation helped my studies and made me a learner and beginner in the research path. I am also thankful to my GEC members, **Dr. Muhammad Adil Mansoor** and **Dr. Khadija Munawar**.

I would like to thank my senior, **Syeda Aqsa Batool**, for always helping me out. I would also like to acknowledge my friends, especially **Muhammad Mohsin Khan, Muhammad Ahmed, Awais Nawaz, Khadija-Tul-Kubra**, and **Farwa Batool**, for their help and support throughout my research, for cheering me up in my difficult times and for making my journey memorable.

Table of Contents

Dedication	i
Acknowledgments	ii
Table of Contents	iii
List of Figures.....	vii
Abstract.....	x
Chapter 1	1
1 Introduction.....	1
1.1 Neurotransmitters	1
1.2 Parts of nerve cell	1
1.3 Functioning of neurotransmitters	1
1.4 Types of neurotransmitters	2
1.4.1 Amino acids neurotransmitters	3
1.4.2 Monoamines neurotransmitters.....	3
1.4.3 Peptide neurotransmitters.....	4
1.5 Significance and working of dopamine neurotransmitters.....	5
1.6 Abnormalities related to dopamine	8
1.7 2-D materials	8
1.7.1 Graphene and boron nitride	9
1.7.2 Transition Metal Dichalcogenides (TMDCs)	10
1.7.3 Phosphorene.....	10
1.7.4 Xenex.....	11
1.8 Synthesis of 2-D materials.....	12
1.8.1 Top-down method	12
1.8.2 Bottom-up approach.....	14

1.9	2-D materials vs. bulk materials	16
1.9.1	Weaking of van der Waals interactions	16
1.9.2	Increased surface area-to-volume ratio	17
1.9.3	Electrons confinement in a plane	17
1.10	Uses of 2D Materials	18
1.10.1	Photodetectors.....	18
1.10.2	Battery electrodes.....	19
1.10.3	Topological insulators	19
1.10.4	Valleytronics	20
1.10.5	Semiconductors and sensors	20
1.11	Molybdenum disulfide (MoS ₂).....	21
1.12	Bulk to nano MoS ₂	21
1.13	Synthesis of MoS ₂	22
1.13.1	Mechanical exfoliation.....	22
1.13.2	Chemical exfoliation.....	23
1.13.3	Chemical Vapor Deposition (CVD)	24
1.14	Properties.....	26
1.14.1	Electronic and Electrical Properties.....	26
1.14.2	Optical Properties.....	26
1.14.3	Mechanical Properties.....	27
1.15	Applications of MoS ₂	28
1.15.1	Mechanical.....	28
1.15.2	Biosensors	30
1.15.3	Gas sensing	31
1.15.4	Catalytic activity	32
1.15.5	Supercapacitors	32
1.16	Phthalocyanines.....	33

1.17	History	33
1.18	Introduction	33
1.19	Preparation methods	37
1.20	Copper Phthalocyanine (CuPc)	38
1.21	History of CuPc	39
1.22	Synthesis of CuPc.....	40
1.23	Structural properties of CuPc	41
1.23.1	Crystalline structures of CuPc	41
1.24	Harmful nature of CuPc.....	41
1.25	Applications of CuPc.....	42
1.25.1	Catalysis.....	42
1.25.2	Colorant.....	42
1.26	Types of sensors.....	43
1.27	Challenges	45
1.28	Electrode material used in electrochemical sensing of dopamine.....	47
Chapter 2	49
2	Literature review.....	49
Chapter 3	58
3	Synthesis.....	58
3.1	Materials and reagents.....	58
3.2	Synthesis of CuPc.....	58
3.3	Synthesis of MoS ₂	59
3.4	Synthesis of CuPc/MoS ₂ composites.....	60
3.5	Slurry formation and deposition on GCE.....	61
Chapter 4	63
4	Results and discussion	63

4.1	Structural and morphological studies	63
4.1.1	XRD	63
4.1.2	Raman spectroscopy	64
4.1.3	FTIR analysis	65
4.1.4	SEM-EDX.....	67
4.2	Electrochemical studies	69
4.2.1	Response towards $K_3 Fe (CN)_6$	69
4.2.2	Optimization of pH	71
4.2.3	Electrochemical response with dopamine.....	72
4.2.4	Scan rate studies with $MoS_2/CuPc$ (1:0.5).....	74
4.2.5	Concentration studies with $MoS_2/CuPc$ (1:0.5).....	75
4.2.6	Reproducibility in electrochemical response for $MoS_2/CuPc$ (1:0.5).....	77
4.2.7	Stability studies of $MoS_2/CuPc$ (1:0.5).....	78
4.2.8	Effect of interferents with $MoS_2/CuPc$ (1:0.5)	80
4.2.9	Scan rate studies with MoS_2	80
4.2.10	Concentration studies with MoS_2	81
4.2.11	Effect of Interferents on MoS_2	84
4.2.12	Stability studies with MoS_2	85
Chapter 5	87
5	Conclusion	87
5.1	Future Recommendations	88
6	References.....	89

List of Figures

Figure 1: Metabolic pathway of dopamine.	7
Figure 2: Catechol biosynthesis.	7
Figure 3: Metabolic pathway of dopamine.	8
Figure 4: Structure of graphene (a) and hexagonal boron nitride (b).	9
Figure 5: Structure of molybdenum disulfide (a) and tungsten ditelluride (b).	10
Figure 6: Layered structure of phosphorene.	11
Figure 7: Structure of silicene (a), germanene (b) and stanene (c).	12
Figure 8: Process of mechanical exfoliation.	13
Figure 9: Process of liquid exfoliation.	14
Figure 10: Process of chemical vapor deposition.	15
Figure 11: Process of solvothermal synthesis.	16
Figure 12: Band alignment of MoS ₂ bulk (a) and monolayer (b).	18
Figure 13: Polytypes of the layered structure of MoS ₂	22
Figure 14: Mechanism of the tribological action of nano lamellar disulfides.	30
Figure 15: Structure of metal-free phthalocyanine.	37
Figure 16: Methods of synthesis of metal-free phthalocyanine.	38
Figure 17: Methods of preparation of metal phthalocyanine.	38
Figure 18: Structure of copper phthalocyanine.	40
Figure 19: Types of biosensors.	43
Figure 20: Advantages of electrochemical sensors.	45
Figure 21: CV (A) and DPV curves (B) for bare GCE and modified GCE.	47
Figure 22: Common electrode materials for DA sensing.	48
Figure 23: Synthesis scheme of copper phthalocyanine.	59
Figure 24: Synthesis scheme of molybdenum disulfide.	60
Figure 25: Synthesis schemes of different composites of MoS ₂ /CuPc.	61

Figure 26: Synthesis schemes of composite of MoS ₂ /CuPc.....	62
Figure 27: XRD analysis of CuPc, MoS ₂ and composites.....	64
Figure 28: Raman analysis of CuPc, MoS ₂ and composites.....	65
Figure 29: FTIR analysis of CuPc, MoS ₂ and composites.....	66
Figure 30: SEM images of MoS ₂ and CuPc.....	67
Figure 31: SEM images of composite of MoS ₂ /CuPc (1:0.5).....	68
Figure 32: EDX analysis of composite of MoS ₂ /CuPc (1:0.5).....	68
Figure 33: Electrochemical response with CV towards K ₃ Fe (CN) ₆	70
Figure 34: EIS response towards K ₃ Fe(CN) ₆	70
Figure 35: Different pH responses with composite MoS ₂ /CuPc (1:0.5) through CV.	71
Figure 36: Different pH response for MoS ₂ /CuPc (1:0.5) with DPV.....	72
Figure 37: Electrochemical response with CV towards dopamine with all electrodes.....	73
Figure 38: Electrochemical response with DPV towards dopamine with all electrodes.	73
Figure 39: Effect of scan rate with CV for MoS ₂ /CuPc (1:0.5).....	74
Figure 40: Effect of concentration with CV for MoS ₂ /CuPc (1:0.5).	75
Figure 41: Linear regression curve graph through CV for MoS ₂ /CuPc (1:0.5) with linear range 1-300 μM (a) and 350-1000 μM (b).	76
Figure 42: Effect of concentration with DPV for MoS ₂ /CuPc (1:0.5).....	76
Figure 43: Linear regression curve through DPV for MoS ₂ /CuPc (1:0.5) with linear range 1- 200 μM (a) and 200-600 μM (b).....	77
Figure 44: Electrochemical response for MoS ₂ /CuPc (1:0.5) with 3 different electrodes.....	78
Figure 45: One day stability of MoS ₂ /CuPc (1:0.5) electrode.	79
Figure 46: Different days stability with MoS ₂ /CuPc (1:0.5) electrode.....	79
Figure 47: Effect of interferences on MoS ₂ /CuPc (1:0.5) electrode.	80
Figure 48: Effect of different scan rates through CV with MoS ₂	81
Figure 49: Effect of varying concentration with CV for MoS ₂	82
Figure 50: Linear regression curve through CV for MoS ₂ with linear range 1-300 μM (a) and 500-1000 μM (b).....	83

Figure 51: Effect of varying concentration with DPV for MoS ₂	83
Figure 52: Linear regression curve through DPV for MoS ₂ with linear range 1-300 μM (a) and 500-1000 μM (b).	84
Figure 53: Effect of interferences with MoS ₂	85
Figure 54: Stability studies for MoS ₂ with CV.	86
Figure 55: Stability studies for MoS ₂ with DPV.	86

Abstract

Detection of chemical compounds has always been a significant concern since it covers a wide range of areas ranging from environmental control to clinical diagnosis. With the advancement of nanotechnology, using carbon nanomaterials in the sensing field has improved the sensors' signal response. Standard analytical techniques characterized the as-prepared materials (pristine and nanocomposites). Here, we synthesized composites of MoS₂ and CuPc of different ratios 1:0.5, 1:1, and 1:2. Cyclic voltammetry (CV), electrochemical impedance spectroscopy (EIS), and differential pulse voltammetry (DPV) were used to characterize and evaluate the performance of the prepared nanosensors. The characteristics of the as-prepared nanosensors, like accuracy, reproducibility, repeatability, selectivity, linear range, the limit of detection (LoD), the limit of quantification (LoQ), and sensitivity, were also evaluated. The respective values of LoD, LoQ, and sensitivity for the concentration studies with CV for the linear range 1-300 μM is 4.70 μM , 15.68 μM and 0.21 $\mu\text{A } \mu\text{M}^{-1} \text{ cm}^{-2}$, and for the linear range 350-1000 μM is 11 μM , 36.6 μM and 0.091 $\mu\text{A } \mu\text{M}^{-1} \text{ cm}^{-2}$, respectively. For the DPV, the values of LoD, LoQ, and sensitivity with the linear range 1-200 μM is 8.21 μM , 27 μM , and 0.06 $\mu\text{A } \mu\text{M}^{-1} \text{ cm}^{-2}$, and for linear range 200-800 μM is 3.13 μM , 10.45 μM and 0.19 $\mu\text{A } \mu\text{M}^{-1} \text{ cm}^{-2}$, respectively. But here, MoS₂ as a pristine compound gave more electrochemical response towards dopamine sensing. In the first half with the linear range 1-300 μM , the value of LoD, LoQ, and sensitivity with CV for MoS₂ is 22.1 μM , 73.8 μM and 0.12 $\mu\text{A } \mu\text{M}^{-1} \text{ cm}^{-2}$, and for the linear range 500-1000 μM is 22.5 μM , 75 μM and 0.12 $\mu\text{A } \mu\text{M}^{-1} \text{ cm}^{-2}$, respectively and with DPV and linear range 1-300 μM is 0.4 μM , 1.36 μM and 0.07 $\mu\text{A } \mu\text{M}^{-1} \text{ cm}^{-2}$ and for the linear range 500-1000 μM is 0.48 μM , 1.6 μM and 0.06 $\mu\text{A } \mu\text{M}^{-1} \text{ cm}^{-2}$, respectively.

Chapter 1

1 Introduction

1.1 Neurotransmitters

Around 86 billion neurons are expected to occur in the human mind. Those billions of synapses are conveyed by passing compound messages at the neurotransmitter, the little hole between cells, in a process called neurotransmission. Those chemical messages are special particles called synapses. Their responsibility is to convey compound sign "messages" from one neuron (nerve cell) to the following objective cell. The following objective cell can be another neuron, a muscle, or any other organ [1].

1.2 Parts of nerve cell

The cell body is an essential part of creating neurotransmitters and keeping up with the capability of the nerve cell. The axon conveys the electrical signs along the nerve cell to the axon terminal.

The axon terminal is where the electrical message is changed to a compound sign utilizing neurotransmitters to speak with the following gathering of nerve cells, muscle cells, or organs. Neurotransmitters are situated in a piece of the neuron called the axon terminal. They're put away inside slender walled sacs called synaptic vesicles. Every vesicle can contain a vast number of neurotransmitters [2].

1.3 Functioning of neurotransmitters

As a message or sign passes along a nerve cell, the electrical charge of the sign causes the vesicles of neurotransmitters to combine with the nerve cell film at the cell's edge. The

synapses, which currently convey the message, are then let out of the axon terminal into a liquid-occupied space between one nerve cell and the following objective cell (another nerve cell, muscle cell, or organ).

This region, known as the synaptic junction, is where neurotransmitters transmit messages across a gap of less than 40 nanometers in width. For context, the average width of a human hair is approximately 75,000 nanometers, highlighting the incredibly small scale of this communication system. Each neurotransmitter is highly specific, binding only to a particular receptor site on the target cell, similar to how a unique key fits and operates a specific lock. Once the neurotransmitter binds to its receptor, it triggers a response or action in the target cell. This response could manifest as the transmission of an electrical signal in a neighboring nerve cell, the contraction of a muscle, or the release of chemicals from a cell within an organ. This intricate and precise signaling system is vital for coordinating the body's various physiological functions [2].

1.4 Types of neurotransmitters

Synapses are responsible for transmitting one of three types of signals depending on the neurotransmitter involved. Excitatory synapses stimulate the receiving neuron, encouraging it to pass on the signal to the next cell. Neurotransmitters like glutamate, epinephrine, and norepinephrine are commonly associated with this excitatory response. Conversely, inhibitory synapses halt the transmission of signals with neurotransmitters such as gamma-aminobutyric acid (GABA), glycine, and serotonin performing this role.

In addition, modulatory synapses adjust the effects of other neurotransmitters, altering how brain cells communicate. They can simultaneously impact the functioning of numerous neurons, adding an additional layer of complexity to neural signaling. Although scientists have

cataloged around 100 neurotransmitters, evidence suggests many more may exist but remain undiscovered. These neurotransmitters are classified based on their chemical properties, and their effects depend on how they interact with the nervous system.

1.4.1 Amino acids neurotransmitters

Glutamate is the primary excitatory neurotransmitter in the central nervous system and is the most abundant neurotransmitter in the brain. It plays a vital role in cognitive processes such as learning, memory, and thinking. However, elevated levels of glutamate have been associated with neurological disorders, including Alzheimer's disease, dementia, Parkinson's disease, and seizures.

On the other hand, gamma-aminobutyric acid (GABA) is the brain's main inhibitory neurotransmitter. It helps regulate brain activity by suppressing overactive signals, which play a role in controlling anxiety, depression, sleep patterns, seizures, and difficulty maintaining focus. Additionally, glycine is the principal inhibitory neurotransmitter in the spinal cord. Glycine is essential for regulating sensory processing, pain transmission, auditory processing, and reflex responses within the nervous system.

1.4.2 Monoamines neurotransmitters

Neurotransmitters play diverse and essential roles in the central nervous system, particularly within the brain, and influence cognition, emotions, attention, and behavior. Monoamine neurotransmitters are vital for regulating mood, attention, and perception, and imbalances in these neurotransmitters are linked to numerous neurological and psychological disorders. Additionally, many commonly prescribed medications impact these neurotransmitters.

Serotonin is an inhibitory neurotransmitter that regulates mood, sleep patterns, appetite, anxiety, pain, and sexual behavior. An imbalance in serotonin levels is linked to conditions

such as seasonal affective disorder, anxiety, depression, fibromyalgia, and chronic pain. Medications like selective serotonin reuptake inhibitors (SSRIs) and serotonin-norepinephrine reuptake inhibitors (SNRIs) are commonly prescribed to manage these conditions by adjusting serotonin levels.

Histamine regulates processes such as alertness, feeding behavior, and motivation. It has been implicated in conditions like asthma, bronchospasm, mucosal edema, and multiple sclerosis.

Dopamine is involved in the body's reward system, contributing to sensations of pleasure, motivation, learning, and emotional experiences. It also supports focus, memory, sleep, mood, and motivation. Dysfunctions in dopamine levels are associated with diseases such as Parkinson's disease, schizophrenia, bipolar disorder, restless leg syndrome, and attention deficit hyperactivity disorder (ADHD). Drugs like cocaine, methamphetamines, and amphetamines act on dopamine pathways, leading to their addictive properties.

Epinephrine (adrenaline) and norepinephrine (noradrenaline) are critical for the body's "fight or flight" response during stressful situations. Epinephrine prepares the body for emergency responses by increasing heart rate, blood pressure, breathing rate, and glucose levels while directing blood to muscles. It is also used medicinally to treat severe allergic reactions, asthma, heart failure, and other conditions. On the other hand, norepinephrine primarily impacts attention, arousal, and mood regulation. Medications targeting norepinephrine are used to treat conditions such as ADHD and depression by enhancing its availability in the nervous system.

1.4.3 Peptide neurotransmitters

Peptides are chains or polymers composed of amino acids that play important roles in various biological processes. Endorphins are natural painkillers produced by the body, functioning as the body's own method of pain relief. They influence the perception of pain and trigger feelings

of happiness or pleasure. The release of endorphins reduces pain and can lead to euphoric sensations. Low levels of endorphins have been linked to conditions such as fibromyalgia and certain types of headaches.

Acetylcholine is a neurotransmitter involved in numerous functions within both the central nervous system (CNS), which includes the brain and spinal cord, and the peripheral nervous system (nerves branching from the CNS). Acetylcholine plays a vital role in regulating autonomic nervous system processes, such as controlling heart rate, blood pressure, and gastrointestinal motility. Additionally, it is essential for functions like muscle contraction, memory, motivation, sexual desire, learning, and sleep. Elevated acetylcholine levels are associated with neurological conditions such as Alzheimer's disease, seizures, and muscle spasms [2].

1.5 Significance and working of dopamine neurotransmitters

The understanding of dopamine's (DA) role in brain function has rapidly evolved over recent years. Initially proposed as a precursor in the biosynthesis of norepinephrine and epinephrine upon its discovery in 1939, dopamine's independent role as a neurotransmitter was established in 1958 when it was found in brain concentrations comparable to norepinephrine. This discovery indicated that dopamine could act as a neurotransmitter on its own. A major breakthrough came when researchers discovered that the striatum contained 70–80% of the brain's dopamine and that striatal dopamine depletion was critically involved in the development of Parkinson's disease. This finding led to a surge of interest in dopamine among neuropharmacologists.

The study of dopamine and other catecholamines was significantly advanced by the development of fluorescence histochemical techniques. These methods allowed for the

visualization of dopaminergic neurons and their fibers, enabling the spatial mapping of these neurons within the brain. This technique, combined with biochemical analysis, demonstrated the presence of a specific population of dopamine-containing neurons distinct from other catecholamines. The fluorescence histochemistry method proved essential for understanding the neurophysiological aspects of dopamine pathways by providing insights into neuronal location and their projection regions.

Figures 1-3 are explaining the metabolic pathway of dopamine. Although formaldehyde or glyoxylic acid-induced fluorescence histochemistry can visualize catecholamine systems in the brain, determining the specific catecholamine involved at a particular location is more challenging. Immunocytochemical methods have emerged as a solution by detecting specific proteins linked to neurotransmitter synthesis. Tyrosine hydroxylase serves as a general marker for catecholamine-producing neurons because it catalyzes the conversion of tyrosine into L-DOPA, the precursor of dopamine. However, tyrosine hydroxylase cannot distinguish between dopamine neurons and those that synthesize norepinephrine or epinephrine. L-DOPA itself is converted into dopamine by the enzyme DOPA decarboxylase, which is widely distributed across various neuronal pathways, limiting its specificity as a marker.

A key enzyme for differentiating dopamine neurons from other catecholamine pathways is dopamine β -hydroxylase. This enzyme converts dopamine into norepinephrine and is exclusive to norepinephrine- and epinephrine-producing neurons. Therefore, dopamine β -hydroxylase serves as a distinguishing marker, helping to identify dopaminergic neurons and differentiate them from other catecholamine-containing neuronal systems [3].

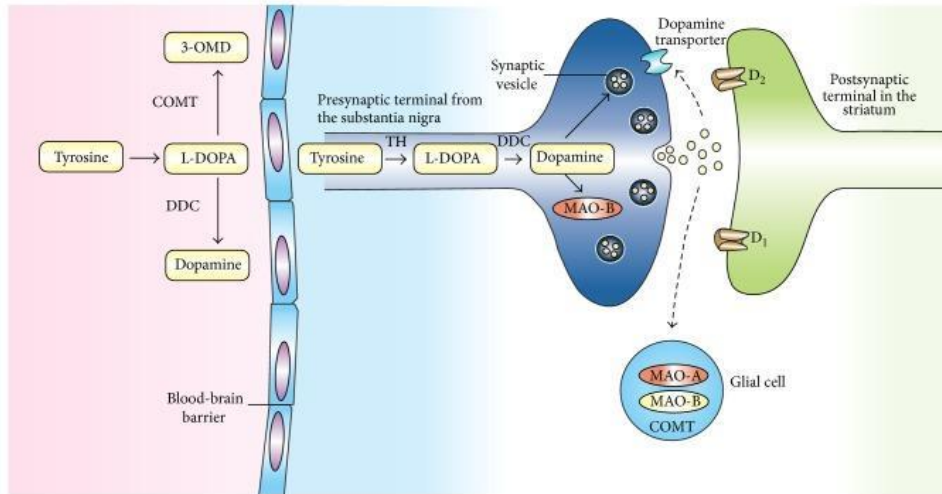


Figure 1: Metabolic pathway of dopamine.

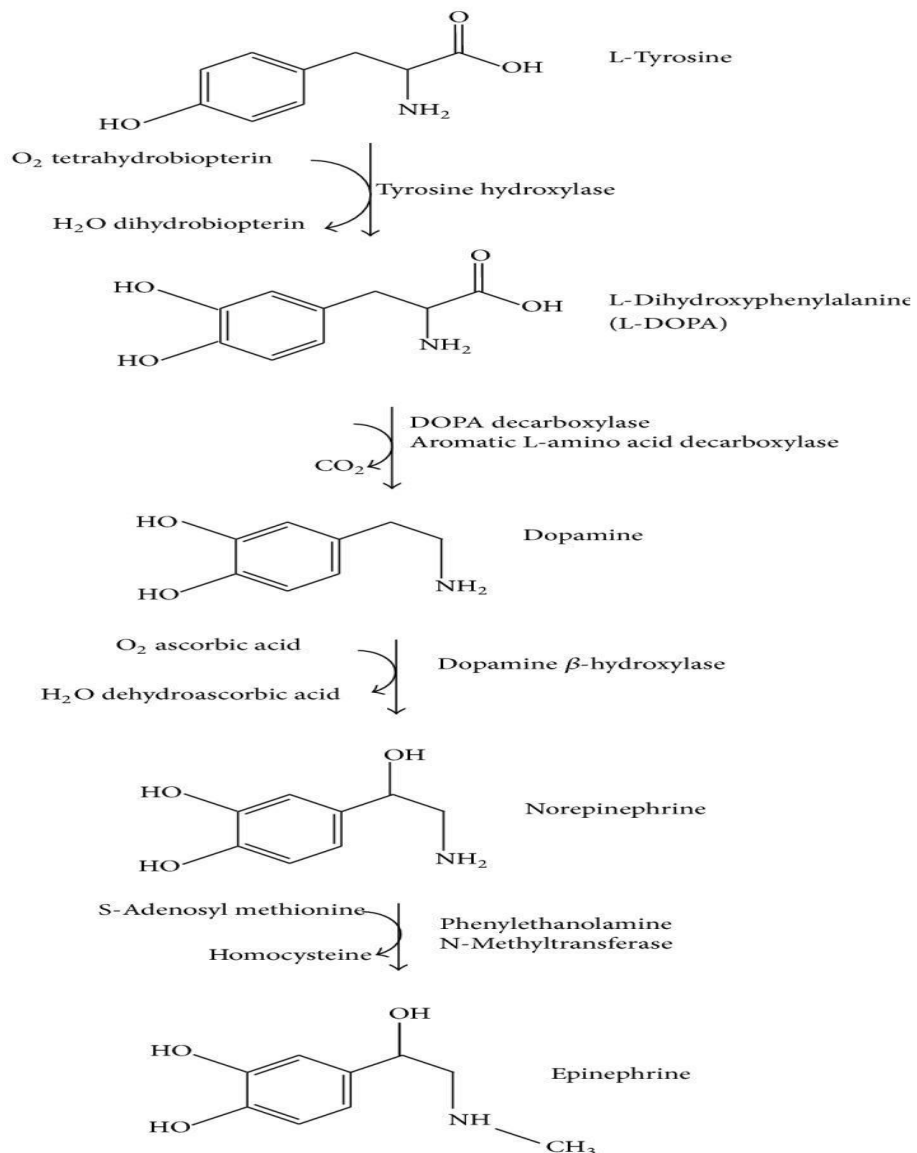


Figure 2: Catechol biosynthesis.

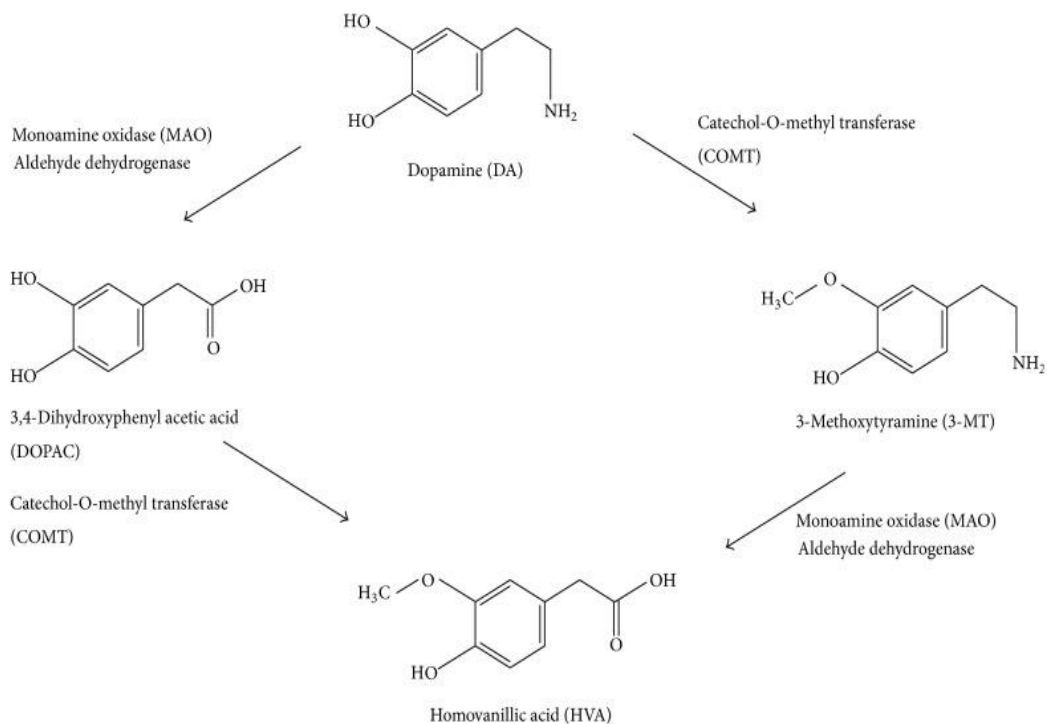


Figure 3: Metabolic pathway of dopamine.

1.6 Abnormalities related to dopamine

In low amounts, it very well might be a contributing element in Parkinson's infection, Discouragement, and Dopamine carrier lack disorder. In excess amount, it very well might be a contributing element in Insanity, fantasies and dreams, heftiness, fixation, schizophrenia [4].

1.7 2-D materials

Nanomaterials are materials extensively characterized through the all-out dimensions of their nanoscopic dimensions:

When all three dimensions of a material fall at the nanoscale, it will be referred to as a 0D (zero-dimensional) material; mostly, they will be denoted as a nanoparticle. If two dimensions of a material are at the nanoscale while the third dimension is significantly larger (analogous to a string that has been shrunk to microscopic size), it is classified as a 1D type of nanomaterial, or they will be denoted as nanotubes or nanowires. When only a single dimension

is at the nanoscale, the material is termed a 2D (two-dimensional) material having a resemblance to a large but highly thin sheet of paper. Conversely, if none of the dimensions meet the nanoscale threshold, the material is not considered a nanomaterial and is categorized as a bulk material, which represents the category of materials encountered in everyday life. Examples of 2D materials include the following:

1.7.1 Graphene and boron nitride

Graphene consists of a single layer of carbon atoms arranged in a hexagonal lattice structure, with a thickness of just one atom (0.14 nm). This unique configuration gives graphene semiconductor-like behavior due to the overlap between its conduction and valence bands. Its distinctive electronic band structure allows electrons to move at exceptionally high speeds, nearly 1/300 of the speed of light, which contributes to its extraordinary properties, such as superior thermal conductivity. Furthermore, graphene exhibits optical transparency, absorbing only about 2% of visible light, and demonstrates remarkable flexibility. Theoretically, a single graphene monolayer, measuring around 0.3 nm in thickness, is strong enough to support the weight of a football [5]. The structures of both are shown in Figure 4.

Boron nitride is structurally similar to graphene, having a hexagonal crystal structure like graphene but consisting of B and N atoms instead of C. Unlike graphene, boron nitride has a large bandgap and is an insulator rather than a conductor.

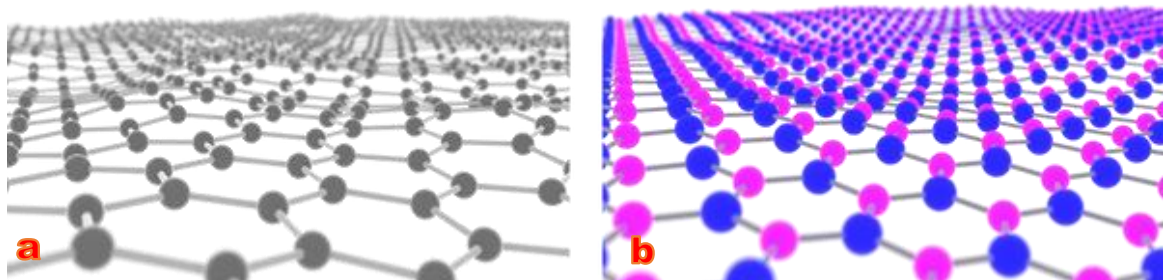


Figure 4: Structure of graphene (a) and hexagonal boron nitride (b).

1.7.2 Transition Metal Dichalcogenides (TMDCs)

Transition metal dichalcogenides (TMDCs) are compounds having the general formula MX_2 , where M represents a transition metal such as Mo or W and X represents a chalcogen such as S, Se, or Te. Bulk TMDCs have van der Waals interaction, consisting of layers that are three atoms thick, with each single metal layer interconnected between two chalcogenide layers. TMDCs can adopt different crystal structures, among which the most common being the 2H phase, which has a trigonal prismatic structure leading to semiconductor properties as observed in materials like MoS_2 , WS_2 , and MoSe_2 . These semiconductors have an indirect bandgap in their bulk form; however, when reduced to monolayer thickness, the bandgap becomes direct and lies within the visible spectrum, making them more favorable for optoelectronics applications. Having charge mobilities of $100\text{-}1000\text{ cm}^2\text{V}^{-1}\text{s}^{-1}$, TMDCs are highly sought after as 2D semiconductors. Another notable structure in TMDCS is the 1T phase, which exhibits metallic properties and is the most stable polymorph of WTe_2 . The structures of both compounds are shown in Figure 5 [6].

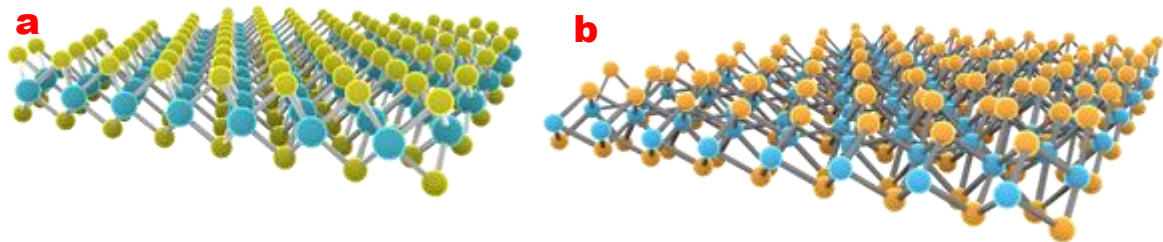


Figure 5: Structure of molybdenum disulfide (a) and tungsten ditelluride (b).

1.7.3 Phosphorene

Phosphorene (Figure 6) is a monolayer derived from black phosphorus and represents a stable and layered allotrope of elemental phosphorus. It is characterized as a direct bandgap semiconductor with a distinct puckered honeycomb lattice. The bandgap of phosphorene is

adjustable across the visible spectrum by altering the number of stacked layers. With a high charge carrier mobility of approximately $1000 \text{ cm}^2\text{V}^{-1}\text{s}^{-1}$, it holds significant potential for use in optoelectronic and semiconductor technologies. Additionally, its anisotropic layered configuration causes its physical and electronic properties to vary considerably based on the crystallographic direction of measurement [7].

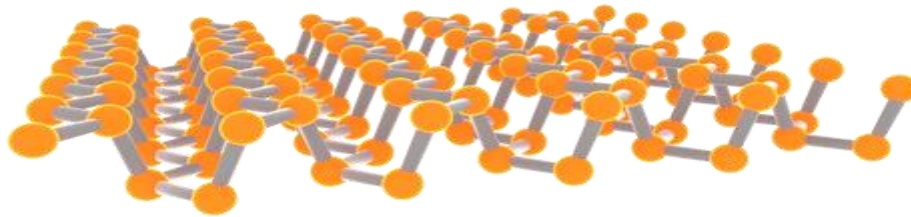


Figure 6: Layered structure of phosphorene.

1.7.4 Xenos

Monolayers of silicon (silicene), germanium (germanene), and tin (stanene), collectively known as Xenos (Figure 7), possess a hexagonal structure akin to graphene but with varying levels of curvature. Unlike graphene, these materials cannot be obtained through exfoliation from bulk forms. Instead, they are produced epitaxially on substrates, where they generally exhibit strong interactions with the underlying material. While Xenos are still in the early stages of exploration, they hold significant potential for applications in advanced technologies, including field-effect semiconductors and topological insulators [8].

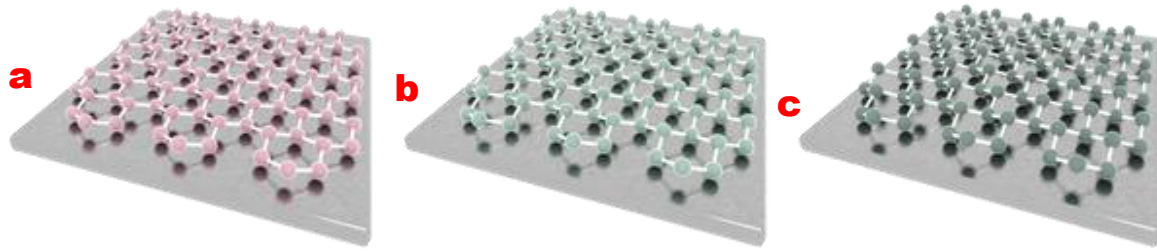


Figure 7: Structure of silicene (a), germanene (b) and stanene (c).

1.8 Synthesis of 2-D materials

There are two ways to synthesize 2D materials:

1. Top-down way (begin with a mass material and making it divide into smaller parts)
2. Bottom-up way (begin with the nuclear entities and make a large lump)

Inside every one of these methodologies are a few subtypes, each having its own perks and drawbacks.

1.8.1 *Top-down method*

Mechanical exfoliation, the "Scotch-tape method," a widely recognized technique (Figure 8), was initially used to isolate monolayer graphene. This method involves pressing a piece of adhesive tape onto the surface of a layered material and peeling it away, thereby detaching flakes consisting of a few layers from the bulk material. These flakes are subsequently transferred onto a substrate for further examination. Although this approach typically yields a low percentage of monolayer material, most flakes are multilayered; it can produce monolayer flakes ranging in size from a few microns to approximately 100 microns. The monolayers

obtained using this technique are usually of high quality, with minimal structural defects, as the process does not involve chemical treatment. Performing the method in a glove box can further improve the structural integrity and quality of the resulting monolayers by reducing deformations. While effective for lab-scale research, this mechanical exfoliation technique is limited in its scalability and is not suitable for large-scale production or integration with new ideas and technologies [9].

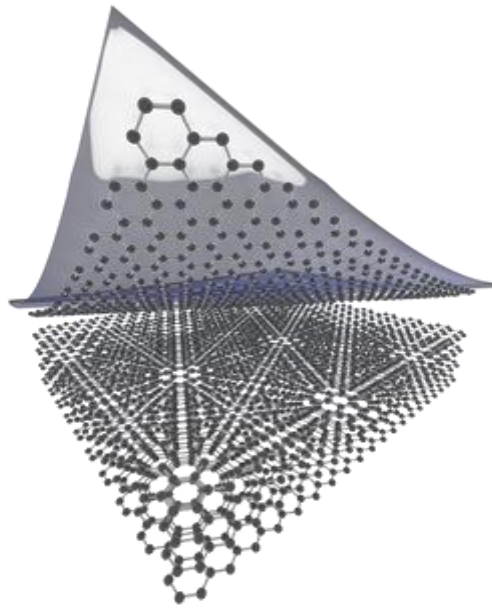


Figure 8: Process of mechanical exfoliation.

Liquid phase exfoliation (Figure 9) is another mechanical method used to isolate layered materials. This technique employs a natural solvent as a medium in which powdered layered materials are suspended, and mechanical energy is applied to separate the layers. Sonication generates flexible strain, facilitating the exfoliation of layers. To enhance the yield of monolayers, additional strategies can be utilized, such as introducing reactive species that produce hydrogen bubbles between the layers, pushing them apart, or employing rapid mixing to generate extra shear forces.

This technique is more versatile than mechanical peeling but has some drawbacks. Its monolayer form remains generally low, having flakes size under 100 nm due to the applied mechanical strength. Additionally, the flakes may possess a high chance of various defects or remaining solvent after exfoliation, which can limit their use in many optoelectronic applications [10].

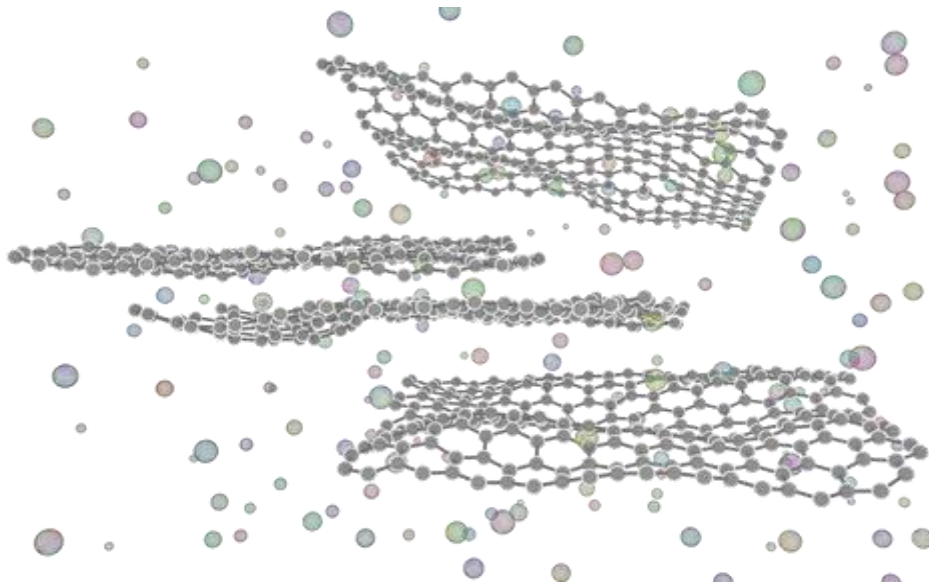


Figure 9: Process of liquid exfoliation.

1.8.2 Bottom-up approach

The chemical vapor deposition (CVD) technique (Figure 10) involves introducing one or more precursor gases, typically containing the essential elements of the target material, into a heated chamber. Within this chamber, the gases react either with one another or with the substrate, forming a thin film of the desired material. This method has proven effective for synthesizing materials such as graphene and transition metal dichalcogenides (TMDCs). Critical parameters, including gas pressure, reaction temperature, and reaction time, require precise control, as they

play a crucial role in determining the thickness, quality, and structural properties of the resulting films.

Although this technique is more compact and has a high cost compared to mechanical methods, it offers remarkable versatility, and the quality of films being produced is comparable to that of mechanically exfoliated layers [11].

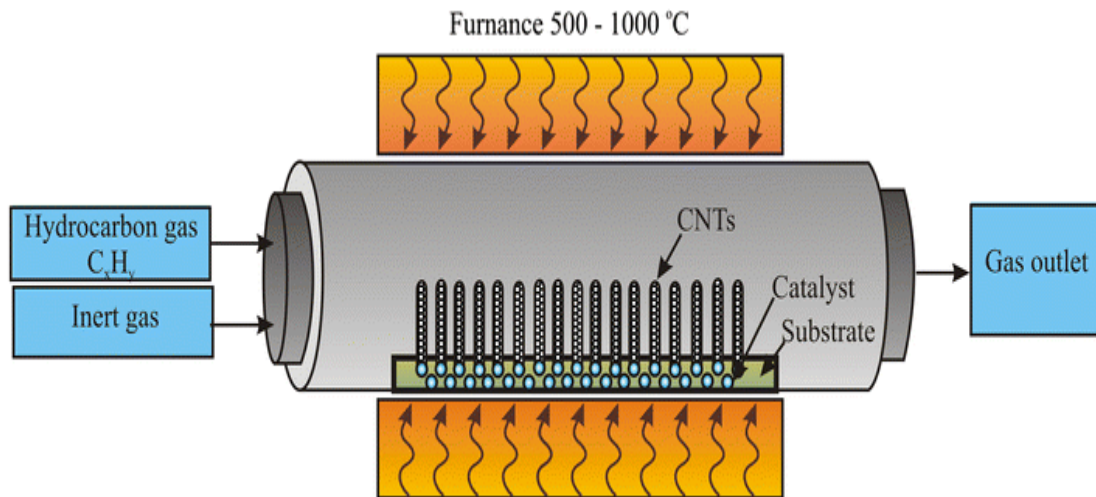


Figure 10: Process of chemical vapor deposition.

The solvothermal synthesis technique (Figure 11) offers diverse methods for producing 2D materials. These approaches include high-temperature chemical reactions under controlled conditions, interface-mediated growth (where reactions occur at the liquid's surface), and the incorporation of nanoparticles into larger nanosheet structures. Each technique is optimized for specific types of 2D materials, enabling the synthesis of a variety of materials, such as graphene, TMDCs, and monolayer metals, depending on the chosen process.

The flakes produced through these methods typically have lateral dimensions smaller than 100 nm and often exhibit characteristics similar to those obtained using liquid exfoliation, including the presence of residual solvents. Despite these limitations, solvothermal synthesis techniques

are highly versatile, cost-effective, and scalable, making them an excellent choice for large-scale production in specific applications [12].

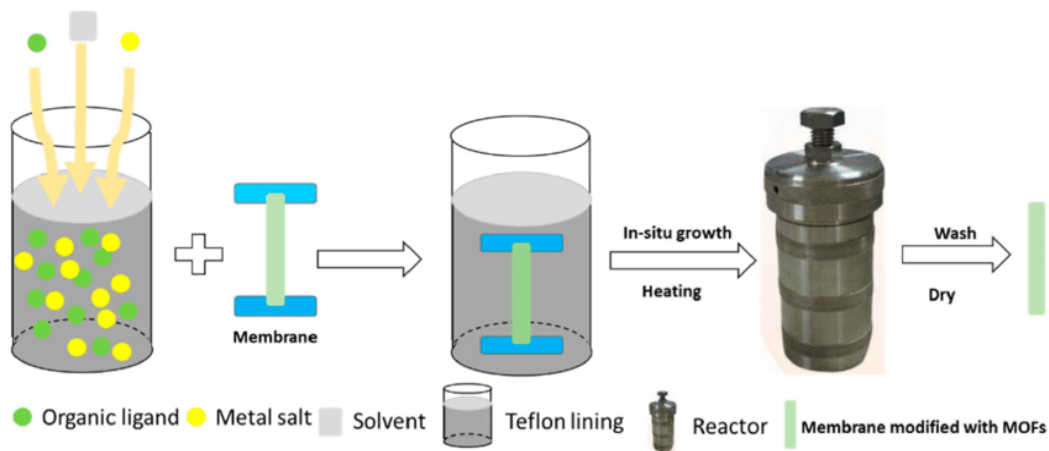


Figure 11: Process of solvothermal synthesis.

1.9 2-D materials vs. bulk materials

It is because of the reasons mentioned below:

1.9.1 Weaking of van der Waals interactions

Layered bulk materials are composed of multiple planes held together by weak van der Waals forces, while the atoms within each plane are bonded covalently. The weak van der Waals interactions make these materials appear fragile, as they can be easily disrupted by external forces. In contrast, monolayers are solely comprised of covalent bonds, eliminating the weak interlayer interactions that act as structural "failure points" in bulk materials. This unique bonding structure significantly enhances their strength. For example, graphene exhibits exceptional tensile strength, far surpassing that of graphite. While graphite, such as in a pencil, can be easily broken, graphene is remarkably strong, up to several times stronger than steel.

1.9.2 Increased surface area-to-volume ratio

The surface area-to-volume ratio of a material defines the amount of its surface exposed to its surrounding environment. This ratio is crucial in chemical reactions because a higher surface area allows more reactants to interact with the material, leading to faster reaction rates. 2D materials, with their increased surface area compared to their bulk counterparts, are more accessible for such interactions. Additionally, this high surface area makes 2D materials more responsive to environmental factors, a property that is utilized in the design of sensors based on 2D materials.

1.9.3 Electrons confinement in a plane

The electronic and optical properties of a material are determined by its electronic band structure, which describes how electrons move through the material and is influenced by the periodicity of its crystal structure. When a material transitions from its bulk form to a 2D structure, the periodicity is disrupted along the direction perpendicular to the plane, leading to significant changes in the bandgap. These changes are responsible for unique properties, such as the exceptional conductivity of graphene and the fluorescence observed in monolayer MoS₂.

Additionally, the confinement of electrons in 2D systems leads to a decreased dielectric shield between electrons and holes in semiconductor materials. Due to the low material available for shielding the electric field, Coulombic interactions are large enough, resulting in more tightly bound excitons that are more consistent than those materials present in bulk form. Quantum confinement effects can lead to excitons being confined within a distance smaller than their Bohr radius, which raises their energy levels compared to excitons in bulk materials. This change in energy alters the frequency of light that these excitons can absorb and emit, leading to distinct optical behaviors [13].

1.10 Uses of 2D Materials

Properties of materials are changed (favorable properties achieved) when the dimensions of materials are decreased as compared to bulky materials (as in Figure 12). Coming up next is a summary of likely the most reassuring applications.

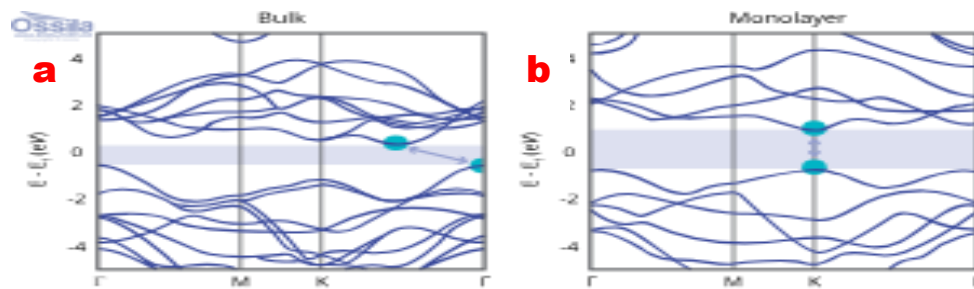


Figure 12: Band alignment of MoS₂ bulk (a) and monolayer (b).

1.10.1 Photodetectors

TMDCs such as MoS₂, MoSe₂, WS₂, and WSe₂, as well as black phosphorus, feature bandgaps within the optical or near-infrared range and exhibit excellent charge transport properties. A single monolayer of a TMDC, with a thickness of less than 1 nm, permits up to 10% of incident visible light to pass through, comparable to the transparency of approximately 100 nm of silicon. While their ultrathin nature limits their application in high-efficiency photovoltaics, these materials are well-suited for developing highly sensitive photodetectors. For example, a device constructed from a precisely exfoliated MoS₂ monolayer achieved a remarkable photo response of 10³ A/W within the 400 nm to 680 nm wavelength range. Furthermore, combining MoS₂ with graphene to form a heterostructure significantly boosts sensitivity, reaching levels as high as 10⁸ A/W.

1.10.2 Battery electrodes

Electrodes used in batteries and supercapacitors require conductive materials with a high surface area to store large quantities of charge-carrying ions efficiently. Graphene has garnered significant attention as a superior alternative to traditional graphite cathodes thanks to its exceptional surface-to-mass ratio, outstanding conductivity, mechanical strength, and flexibility. These attributes could pave the way for stronger, lighter batteries with higher power densities and faster charging capabilities.

Similarly, 2D MoS₂ has emerged as a highly promising electrode material. While its most stable 2H crystal structure exhibits semiconducting properties, chemical treatments such as exfoliation can induce a phase transition to the metallic 1T phase. Electrodes composed of stacked 1T monolayers of MoS₂ have shown superior energy and power densities compared to graphene-based electrodes, emphasizing its potential for next-generation energy storage technologies [14].

1.10.3 Topological insulators

Topological insulators (TIs) are a class of materials that behave as insulators in their interior but allow electrons to move freely along their edges. A key feature of these edge states is that electrons with opposite spins travel in opposite directions, a property that makes TIs highly promising for low-power electronic devices and spintronic applications, where electron spin can be exploited for data storage and device optimization.

Xenes such as bismuthene and stanene are emerging as potential candidates for topological insulators due to their unique electronic characteristics. Additionally, WTe₂, a transition metal dichalcogenide, is particularly versatile because it can transition between a topological

insulator and a superconductor when exposed to an electric field, broadening its range of possible technological applications.

1.10.4 Valleytronics

Valleytronics is a concept that exploits a unique property of charge carriers in certain transition metal dichalcogenides (TMDCs), such as MoS₂ and WS₂, known as valley polarization. This property refers to the association of electrons and holes with specific valleys in the electronic band structure, linked to their spin and angular energy. Optical excitation can selectively target a particular valley, allowing the excitation of carriers in that specific valley, thereby creating a degree of freedom for carriers. These extensive degrees of freedom entitle the development of innovative optoelectronic devices for information processing, storage, and computation by utilizing valley degrees of freedom for encoding data.

1.10.5 Semiconductors and sensors

Field-effect transistors (FETs) have been fabricated using a variety of 2D semiconducting materials, including transition metal dichalcogenides (TMDCs) and black phosphorus, owing to their high charge carrier densities and moderate bandgaps, which make them ideal for these applications. Hexagonal boron nitride is often used as the gate dielectric in these devices because of its excellent insulating properties. Although graphene does not possess an inherent bandgap, it has been employed as an active channel material in semiconductors by engineering bandgaps through techniques such as edge state engineering, chemical doping, or the application of external electric fields.

One of the main advantages of 2D materials over conventional silicon is their natural flexibility, which allows them to be integrated with flexible substrates for the development of wearable and flexible electronic circuits. Despite the challenges associated with scaling up the

production of high-quality 2D layers for commercial applications, their potential in semiconductor technology remains strong. Additionally, FET-based sensors have been developed using 2D TMDCs, demonstrating the ability to detect a variety of chemical compounds at parts-per-million concentrations or lower. These sensors can identify compounds such as triethylamine, nitric oxide, ammonia, and nitrogen dioxide by observing changes in their electrical conductance upon exposure to these gases [15].

1.11 Molybdenum disulfide (MoS₂)

Molybdenum disulfide (MoS₂) belongs to the family of transition metal dichalcogenides (TMDs). It is a layered material where a molybdenum atom is sandwiched between two sulfur layers (S-Mo-S). Within the structure, strong covalent bonds hold the atoms together, while weak Van der Waals forces exist between the layers. This unique structural arrangement underpins MoS₂'s application as a lubricant, especially in aerospace machinery.

1.12 Bulk to nano MoS₂

The crystalline structure of bulk MoS₂ features a stacking arrangement where molybdenum atoms are coordinated with six sulfur atoms in a trigonal prismatic geometry. The layers, separated by weak van der Waals forces, allow for interlayer sliding. This property facilitates shear along the basal planes of the crystal, making it an excellent lubricant.

At the atomic level, research by Kim et al. demonstrated that MoS₂ exhibits a shear strength of 24.6 MPa under normal pressure, indicating its unique mechanical properties, including superlubricity. These attributes have been extensively studied to understand their implications for industrial applications.

MoS₂, like other TMDs, exhibits rich polytypism (Figure 13) with three primary crystallographic phases:

1. 1T Phase: A metallic structure with octahedral geometry and D6d symmetry.
2. 2H Phase: A semiconducting structure with hexagonal symmetry and a D6h point group.
3. 3R Phase: A rhombohedral structure with C3v symmetry.

In addition to these, a theoretical tetragonal 2T phase has been proposed. The nomenclature reflects the number of layers (e.g., "1" for monolayer) and the crystallographic arrangement, with "T" indicating trigonal, "H" for hexagonal, and "R" for rhombohedral stacking [16].

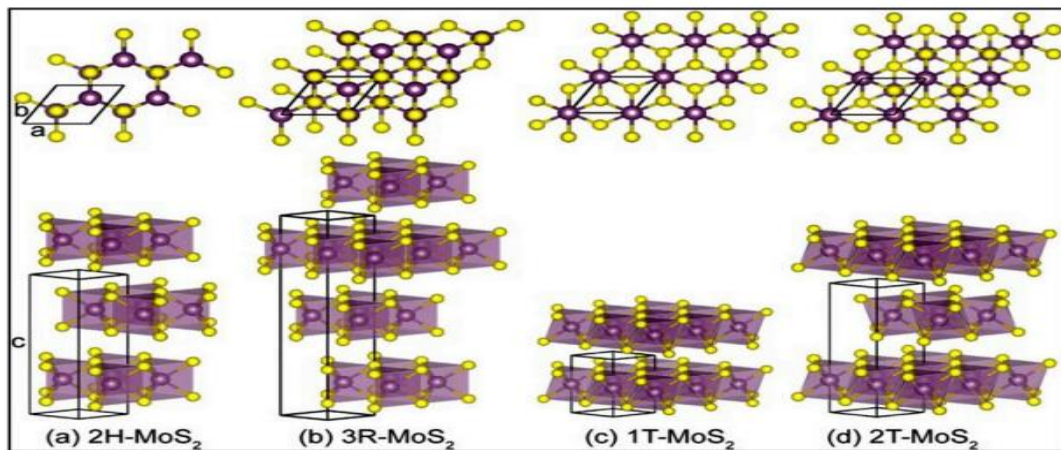


Figure 13: Polytypes of the layered structure of MoS₂.

1.13 Synthesis of MoS₂

1.13.1 Mechanical exfoliation

The Scotch tape method, pioneered by Novoselov et al. [17], remains a foundational approach for isolating few-layer or monolayer MoS₂. This method relies on the adhesive properties of tape to separate thin layers from bulk crystals. A key advantage is the production of high-quality flakes with thicknesses ranging from a few layers to several micrometers. However, the primary limitation is its low yield, making it unsuitable for large-scale applications.

An improved method is wafering anodic bonding, where bulk MoS₂ is placed on a Pyrex glass substrate and subjected to a voltage of 200–1500 V at temperatures of 130–200 °C. This process uses tape to exfoliate the MoS₂ onto the substrate, yielding thin films with better precision and scalability [18].

1.13.2 Chemical exfoliation

Jensen et al. [19] were among the first to employ the molecule intercalation method, also known as the Morrison approach, for the exfoliation of MoS₂. This technique involves two key steps: initially, small particles such as lithium ions are introduced into the interlayer spaces of MoS₂. This process causes the layers to expand and weaken the van der Waals forces holding them together. In the second step, the intercalated compound is reacted with water, generating hydrogen gas and effectively separating the layers into single-sheet structures that are suspended in a solution.

The process can be further optimized by using alternative solvents, such as methanol, ethanol, or isopropyl alcohol, combined with mild heating to enhance the exfoliation. The final product is referred to as "exfoliated MoS₂," which consists of reassembled layers that can be used in various applications. However, the method has several limitations, including prolonged reaction times (up to three days) and limited control over the intercalation process. Insufficient intercalation may result in low yields, while excessive intercalation can degrade MoS₂ into Li₂S. Another drawback is the potential conversion of the desirable 2H phase (semiconducting) to the 1T phase (metallic, octahedral), which is less favorable for electronic applications. To recover the semiconducting properties, an additional thermal treatment process is necessary to convert 1T-MoS₂ back to the 2H phase.

Gentle annealing has been shown to gradually restore the semiconducting nature of chemically exfoliated MoS₂ crystals. Moreover, annealing above 300°C has been reported to enhance

photoluminescence by reopening the band gap. To address the lengthy reaction time, microwave-assisted processes have been introduced, significantly reducing the time required for intercalation and exfoliation. Additionally, microwave energy has been utilized to synthesize 2H-MoS₂ nanosheets and nanocomposites and facilitate the phase transition from 1T to 2H.

Another advancement in this field is the electrochemical exfoliation technique. Instead of lithium in hexane, a voltaic cell setup is used, with MoS₂ serving as the cathode and lithium foil as the anode. The controlled voltage applied in this system provides better regulation of the intercalation process, leading to improved results.

Solvent-based exfoliation, commonly referred to as the Coleman method, is another widely used approach. This technique involves reducing the energy required for layer separation by dispersing bulk MoS₂ crystals in organic solvents such as isopropyl alcohol or N-methyl-2-pyrrolidone (NMP) and applying sonication. This process results in 2D MoS₂ flakes suspended in the solvent, which are particularly useful for optical, vibrational, and biosensing applications. Additionally, this method preserves the 2H crystal structure of MoS₂, making the resulting suspensions highly compatible with microfluidic systems [20].

1.13.3 Chemical Vapor Deposition (CVD)

The chemical vapor deposition (CVD) process is a highly effective technique for producing high-quality 2D nanomaterials like MoS₂. This method provides precise control over the morphology, crystallinity, and defect levels of the resulting materials. The ability to manipulate various parameters during the process allows for the fabrication of 2D nanosheets with tailored properties, making CVD a valuable tool for advancing novel 2D material systems and their composites.

In the CVD process, thin films are deposited on a substrate through a chemical reaction of vapor-phase precursors. This approach facilitates the synthesis of high-purity materials with well-defined structures and is particularly advantageous for large-scale production. The primary methodology involves a direct deposition technique, sometimes referred to as a strong vapor-phase reaction process, where the precursors react on the substrate's surface to form the desired material.

CVD has demonstrated its potential for growing monolayer and few-layer MoS₂ films with exceptional uniformity and quality. However, early attempts with CVD produced fragmented or discontinuous films, which posed challenges for achieving high-performance 2D materials. These limitations were overcome with the development of vapor-phase growth methods, which enabled the formation of continuous films by carefully controlling the precursor flow, reaction temperature, and substrate conditions.

A common approach involves depositing a thin molybdenum layer on a substrate, followed by exposing it to sulfur vapor. The sulfur reacts with molybdenum to form MoS₂ films. This process can yield uniform and continuous films with a precise thickness, determined by the growth parameters. Various advancements in CVD techniques have enabled wafer-scale production, creating MoS₂ films with large triangular domains and high-quality crystallinity. These features are critical for applications in electronics, optoelectronics, and catalysis.

Additionally, CVD methods allow for the fabrication of 2D MoS₂ with unique morphologies and properties by combining different precursors and modifying the growth conditions. This flexibility has paved the way for the development of MoS₂-based heterostructures and composites, broadening the scope of applications in emerging technologies [21].

1.14 Properties

1.14.1 *Electronic and Electrical Properties*

In its bulk form, MoS₂ exhibits an indirect bandgap of approximately 1.29 eV, with the valence band maximum (VBM) occurring at the Γ -point and the conduction band minimum (CBM) at the K-point of the Brillouin zone. This configuration results in metallic characteristics. As the number of MoS₂ layers decreases, the electronic structure undergoes significant changes. The energy difference at the Γ -point decreases, while the CBM between Γ and K points shifts, driven by hybridization between the d-orbitals of molybdenum atoms and the p-orbital of sulfur atoms.

Notably, the energy at the K-point, determined by the d-orbital of molybdenum, remains constant regardless of the number of layers. When the VBM at the Γ -point drops below zero energy, the K-point becomes the new VBM, and the material transitions from an indirect to a direct bandgap semiconductor. This shift is most evident in monolayer MoS₂, where a direct bandgap of approximately 1.9 eV is observed, marking its potential in optoelectronic and semiconducting applications [22].

1.14.2 *Optical Properties*

Unlike graphene, monolayer MoS₂ is a non-centrosymmetric material with a direct bandgap, which can be attributed to the d-orbital electron occupation. This property results in distinctive optical features, including:

Monolayer MoS₂ exhibits strong photoluminescence due to its direct bandgap, in contrast to bulk MoS₂, which shows weak photoluminescence due to its indirect bandgap. The quantum yield (QY) of photoluminescence decreases as the number of layers increases.

Reflection spectroscopy reveals two prominent peaks, A_1 and B_1 , located at wavelengths of 670 nm and 627 nm, respectively. These peaks are caused by the splitting of the VBM at the K-point due to spin-orbit coupling. In multilayered MoS₂, the peaks reflect a combination of spin-orbit coupling and interlayer interactions, while in monolayers, the effects are dominated by spin-orbit coupling alone.

Monolayer MoS₂ features six CBMs and VBMs at the K-points in the Brillouin zone, often referred to as "valleys." These valleys exhibit spin-valley coupling, resulting in opposite spin orientations at the K and K' valleys. However, because monolayer MoS₂ lacks inversion symmetry and maintains time-reversal symmetry, inter-valley transitions are prohibited, making valley polarization observable only under specific conditions, such as broken inversion symmetry.

Strain engineering further influences MoS₂'s optical properties by shifting the band structure. For instance, strain reduces the intensity and energy of the A_1 peak, allowing for fine-tuning of photonic and optoelectronic devices [23].

1.14.3 Mechanical Properties

MoS₂'s unique mechanical properties, combined with its electronic and valley properties, make it an excellent candidate for nanodevices. Its remarkable mechanical robustness includes properties such as Young's modulus, yield stress, and bending modulus.

Monolayer MoS₂ can endure elastic deformations up to 25% before failure, making it highly resilient. This mechanical flexibility is critical for applications in flexible electronics and strain-engineered devices.

The effective Young's modulus for monolayer MoS₂ has been reported to range between $120 \pm 30 \text{ Nm}^{-1}$ and $180 \pm 60 \text{ Nm}^{-1}$, depending on the thickness and test methods. This corresponds to a bulk Young's modulus of approximately $270 \pm 100 \text{ GPa}$, comparable to steel.

Nanoindentation experiments estimate the yield strength of monolayer MoS₂ to be around $15\text{--}16.5 \text{ Nm}^{-1}$, with a fracture strength averaging 23 GPa . The material displays an effective strain range of $6\text{--}11\%$ before breaking, demonstrating its excellent mechanical stability at the nanoscale.

Thermoelectric Performance: MoS₂ possesses a significant Seebeck coefficient and a suitable intrinsic bandgap, enabling its use in thermoelectric devices [24].

1.15 Applications of MoS₂

1.15.1 Mechanical

MoS₂ is primarily utilized as a solid lubricant due to its superior performance (as in Figure 14) in extreme conditions where traditional liquid lubricants fail. It minimizes friction between surfaces under varying operational environments, including very high or low temperatures, varying pressure conditions, and high-speed scenarios. Unlike liquid-based lubricants, which may freeze, degrade, or fail under extreme conditions, MoS₂ offers a reliable and stable alternative.

MoS₂ is preferred due to its solid lubricant stem from its hexagonal layered structure. These layers easily slide over each other, which significantly reduces friction and wear. Other key characteristics contributing to its performance include:

Its hexagonal lattice structure leads to exceptional low friction and strong adherence to diverse materials. The weak interlayer interactions in MoS₂ ensure that the material maintains its

lubricating properties even under varying environmental pressures. MoS₂ performs exceptionally well in high temperatures, demonstrating stability and thermal durability.

Additionally, MoS₂'s low frictional properties result from sliding motion between the individual layers and the presence of six nonbonding electrons that entirely occupy the conduction band. These properties give MoS₂ a net positive charge on its outer layer, further enhancing its performance as a lubricant.

Amontons-Coulomb Law explains MoS₂'s superior lubricating properties. This law shows that the coefficient of friction can be reduced as low as 0.003 between two MoS₂ surfaces. Research indicates that the unique lamellar (layered) design of MoS₂ offers maximum advantages in reducing friction, particularly in situations involving metal-to-metal contact. Due to its impressive properties, MoS₂ finds widespread use across various industries, including:

MoS₂ is extensively used in automotive and transportation machinery to reduce friction and wear in engines, transmissions, and other moving mechanical parts under varying operational conditions.

In mining machinery, MoS₂ provides lubrication for heavy equipment operating under high loads, pressure, and extreme environmental conditions.

MoS₂ is applied in construction machinery (e.g., cranes and bulldozers) to ensure operational efficiency while enduring heavy workloads and environmental stress.

MoS₂ is employed in agricultural equipment operating across rough terrains and variable weather conditions.

MoS₂'s reliability and ability to perform in extreme temperatures and pressures make it ideal for military and aerospace systems, such as aircraft engines and other mechanical components exposed to harsh operational conditions [25].

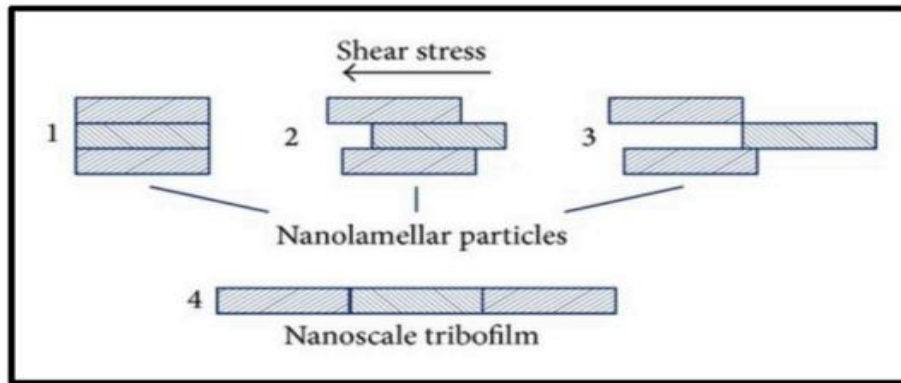


Figure 14: Mechanism of the tribological action of nano lamellar disulfides.

1.15.2 Biosensors

Molybdenum disulfide (MoS₂), especially in its monolayer form, possesses outstanding electrical, optical, and vibrational properties along with a high surface-to-volume ratio. These features make it an excellent choice for creating advanced biosensors. MoS₂ offers superior sensitivity and responsiveness compared to graphene, positioning it as a more effective material for biosensor development.

Primary Properties Contributing to Biosensor use MoS₂ shows an impressive sensitivity level of over 700 for a change of pH by just one unit. Additionally, its signal-to-noise ratio is nearly ten times higher than that of graphene, further emphasizing its potential for biosensor use.

Biosensors utilizing MoS₂ operate by detecting changes in Electrical parameters or fields, Optical signals (e.g., photoluminescence), Electro-optical responses, and plasmonic or intercalation effects. These mechanisms depend on the interaction of target biological or chemical species with the MoS₂ surface.

The 2D monolayer structure of MoS₂ provides increased surface exposure, allowing more efficient interaction with target molecules. Its structure supports the binding of a wide range of chemical and biological species, making it effective for biosensing.

MoS₂ is frequently combined with other materials like graphene, carbon nanotubes, and polymers to form composites. These combinations integrate MoS₂'s unique properties while adding additional effects, such as heterojunctions. These interfaces improve the biosensor's sensitivity and response time.

The intercalation of organic molecules into MoS₂ layers modifies its electronic properties by reducing its bandgap and causing photoluminescence (PL) quenching at varying levels. This allows for fine-tuning the sensor's sensitivity and optimizing its performance for target biomolecule detection.

Biosensors must be carefully engineered to detect specific molecules or ranges of concentration. An external electric field is necessary for the intercalation process, requiring precise control. Voltage must align with the electric field generated by the bilipid membranes of cells to enable the intercalation process.

1.15.3 Gas sensing

MoS₂ demonstrates significant potential for gas and pH sensing applications by utilizing changes in electrical conductivity at the interface between MoS₂ and the substrate. It is being employed for the detection of gases such as NO₂, ammonia (NH₃), and hydrogen (H₂), with sensitivity levels as low as 1.2 ppm, resulting in a high signal-to-noise ratio. The gate effect and light exposure can further enhance these properties. Similarly, MoS₂ is being developed for pH detection by monitoring shifts in electrical conductivity as pH levels change. Both gas and pH sensing performance are influenced by factors such as the number of MoS₂ layers, with

thicker layers improving charge density and exposure time, which allows for better signal responses. These properties make MoS₂-based sensors promising for a variety of environmental and biological sensing applications [26].

1.15.4 Catalytic activity

MoS₂ has extensive applications in the chemical industry, particularly in the production of clean hydrogen fuel. Theoretical and experimental studies have confirmed that the hydrogen evolution reaction (HER) occurs efficiently at the active sites on the MoS₂ plane edges. Hydrogen is considered a promising clean alternative to petrochemical fuels due to its high energy density, excellent chemical stability in acidic environments, and its role as a clean energy carrier. Consequently, there is a growing interest in exploring MoS₂ for hydrogen production, which can be achieved through photocatalysis or electrocatalysis. Although MoS₂ was initially a favored material due to its chemical inertness with solid electrolytes, its bulk structure displayed limitations. Specifically, its threefold sulfur coordination led to closed planes, restricting interaction with the electrolyte. To address this challenge, research has shifted toward enhancing the active sites of MoS₂, with nanoscale engineering playing a pivotal role in improving its catalytic performance and efficiency [27].

- Make more dynamic structures according to mass or volume ratio.
- Electronically adjust the dynamic site to make it more dynamically favorable.

1.15.5 Supercapacitors

The porous morphology of MoS₂ enhances electrochemical performance due to the increased contact area between the active material and the electrolyte, allowing for rapid ion and electron transport. MoS₂ nanostructures exhibit desirable properties such as high charge transfer capabilities and long cycling stability, making them ideal for use in supercapacitors.

Mesoporous MoS₂ cathodes have demonstrated improved specific capacitance values of 376–403 F g⁻¹ at a scan rate of 1 mV s⁻¹ while maintaining exceptional long-term cycling stability, retaining 80 % of their charge even after 2000 cycles. These superior properties result from two mechanisms: the pseudocapacitive behavior driven by Faradaic charge transfer processes and a non-Faradaic process at the electrode/electrolyte interface, where a double layer is formed. The latter is considered a purely surface-related phenomenon, contributing significantly to the overall electrochemical performance [28].

1.16 Phthalocyanines

1.17 History

In 1928, at Grangemouth, Scotland, as crafted by Messrs. Scottish Colors Ltd., hits of a light blue insoluble complex were seen in the iron vessels, which were used to get ready phthalimide from phthalic anhydride and ammonia. This compound was, therefore, demonstrated to be ferrous phthalocyanine. From that point forward, in a real sense, a huge number of patents and publications concerning phthalocyanines have shown up. It is likely that the phthalocyanines have been the subject of additional actual investigations than some other single class of compound, part of the way because of their exceptional construction and incompletely due to their highly warm and chemically stable [29].

1.18 Introduction

Phthalocyanine takes its name from the Greek language naphtha, meaning rock oil, and cyanine, meaning dark blue. The term was first coined by Professor Reginald P. Linstead in 1933 at the Royal Institute of Science and Technology in describing a family of organic compounds, which includes both metal-free phthalocyanine (dihydrogen phthalocyanine) and metal phthalocyanines. These metal derivatives are formed by substituting the two central

hydrogen atoms with metals from the periodic table, with at least 70 different metal phthalocyanines having been identified to date. The four benzene units in the core of phthalocyanines have 16 reactive sites, which has allowed the synthesis of over 5,000 unique phthalocyanine derivatives.

The discovery of phthalocyanines occurred by accident. In 1907, Braun and Tcherniac at the South Metropolitan Gas Company in London discovered a blue compound by heating o-cyanobenzamide, which is believed to have been phthalocyanine. Later on, in 1927, de Diesbach and von der Weid named scientists at the University of Fribourg, reacted o-bromobenzene along with cuprous cyanide in order to synthesize nitriles of benzene, resulting in a blue compound that was mostly similar to copper phthalocyanine. Moreover, in 1928, with the Grangemouth Works project of Scottish Colors Ltd., a blue-colored impurity was discovered during the synthesis of phthalimide that was synthesized from a reaction of phthalic anhydride and ammonia. This impurity was identified as iron phthalocyanine, which was formed as a result of the reaction between phthalimide and iron in the reaction vessel.

The unique structure of phthalocyanines consists of a macrocyclic ligand with four aromatic benzene rings interconnected by nitrogen atoms (as in Figure 15). Two central hydrogen atoms can be replaced by various metals, forming stable metal phthalocyanines. These compounds exhibit remarkable stability and versatility due to their aromaticity and metal coordination, making them resistant to acids, light, moisture, and other environmental factors. Their discovery and subsequent study paved the way for a variety of technological and industrial applications.

X-ray studies of phthalocyanine compounds and their relative metal derivatives, such as Ni, Cu, and Pt phthalocyanines, were conducted by Professor J. Monteath Robertson and his colleagues between the time span of 1933 and 1940. These studies revealed that phthalocyanine

compound and its metal derivatives adopt monoclinic crystal structures with the space group P2/a. Each unit cell contains two molecules within central symmetry, and the entire molecule is typically lying in a single plane, with one exception being the two central hydrogen atoms present in dihydrogen phthalocyanine.

Efficient stability of phthalocyanines can be assigned to the strong coordination bond and covalent bond of the central metal with the surrounding aromatic benzene and nitrogen structures. This high degree of aromaticity and coordination contributes to their exceptional resistance to environmental degradation. Phthalocyanines exhibit remarkable stability against acids, bases, moisture, heat, light, and most solvents. However, they tend to decompose through pyrolysis at high temperatures like 500° C. Copper phthalocyanine is soluble in concentrated H₂SO₄ and can precipitate out of diluted sulfuric acid solutions, though phthalocyanines are only sparingly soluble in organic solvents and shows insoluble character in water.

The outstanding stability, coupled with the exceptional color properties of phthalocyanines, especially copper phthalocyanine, led to their widespread use as pigments. In 1935, the discovery of copper phthalocyanine as a pigment, later named Monastral Blue, marked a significant development as it was described by The New York Times as the first new blue pigment discovered in over 100 years. This discovery came from Royal Chemical Ventures Ltd., where the demand for copper phthalocyanine as a colorant grew, and in 1936, companies like I.G. Farbenindustrie and DuPont began producing it on an industrial scale. By 1985, production had reached approximately 14 million pounds annually in the United States alone, supported by about 12 manufacturers.

Between the 1930s and 1950s, extensive studies were carried out on the physical, chemical, and electronic properties of phthalocyanines, including X-ray spectra, polymorphism, photoconductivity, dielectric properties, and their potential as semiconductors. During this

period, 45 distinct metal phthalocyanines from all over the periodic table were made and studied for their various properties and applications. These investigations highlighted their wide potential across many fields, from colorants to advanced technological applications.

Commercial manufacturing techniques for phthalocyanine and copper phthalocyanine saw significant advancements, including methods to prevent the crystallization process and flocculation process of the pigment structure. Additionally, processes were developed to synthesize both partial-chlorinated and full-chlorinated copper phthalocyanines. The discovery of polymorphism among these compounds further expanded their versatility, with different crystalline forms identified, such as α , β , γ , δ , $\pi\rho$, R, and ϵ types of copper and other metal phthalocyanines. Notably, the p structure was spotted in 1977, while in 1967, the x type of phthalocyanine without metal was reported within electrophotographic applications.

In the mid-1980s, η and τ types of metal-containing and metal-free phthalocyanines were discovered and found promising as photoreceptors in the photoconductive layers used in electrophotographic applications. From 1930 to 1960, phthalocyanines were widely explored for their use as colorants in various applications. They were used in the paint industry, plastic industry, inks used in the printing and textiles industry, ballpoint and pen inks, leather treatment, fuel, oil, and visual color printing. Furthermore, phthalocyanines were also employed as food coloring agents due to their stability and color properties. During this period, research discovered the ability to polymerize phthalocyanines, which opened up additional opportunities for their use in diverse industrial and technological applications [30].

Phthalocyanines frequently exist in at least two polymorphic adjustments, which might be recognized by infrared and X-beam diffraction procedures. In spite of the fact that phthalocyanines in which the focal metal particle has an oxidation condition of 2 are the most widely recognized, buildings are realized in all oxidation states from 0 to 6. Phthalocyanine

manganese edifices, for instance, are realized in oxidation states 0, 1, 2, 3, 4. Phthalocyanines show differing sound qualities toward arrangement in concentrated sulfuric acid. Practically every one of the edifices is uninhibitedly dissolvable in this acid, yet some, like CuPc and NiPc, are reprecipitated unaltered upon weakening, though others, for instance, CaPc and NazPc, are demetallized. The item sans metal phthalocyanine (shortened HZPc) itself gradually deteriorates in concentrated sulfuric acid. Berezin has exhaustively concentrated on the conduct of amassed sulfuric acid. The phthalocyanine unit is decently steady toward oxidation yet might be separated to phthalimide or phthalic acid by two-electron oxidation with ceric or dichromate particles. Elvidge has formed the dichromate oxidation into a rich strategy for the quantitative assurance of the oxidation condition of the focal metal particle. Under particular conditions, a one-electron oxidation item, having the ring framework unblemished, might be recognized. This item is paramagnetic and shows an electron-turn reverberation range normal for a free extremist [31].

1.19 Preparation methods

Phthalocyanine metal complex structures might be prepared by different strategies, the broader techniques being shown in the following conditions (as shown in Figures 16 and 17).

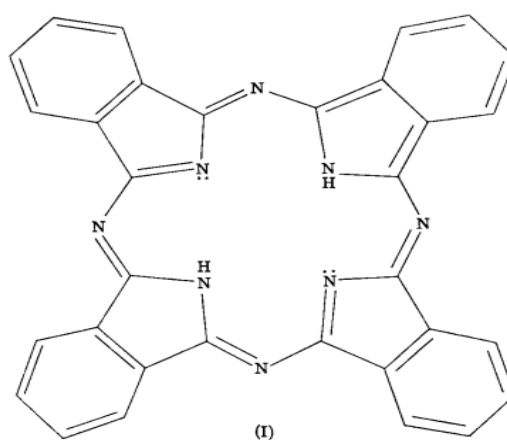


Figure 15: Structure of metal-free phthalocyanine.

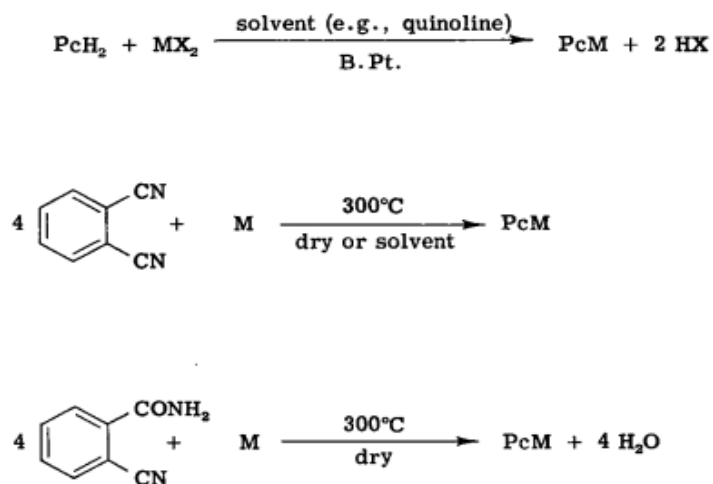


Figure 16: Methods of synthesis of metal-free phthalocyanine.

Free metal phthalocyanine might be ready by various courses, of which models are given below (as shown in Figure 18).

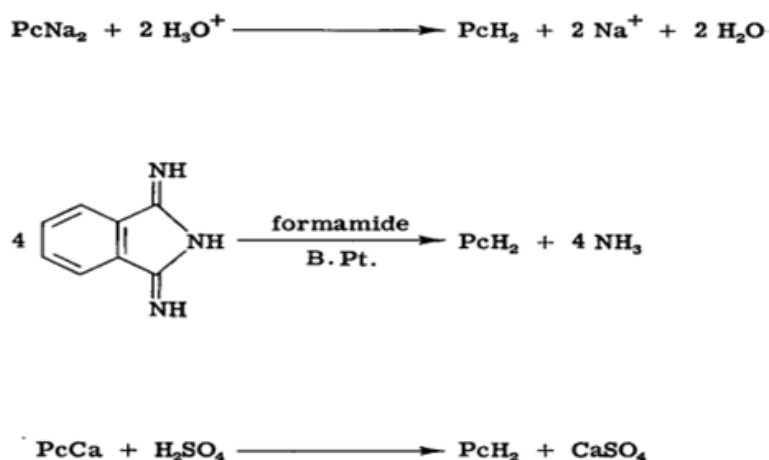


Figure 17: Methods of preparation of metal phthalocyanine.

1.20 Copper Phthalocyanine (CuPc)

Copper phthalocyanine (CuPc), commonly known as phthalocyanine blue or phthalo blue (Figure 18), is a vibrant and intense blue pigment derived from the phthalocyanine group of

compounds. This pigment is widely used in paints, dyes, and other coloring applications due to its exceptional properties. Copper phthalocyanine is highly valued for its remarkable characteristics, including excellent lightfastness, strong color intensity, dramatic covering efficiency, and resistance against the effects of acids and alkalis. It appears as a fine blue powder and is largely insoluble in solvents like water, making it stable and reliable for various industrial and artistic uses.

1.21 History of CuPc

The discovery of metal phthalocyanines can be traced back to the observation of unique colored byproducts formed during reactions involving phthalic acid (benzene-1,2-dicarboxylic acid), its derivatives, and nitrogen-containing compounds or metals. Copper phthalocyanine (CuPc) was first synthesized in 1927 through a reaction between copper(I) cyanide and *o*-dibromobenzene. This reaction primarily yielded dark phthalonitrile along with a distinctive blue byproduct.

A few years later, researchers at Scottish Dyes identified phthalocyanine pigments when phthalimide was mixed in reactions involving phthalic anhydride and an alkali, with metallic iron observed in the process. In 1937, DuPont began producing copper phthalocyanine blue in the United States under the brand name Monastral Blue, following its introduction in the United Kingdom by ICI and in Germany by I.G. Farbenindustrie in 1935.

Initially, producing stable dispersions with certain other pigments, particularly when combined with rutile titanium, presented challenges due to the tendency of the blue pigment to flocculate. The beta structure of copper phthalocyanine proved to be more stable than the primary alpha structures and, therefore, became the preferred configuration. Over time, a variety of isomeric

structures of copper phthalocyanine have been discovered, further expanding the diversity of its molecular configurations [32].

1.22 Synthesis of CuPc

Two main processes have commercial significance for the successful synthesis of CuPc.

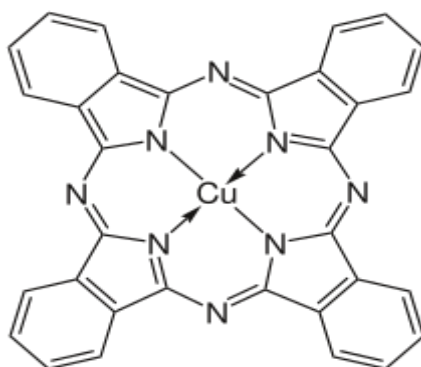


Figure 18: Structure of copper phthalocyanine.

Process involving Phthalonitrile: This method is predominantly used in Germany and involves the synthesis of copper phthalocyanine via reactions with phthalonitrile intermediates.

Process involving Phthalic Anhydride/Urea: Developed and utilized in the UK and US. This method relies on the reaction between phthalic anhydride and urea to produce copper phthalocyanine.

Both of these processes can be carried out either with or without the use of a solvent. The solvent-based process tends to produce a higher yield (> 95%) compared to the solvent-free or "baking" method, which typically achieves yields of 70 to 80%. Consequently, the solvent-based method has historically generated greater commercial demand due to its higher efficiency. However, recent trends indicate a shift toward the solvent-free baking process,

driven by economic and environmental factors. The baking method is favored because it eliminates the use of solvents, reduces waste, and shortens production lead time.

1.23 Structural properties of CuPc

Copper phthalocyanine (CuPc) is a coordination complex compound consisting of Cu (II) ions (Cu^{2+}) linked to the phthalocyanine ligand, forming the structure $\text{Cu}^{2+}\text{Pc}^{2-}$. Its structure is closely related to copper porphyrins, which are derived from the double deprotonation of porphyrins. CuPc has the D_{4h} point group in symmetry and exhibits Para magnetism due to one electron that is not paired in a molecule.

CuPc apparently shows insolubility in water (0.1 g/100 ml) but is highly soluble in concentrated H_2SO_4 . The density of the CuPc has a value of 1.6 g/cm³. The distinct blue color of CuPc arises from a π - π^* transition of electrons, with a λ_{max} value of 610 nm.

1.23.1 Crystalline structures of CuPc

Copper phthalocyanine (CuPc) exists in several polymorphic forms, with five distinct polymorphs identified: α , β , η , γ , and χ . Among these, the β phase and the α phase that is metastable can be readily converted into β phase. These polymorphs differ in the degree of overlap between their coordinating molecules, which can be used as distinguishing features.

The α phase exhibits a greater molecular overlap, resulting in a smaller copper-to-copper distance of approximately 3.8 Å. β phase has a larger distance of about 4.8 Å. This variation in structural arrangement influences the physiochemical properties of the material.

1.24 Harmful nature of CuPc

CuPc is non-biodegradable, although it is not considered non-toxic to aquatic animals and plants. None of the hazards have been directly linked with CuPc. The LD50 value in vertebrates

is considered to be more than 5g/kg, and no special harmful effects have been observed at this level of intake. A consistent intake of 0.2 mg/kg daily in rodents has been evaluated as low concern. There is no evidence to suggest that this compound causes cancer problems. However, phthalocyanine treated with sulphuric acid has been observed to induce neuroanatomical changes in growing chickens that lack certain biological entities when directly injected into fertilized eggs [33].

1.25 Applications of CuPc

1.25.1 Catalysis

Metal phthalocyanines have been extensively studied as catalysts for redox reactions due to their unique structural and electronic properties. Two primary areas of focus in their application include the oxygen reduction reaction (ORR) and removing hydrogen sulfide from gaseous species. These reactions demonstrate the ability of metal phthalocyanines to act as efficient and selective catalysts, facilitating crucial environmental and industrial processes.

1.25.2 Colorant

Phthalo blue, also known as copper phthalocyanine blue, is widely utilized in inks, coatings, and various plastic applications due to its exceptional durability and stability. Despite being insoluble, it tends to migrate within the material over time. This vibrant blue dye is a popular choice in printing through inks and the packing industry. In the era of 1980s and 1990s, production levels in only Japan reached approximately 10,000 tons annually, making it the most widely produced synthetic dye by volume [34].

1.26 Types of sensors

Biosensors and synthetic sensors are the two general classes (Figure 19) into which electrochemical sensors can be isolated. Different sensing techniques for dopamine sensing are featured below.

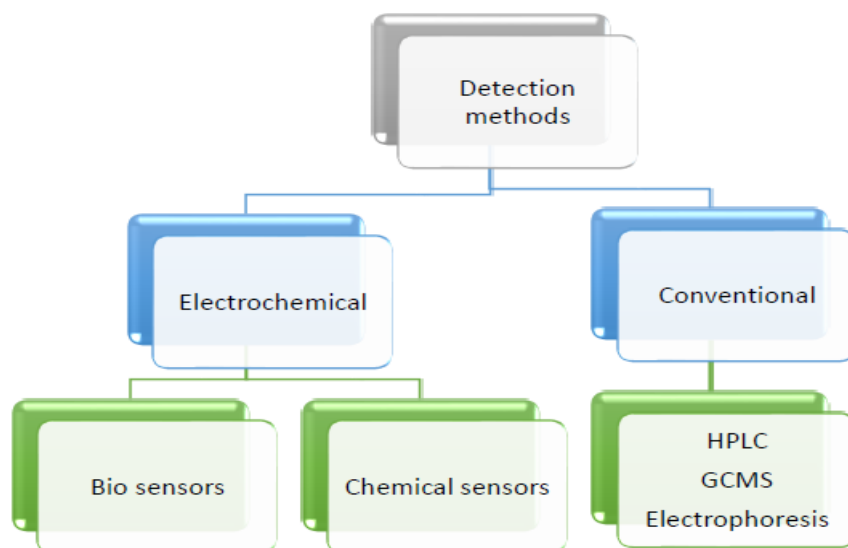


Figure 19: Types of biosensors.

Utilizing a biochemical receptor that is associated with an electrochemical transduction component, the electrochemical biosensor is a device that can give explicit quantitative, logical data. In any case, a few creators utilize a more extensive meaning of biosensors in writing, focusing on the sort of analyte as opposed to the need for a biological recognition component.

Substance sensors, rather than biosensors, contain parts that are not naturally dynamic, which expands their awareness and particularity. Changed anodes are used every now and again as electrochemical sensors. Different natural or inorganic materials with solid electrical conductivity and synergist capacities can be utilized to make these changed terminals.

Biosensors can be made sufficiently little to be embedded into living cells and produce a speedy, sensitive, and quick reaction. However, there are a few issues that should be fixed.

In the first place, biosensors should have the option to answer delicately in the right focus range.

Ascorbic acid, which oxidizes inside a similar potential as DA, are instances of interferents that the biosensors should have the option to recognize from to recognize dopamine and them.

Electrochemical detection of DA typically includes a course of oxidation, bringing about the development of leuco dopamine chrome and, afterward, dopamine chrome. Among various electroscientific procedures, amperometry shows fundamental selectivity and awareness. Due in enormous part to their convenience, speedy reaction times, and prevalent responsiveness, electrochemical dopamine discovery methods have gone through broad exploration in such a manner.

Electrochemical strategies can effectively survey dopamine (Figure 20) since it is oxidized or diminished at electrical possibilities without the requirement for any additional redox catalysts. Be that as it may be, to successfully distinguish dopamine, cathode awareness should be expanded because of a few other interferents in the body, which range from Pico molar to Nano molar scale.

Because of their better capacity than improving the cathode's electro-reactant ability, metal components like gold and platinum have generally been utilized widely in bio-detecting applications. Gold and platinum are not leaned toward for use in that frame of mind in spite of these benefits due to disadvantages like low responsiveness, linearity at low DA focus, and a need for assets. A few benefits of electrochemical sensors for genuine applications are given below.

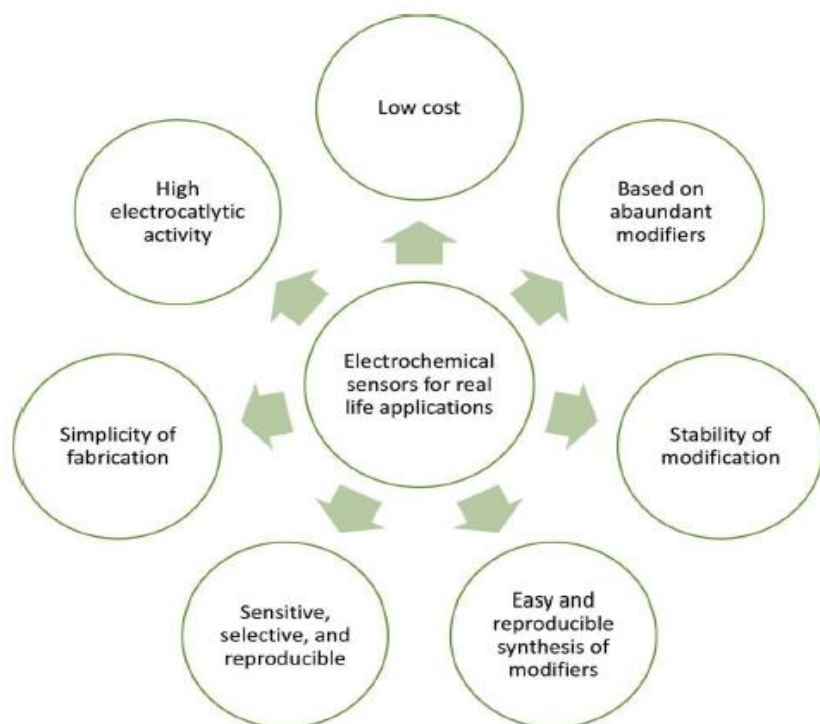


Figure 20: Advantages of electrochemical sensors.

1.27 Challenges

It is broadly acknowledged that DA when presented to a terminal surface, is prepared to undergo electrochemical oxidation to deliver dopamine-quinone (DAQ). In the DA compound, a trade of 2 electrons and 2 protons happens when a voltage is provided to the cathode in the oxidation of the DA compound into DAQ. Subsequently, a sign comprising of a faradaic current was shaped when the electrons were gotten by the cathode. Previously, the immediate assurance of DA was, in many cases, achieved by utilizing a customary electrochemical strategy. When conventional anodes were used, it was noticed that the reaction signal was poor most of the time. This was because of the sluggish electron-move rate characteristics of the cathode. What's more, the fouling impact that happens at the exposed terminal makes it hard to accomplish elevated degrees of responsiveness and selectivity in DA discovery. What's more, the presence of various meddling species simultaneously, like AA and UA, is answerable for the covering

signal reaction, which makes it hard to separate between the different individual pinnacle potentials [35].

Consequently, a surface change procedure applied to the functioning terminal is an effective strategy for settling this issue. This procedure can help evade the overvoltage as well as the deferred energy of the terminal interaction. Electrochemical DA sensors for cerebrum illness conclusion should proficiently control potential interferent species like glucose, uric acid (UA), and ascorbic acid (AA), epinephrine, which have comparable redox conduct.

Dopamine might be identified at exceptionally low amounts in human serum tests by improving its electrochemical signals and recognizing it from interferents. The synergistic impact of numerous NPs adsorbed on the terminal can reduce the previously mentioned issues and work on insightful execution.

Bio and substance sensor stages in light of assorted modifiers are vital on the grounds that nanomaterial communication augments logical proficiency. The synergistic impact ought to increment the surface region and electron move rate between the outer layer of the terminal and DA without impacting the bio similarity of the component (Figure 21), which is vital for dopamine fixation examination. The ultimate objective is to accomplish a proper change that will take into account high selectivity and, what's more, responsiveness toward DA sensors [36].

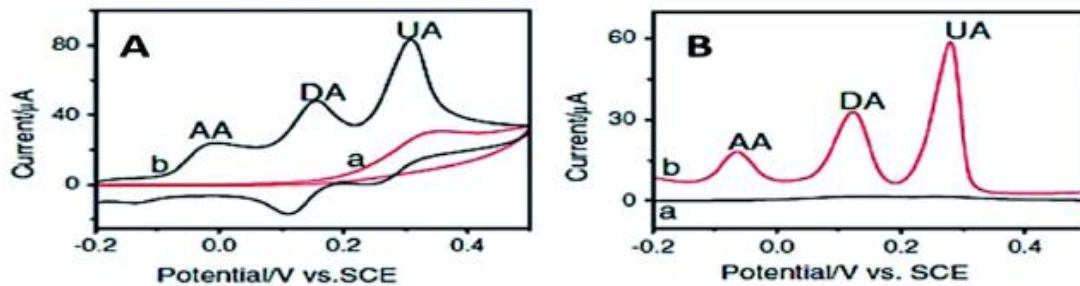


Figure 21: CV (A) and DPV curves (B) for bare GCE and modified GCE.

CV and DPV bend for uncovered GC and artificially changed terminal are outlined in the above picture. Terminals that have been synthetically adjusted are regularly used to recognize DA. Ordinarily, detailed materials are metal NPs (Ag, Au, Pd, Pt, Cu), metal oxide, polymers, carbon nanotubes, zeolite, earth, and metal-organic frameworks (MOF).

1.28 Electrode material used in electrochemical sensing of dopamine

Electrochemical strategies have been made to offer a fast and simple strategy for focusing on particles' redox responses, and they have been demonstrated to be viable possibilities for the identification of an assortment of synapse particles similar to dopamine. Dopamine might be precisely and promptly identified by electrochemical identification when utilized in relation to suitable terminal materials since it is an electro-dynamic material.

Because of their incredible (Figure 22) electrical conductivity, enormous surface regions, and electro-synergist properties, the utilization of conductive materials could essentially upgrade the limit of the anode to identify the analyte. Numerous materials, including metal nanoparticles, polymers, CNTs, and graphene, have been utilized to make an incredibly viable detecting platform to track down focuses of interest, which could determine the issues framed previously. Thus, name-free dopamine discovery utilizing real clinical examples might be

conceivable if electrochemical investigations were utilized utilizing mixture stages modified with nanomaterial [37].

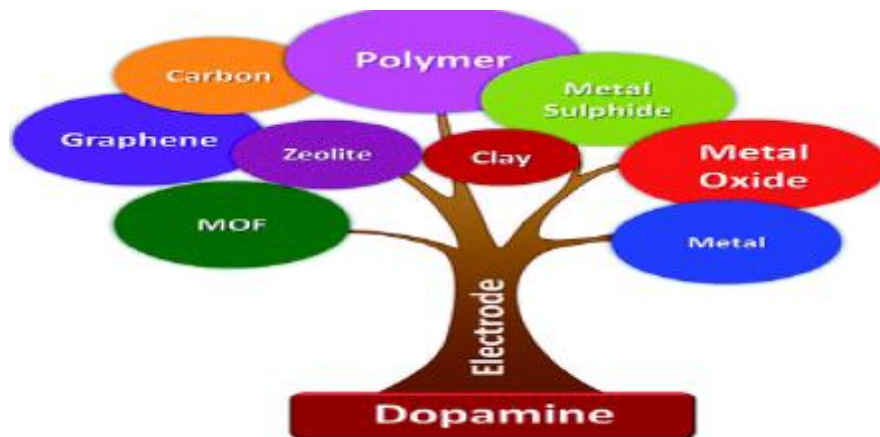


Figure 22: Common electrode materials for DA sensing.

Chapter 2

2 Literature review

Koyan et al. assessed the use of PGE changed with overoxidized nanofiber polypyrrole (OONfPPy) as a sensor for the estimation of DA. The differential pulse voltammetric (DPV) approach was utilized to look at the changed terminal's presentation. EIS and SEM were utilized to evaluate the modified electrode's surface. It was found that the uncovered and changed cathode had different registered electroactive regions. The sensor's LoD of 6.95×10^{-9} M (S/N=3) exhibited areas of sensitivity for its DA [38].

Hareesha et al. manufactured a touchy and sufficiently cost DL-phenylalanine graphite electrode (Poly (DLPA)- GE) that was made in the ongoing sensing for DA detection. Involving CV and DPV in a phosphate buffer solution (PBS) with a pH of 6.5, the movement of DA was inspected at GCE. As per the voltammetric result, the sensor shows an impressive expansion in DA flows, bringing overpotential contrast to the bare electrode. A fine direct increment for DA oxidation (scope of 2.0 μ M to 45.0 μ M) is depicted by poly (DLPA)-GE under the best working conditions, with an expected lower LoD of 28 nM and. The proposed terminal showed an elevated degree of sensitivity and selectivity in the presence of interferents [39].

Khan et al. have accounted for the electrocatalytic execution of 2D-hBN toward DA. The catalytic effect of the electrode was shown utilizing a clear drop casting strategy to rely upon both the substrate and mass or coverage. Modified SPEs were exhibited to deconvolute the signals of DA and normal interferent AA (by around 110 mV). This depended on the extraordinary electrocatalytic oxidation of DA noticed. SPEs showed LoD worth of 0.65 μ M. It is found that the collaboration between supporting terminal and 2D-hBN assumes a huge part in how well 2D-hBN changed cathodes answer. Modification made with 324 ng of 2D-hBN

upgrades the electrochemical reaction, bringing down the DA's electrochemical oxidation V by around 90 mV. Then again, when contrasted with a cathode that hadn't been changed, a GC electrode that had been treated with 320 ng of 2D-hBN had an 80 mV higher oxidation potential for DA [40].

An exceptionally sensitive electrochemical sensor for the recognition of DA in light of a blend of graphene quantum dots and multiwalled carbon nanotubes (GQDs-MWCNTs) was made by Huang et al. GQDs, which are carbon nanomaterials, have a large surface area, which helps the electrodes' conductivity. As expected, the sensor shows great dopamine selectivity among contending bio-analytes. This electrochemical sensor performed at its most elevated level for DA estimation under ideal conditions, showing great linearity all through a wide straight scope of 0.005-100 μM and LoD of 0.86 μM (3S/N). CVs were acquired to look at the electrochemical reactions of different electrodes. As opposed to GCE and MWCNTs/GCE, the redox peak at last increased at a good observable point. When contrasted with the GQDs/GCE and the exposed GCE, the anodic pinnacle current of the DA at the created cathode was roughly 5.01 and 17.82 times more prominent, respectively [41].

A fruitful 2D-hBN changed SPEs with EDA was made by Yang and collaborators utilizing the fundamental CV methodology, and deciding DA and UA in their blend with responsiveness and precision was then utilized. The electrochemical reaction of DA was additionally worked on by Expert pretreatment. This changed terminal fundamentally expanded the powerful use of CNTs. These elements, for example, the simple creation process, comparing electrocatalytic movement and high CNT accessibility, make the SWCNTs cluster GCE a powerful scientific device with various possibilities involved in sensors.

Yang et al. delivered graphene-adjusted electrodes (GME) for the electrode potentials DA. Through CV and EIS spectra, productive electrocatalytic movement was noticed. Qin et al.

manufactured Polyvinylpyrrolidone (PVP)/graphene changed GCE. An increment of the current sign was noticed when contrasted with bare GCE, showing that PVP/GR/GCE showed good electrocatalytic action e-1 exchange energy towards the DA oxidation. Also, PVP/GR/GCE exhibited solid concealment of the foundation current from a huge overabundance of ascorbic acid. The planned sensor exhibited a wide direct scope of 5×10^{-10} to 1.13×10^{-3} mol/L DA with LoD of 0.21 μ M. Dopamine assurance in human serum and pee tests was investigated [42].

Arroquia. et al. manufactured screen-printed C-electrode adjusted with Au nanoparticles and AuNP/SPCE sensor came about the limit of detection (LoD) and expanded responsiveness towards DA and riboflavin identification in contrast with exposed SPCE [43].

The beat laser removal technique was utilized by Fazio et al. to effectively make molybdenum oxide nanoparticles (MoOx NPs) in water. Artificially and morphologically stable MoOx colloidal nanoparticles were made conceivable by picosecond beats to make the SPCE change. When used to recognize dopamine in PBS (pH = 7) arrangement, (MoOx NPs/SPCE) shows improved electro-reactant execution. With a LoD of 43 nM and a focus scope of 0.1-600 μ M, the peak current of DA rose under ideal circumstances. They were a practical competitor for the detection of DA [44].

Elham et al. did an electrodeposition of Cu/Cu₂O on the PGE surface in a cell containing Cu²⁺ particles and investigated it for DA identification [45]. Nemah and collaborators utilized CV and DPV to identify the presence of DA within sight of other natural, synthetic substances in [46] MIP anodes distinguished by DA with high selectivity, even with obstructions. Studies are being done to investigate altered PGEs for electrochemical detection. Alterations of PGE should be made possible using various strategies. Because of their astounding biocompatibility and conductance, valuable metal materials have increasingly become involved in

electrochemical detection. Pt-based materials have been referenced more. Unadulterated Pt nanoparticles, nonetheless, continue to display various difficult disadvantages, including significant expense, easy agglomeration, and restricted shelf life. Two systems have been explored to expand the synergist proficiency and decline the number of important metals: the first includes controlling the structure, size, and design; the other includes doping. Ag nanoparticles are encouraged to be alloyed with Pt. Li and colleagues fostered a DA sensor that was Pt Ag/WS₂/GCE. WS₂ and dandelion-like Pt Ag NCs were integrated to create a sensor [46]. Zhao et al. fostered an environmentally agreeable, simple, watery arrangement technique used to straightforwardly make Pt Ru ultrafine wavy nanowires. In the first place, they brought Pt Ru nanowires into electrochemical biosensors and found that the Pt₇Ru₃ nanowires have fantastic action to DA with quick reaction and ultralow LoD at 0.3 V in 0.1 M PBS [47].

Li et al. changed DNA aptamers on a multiple-parallel-connected (MPC) silicon nanowire to make a DA nano electronic biosensor. FETs measure nanofabricated semiconductor current. Aptamer restricting controlled the current. This biosensor's linear working reach and LoD were 0.01-10 nM and <10 pM. It recognized dopamine from AA, epinephrine, tyrosine, and norepinephrine. Ongoing DA observing from dynamic PC12 cells with hypoxic excitement was additionally finished with this MPC aptamer/SiNW-FET [48].

An electrochemical (MPC) silicon nanowire field-effect transistor (FET) for estimating DA was portrayed by Zhao et al. It utilized GCE, which is made with a nanocomposite of MWCNTs, block copolymers, and GO. Since DA is an electroactive species, DPV quickly recognized it. The made anode effectively recognized DA in examples of human blood serum with LoD of 42 nM. Hira et al., as of late, revealed the improvement of a minimal-expense MIP biosensor for the discovery and evaluation of DA. FTIR and XRD were utilized to break down the material. EIS and CV were utilized to break down the properties of the proposed sensor.

For the electrochemical recognition of DA, it showed a wide linear slope of 10-110 μM and a LoD of 0.3 μM .

By changing nanocomposites of phytic acid/graphene oxide (PA/GO) on a GCE, a DA electrochemical sensor was made. Ultrasonication was utilized to create GO, which has been functionalized with Dad. Nanocomposites were then drop-cast onto shiny GCE. IR spectroscopy was utilized to affirm the attributes of the PA/GO-adjusted GCE. DPV was utilized to track down unmistakable DA fixations using the proposed electrochemical sensor. The arranged sensor was believed to be very delicate to DA at fixations somewhere in the range of 0.05 and 10 μM . What's more, within the interferent phenomenon of AA and UA, the cathode showed an amazing electrochemical response toward DA. The developed electrochemical DA sensor was utilized effectively to distinguish DA in human pee tests that had been spiked with dopamine hydrochloride injection [49].

Because of the consolidated impact of the materials that comprise composite materials, which makes it more straightforward to involve them in new applications, composite materials have drawn in a lot of interest. Silva et al. delivered and immobilized a mixture framework for the location of the DA, which was viewed as the PGE/NiTsPc-ZnONPs-CNT. CA and DPV were utilized to discover the furthest reach of DA, which was still up in the air at 23 nM and 6.9 nM, separately. Furthermore, the effect of specific potential DA interferents on DA reaction was surveyed. These were AA, uric acid, and serotonin. The DA electrochemical reaction was not altogether modified by their presence [50].

A Ni-MOF changed terminal was made for DA detecting by Huang et al. SEM, XRD, TGA, and attenuated total reflection FTIR were utilized to assess the Ni-MOF's shape and structure. Electrochemical responses of the anode to DA were estimated utilizing DPV. Ionic fluid with a direct reach (0.2-100 $\mu\text{mol. L}^{-1}$) and LoD (60 nmol. L⁻¹) expanded the detecting capacity of

the charged cathode. The overhauled cathode showed selectivity to DA in complicated mixtures and highly stable and reproducibility [51].

2D transition metal dichalcogenide nanosheets are acquiring fame in electrochemical detection. Huang et al. made MoS₂-polyaniline (PANI) composites with graphene-like properties utilizing a natural aqueous methodology and a simple in situ polymerization process. An exceptionally open, 2D conductive surface area of redox-dynamic PANI was upheld by MoS₂ and offered an immediate way for electrons. Following this, an electrochemical sensor in light of MoS₂-PANI composites and a GCE changed with gold nanoparticles (AuNPs) was made to gauge dopamine (AuNPs/MoS₂-PANI/GCE). It exhibited higher electrocatalytic movement. With LoD of 0.1 μM (S/N = 3), it exhibited better electrocatalytic oxidation of dopamine in the direct scope of 1 to 500 μM. The made electrochemical sensor was successfully used to recognize DA in an example of human pee, exhibiting its flexibility as a detecting gadget in genuine examples [52].

Ponnada et al. made a straightforward, minimal-cost nanocomposite material that looks like a flower, Ag-Cu brightened ZnO nanoflower-like composite with a vast dynamic surface region. FTIR and XRD were utilized to break down the created Ag@ZnO, and Cu@ZnO improved ZnO. The electrochemical action of composite material showed promising outcomes with a recognition breaking point of 0.21 mM and a high responsiveness use (DPV). The dopamine sensor exhibited security and reproducibility when tried at different pH levels. At last, ongoing observation of tests utilizing the developed sensor created great outcomes. The outcomes showed that the sensor, as pre-arranged, exhibited a huge commitment to recognizing dopamine in real sample analysis [53].

An alternative CV methodology electrochemically enacted a GCE to make an AGCE. Dopamine (DA) electrochemical measures were enhanced utilizing AGCE. The AGCE's electrochemical way of behaving was inspected utilizing CV. The new AGCE increments 4-NP

and DA redox top flows contrasted with the uncovered GCE. OxSFGs, which advance electron transport and electrocatalytic movement of the AGCE, are framed during the enactment stage. States of the AGCE's voltammetric reactions to 4-NP and DA were tuned. The AGCE detecting stage's insightful presentation was inspected utilizing differential pulse voltammetry (DPV). With a lower LoD of 0.01 μM ($S/N = 3$), the AGCE showed direct reactions to DA from 0.02-1.0 and 1.0-100 μM . The AGCE-based DA sensors additionally have incredible responsiveness, selectivity, and repeatability. In genuine examples, the sensors recognized DA with great recuperation [54].

This study inspected the electrochemical polymerization of pyrrole-3-carboxylic acid on electrochemically over-oxidized PGE (p(P3CA)/EOPGE) for DA location. CV observations showed that EOPGE would be wiser to electron transport than PGE. p(P3CA's) ionized carboxyl groups bound emphatically charged DP. p(P3CA)/EOPGE synergistically oxidized DP by means of electrochemical oxidation. By delivering anodes under various circumstances, the voltammetric response was assessed. Recognizing the DA oxidation potential from AA and UA showed exceptional selectivity for DOP. Between 0.025 μM and 7.5 μM , p(P3CA)/EOPGE yielded a 0.0025 μM identification limit. p(P3CA)/EOPGE effectively recognized DA [55].

Palanisamy et al. showed the sonochemical creation of a CuS Nano plate-improved rGO nanocomposite. CuS and GO antecedents were shower sonicated at 80°C for an hour to make the PrGO-CuS nanocomposite. The powerful creation of CuS nanoplates and nanosheets was approved by the outcome's portrayal (FTIR, XRD, SEM, and Raman spectroscopy). The PrGO-CuS nano-composite, as it was made, was likewise utilized for the electrochemical sensing of the DA. The electro-logical information acquired showed that the electrochemical action towards DA of PrGO-CuS nanocomposite is better than that of perfect composite. The

made biosensor shows a diminished LoD (0.022 μM) and a more extensive straight reach (0.1-155.1 μM) [56].

Hayder et al. presented a technique for the production of AGCE-based DA sensors that display noteworthy electrocatalytic capacities. The galvanic replacement of Cu with Ag prompted the development of bimetallic nanostructures, while the format electrodeposition technique was utilized to make Cu nanostructures. Electroanalysis of DA was utilized as a model analyte to represent the action. The sensor had a LoD of 26 nM and adequate recuperation in examinations performed on genuine examples. Taking everything into account, the work uncovered a simple procedure for the creation of bimetallic nano electrocatalysts for minimal price [57].

An electrochemical DA sensor had been concocted and created by Uppachai et al., and it depended on the joining of surfactants with Au nanoparticles. This introduced forward biosensor showed a rapid reaction to DA over a wide direct reach from 0.02 to 1 μM . Because of these better scientific reaction properties, the nanocomposite changed GCE was a promising material for the making of a reasonable and strong electrochemical DA sensor supramolecular [58].

Balu et al. manufactured a simple to make SnS_2 nanorod-finished graphene-cyclodextrin ($\text{SnS}_2/\text{GR}-\beta\text{-Disc}$) nanocomposite. It was inventive DA biosensors. GCE was utilized to fabricate the DA bio-sensor Blend, which has been completed using aqueous and Sono chemical processes. Different physicochemical methods were utilized to check the development of the nanocomposite. The CV reaction of DA was a component of five more prominent than those seen at unmodified GCEs, Disc-changed GCEs, SnS_2 -adjusted GCEs, and GR-altered GCEs. The biosensor's DPV current is direct to DA from 0.01-150.76 μM under ideal conditions. At the point when UA and AA were available as normal meddling species, the SnS_2/GR -Album biosensor showed great selectivity toward DA. The nanocomposite-changed

terminal additionally exhibited OK sound over the long-time span, sensitivity ($2.49 \text{ AM}^{-1} \text{ cm}^{-2}$), and reproducibility for DA identification. Human blood serum and rodent cerebrum tests were effectively used to recognize DA utilizing the developed $\text{SnS}_2/\text{GR}-\beta\text{-Cd}$ biosensor [59].

Sundar et al. planned a straightforward, one-step green interaction that utilizes saponin-rich *Sapindus mukorossi* fruit extract (SMFE) to make copper oxide (CuO) nanowires. The physio-synthetic properties of CuO nanowires have been concentrated on utilizing DPV. CuO nanowires made with SMFE have additionally been utilized as DA sensors, and their electrocatalytic movement has been investigated. It showed an amazing electrochemical reaction with worked on current reaction because of their extraordinary qualities and directly recognizes the DA over $0.2 \text{ }\mu\text{M}$ to 0.105 mM of DA. The acquired outcomes exhibited that the delivered CuO nanowires can undoubtedly advance the electron move between the adjusted anode and DA. CuO nanowires are an extraordinary sensor for DA in light of their uncommon electrocatalytic capacity. Additionally, AA, UA, and other interfering species do not interfere with the sensor. Moreover, interferent results showed that CuO nanowires and GCE may be utilized more accurately and efficiently in sensing DA in real samples [60].

Chapter 3

3 Synthesis

3.1 Materials and reagents

Dopamine, Phthalimide, Ammonium molybdate, Urea, Copper acetate, Methanol, Hydrochloric acid, Sodium Hydroxide, Sulfuric acid, Thiourea, Sodium molybdate, Ethanol, Acetone Deionized water.

3.2 Synthesis of CuPc

CuPc was synthesized with already reported work [61]. The given quantities of the following compounds were taken as phthalimide (0.85 g), ammonium molybdate (0.12 g), urea (0.65 g), and copper acetate (0.18 g) was mixed well into a mortar and further ground to get a uniform mixture. Then, the whole mixture was heated at 200°C for 25 min and then cooled at room temperature to 25 °C. The residue was then washed with methanol (CH₃OH) to give the dark green crude product. The required solid was further treated under 2% Hydrochloric acid (HCl aq.) and 2% Sodium hydroxide (NaOH aq.) in a respective way and then filtered after stirring for the time of 20 min. The crude product was then get dissolved in 20 mL concentrated Sulfuric acid (H₂SO₄ aq.) and diluted with 300 mL DI water. Finally, after crystallization and suction filtration, we obtained pure CuPc and washed it with DI water until it was neutral. Then, we dried it in an oven at 50°C overnight (as shown in Figure 23).

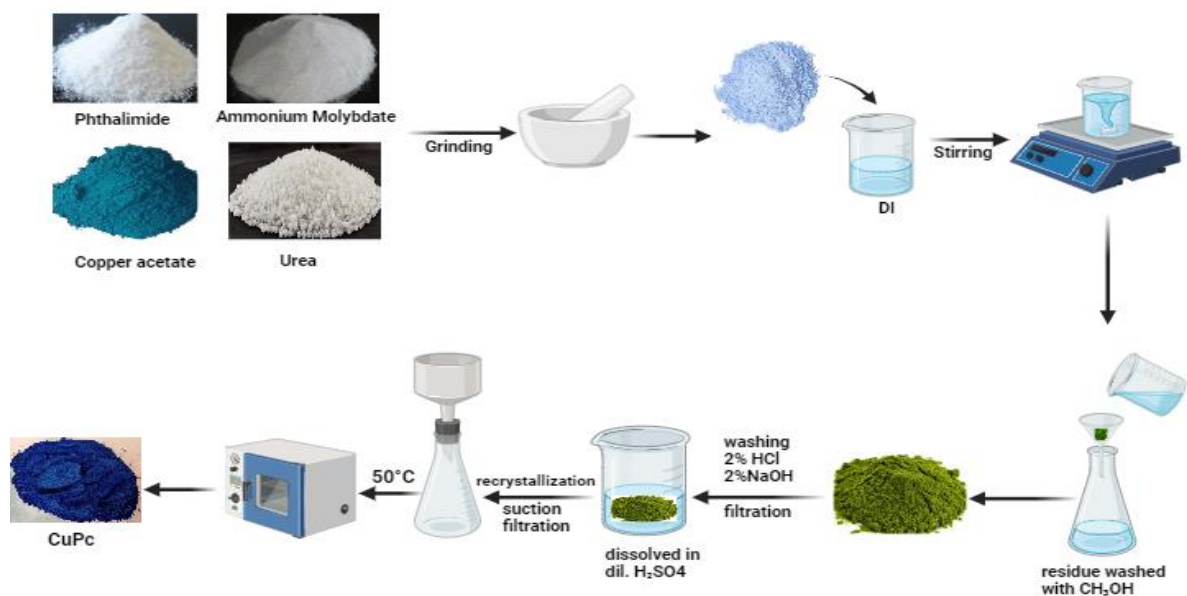


Figure 23: Synthesis scheme of copper phthalocyanine.

3.3 Synthesis of MoS₂

The synthesis of MoS₂ was performed by already reported literature [62]. The hydrothermal method was used to synthesize MoS₂. Thiourea (3.044g) and sodium molybdate (2.419) were dissolved in 70 ml of water and put in a 100 ml stainless steel autoclave. It is then put for 24 h at a temperature of 220° C in a heating oven. The obtained black precipitates were then washed with DI water and then with ethanol and further dried for 24 h at a temperature of 80° C in a vacuum oven. The obtained product was black in color and stored for further use (as shown in Figure 24).

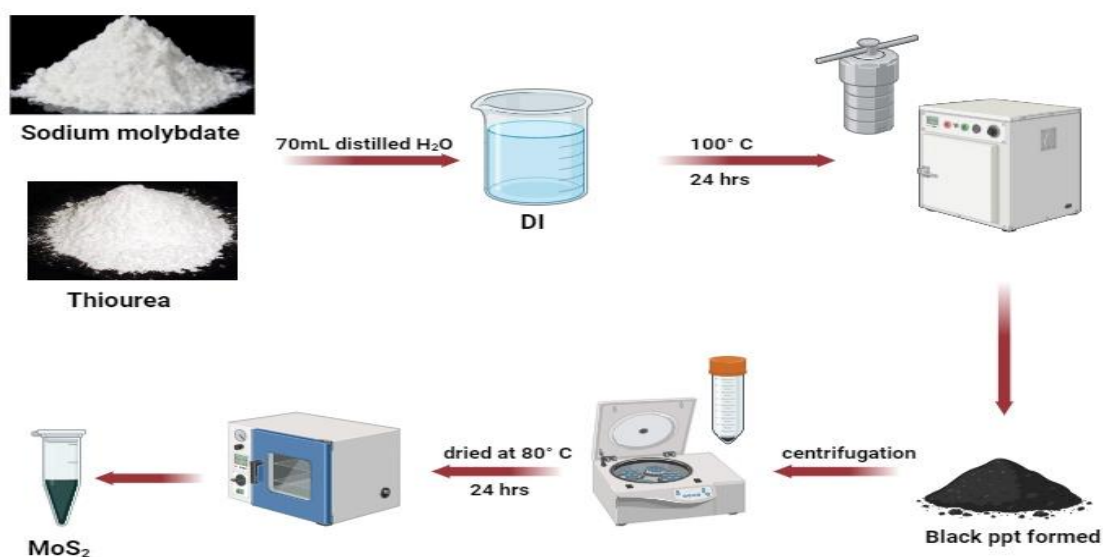


Figure 24: Synthesis scheme of molybdenum disulfide.

3.4 Synthesis of CuPc/ MoS_2 composites

In the present work, the composite of CuPc and MoS_2 was successfully synthesized. Three different composites of different ratios, 1:0.5, 1:1, and 1:2, were synthesized. The amount of MoS_2 was kept constant, and the amount of CuPc was changed according to the specific ratios mentioned above. For the synthesis of all of the composite ratios, quantities of both compounds were taken and dissolved in 10ml DMF. The mixture was mixed well and sonicated for around 30 minutes and then centrifuged for around 40 minutes. The mixture was treated with 20ml ethanol and sonicated for 30 minutes. Then, it was centrifuged at 9000rpm, and finally, the sample was dried at 60°C . Three different ratios of 1:0.5, 1:1, and 1:2 were synthesized. A colored powdered composite of CuPc/ MoS_2 was synthesized (as shown in Figure 25)

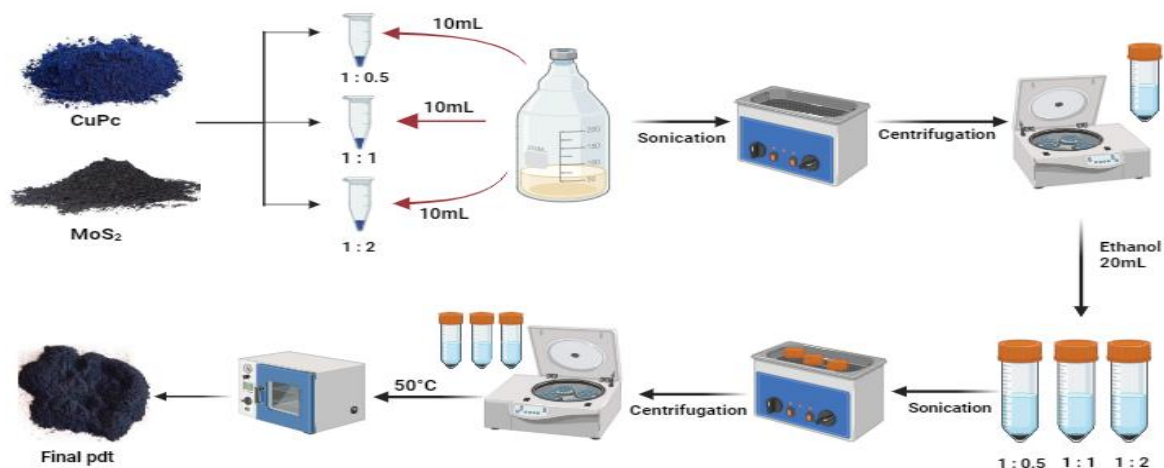


Figure 25: Synthesis schemes of different composites of MoS₂/CuPc.

3.5 Slurry formation and deposition on GCE

For the synthesis of slurry, 2 mg of each composite was taken, dissolved in 0.5 ml DMF, and sonicated for 30 minutes. The slurry of each composite ratio 1:0.5, 1:1, and 1:2 was synthesized. A glassy carbon electrode (GCE) was taken as the working electrode. The GCE surface was polished with a polishing kit with alumina slurry. Then GCE was sonicated in acetone, then in water, and in the last again in acetone. The 8 μ L of slurry was deposited on the surface of GCE. The slurry was dried overnight for equal and homogenous deposition of a layer of composite. It was further tested for electrochemical studies (as shown in Figure 26).

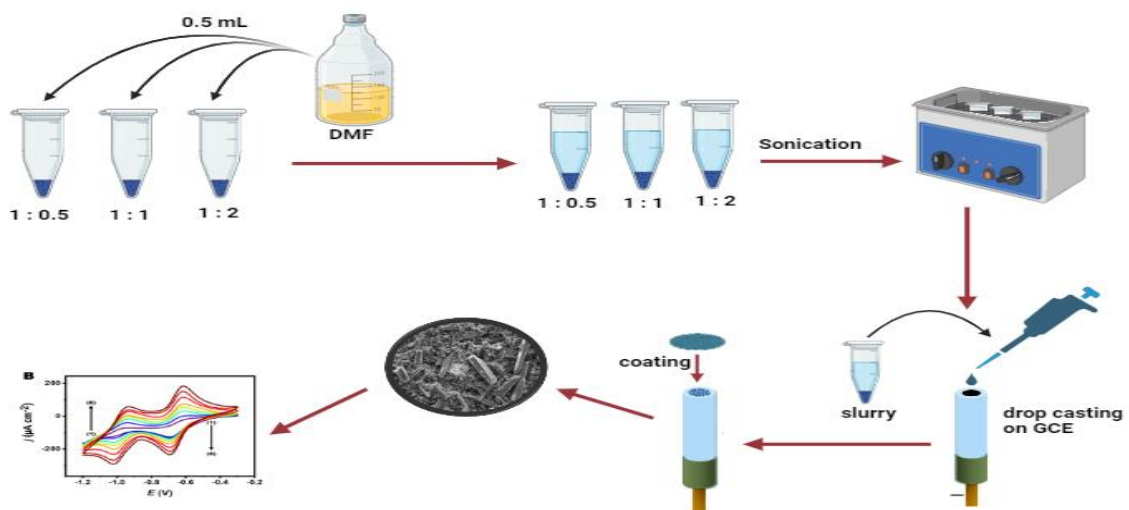


Figure 26: Synthesis schemes of composite of MoS₂/CuPc.

Chapter 4

4 Results and discussion

4.1 Structural and morphological studies

4.1.1 XRD

X-ray diffraction (Figure 27) was performed with two prominent peaks of copper phthalocyanine were observed at $2\theta = 6.87^\circ$ and $2\theta = 8.94^\circ$. These two peaks show the intensity of 100% and 81%, respectively, and planes (-101) and (101), respectively. The other peaks observed at 13.93° had planes (200), and at 17.93° the planes were (103). The values of peaks were matched with the literature reported [63].

X-ray diffraction peaks were observed for MoS_2 as well. The prominent peaks were shown at 13.97° , 32.5° , and 57.5° with the planes (002), (100), and (110), respectively. These are also matched with the reported literature [62].

Then, the peaks of composites of Copper Phthalocyanine and MoS_2 were matched with the peaks of pristine substances. We can see that as the ratio of CuPc is being increased, the peak intensity of the composite is increasing at 6.87° and 8.94° prominently. In the same way, the prominent peaks of MoS_2 are becoming less intense as the CuPc concentration increases.

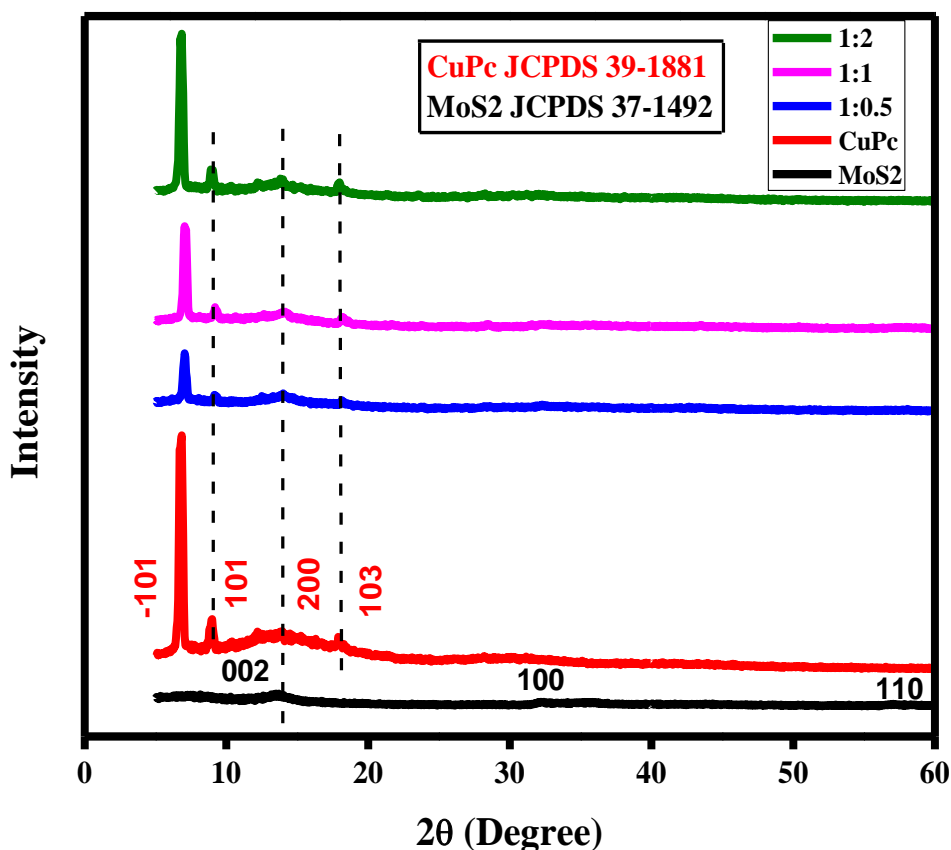


Figure 27: XRD analysis of CuPc, MoS₂ and composites.

4.1.2 Raman spectroscopy

Figure 28 shows the Raman peaks of both pristine compounds and composites. The prominent band at 592 cm⁻¹ was considered due to the macro-cycle ring of CuPc. The band peak at 679 cm⁻¹ is assigned to C–N–C and N–C–C bending vibration. The peak value at 1141cm⁻¹ was assigned to pyrrole breathing vibrational mode, 1332cm⁻¹ was assigned to C-N stretching vibration, and 1518 cm⁻¹ was assigned to isoindole mode. The peak value at 1446 cm⁻¹ could be attributed to C_β–C_β, C_β–C_γ–H and C_α–N_β, N_α–C_α–C_β, C–C–H [61].

Raman analysis of MoS₂ shows two in-plane vibrational modes at peak positions of 281 and 378 cm⁻¹ corresponding to the E_{1g} and E_{2g} modes of the bulk 2H- MoS₂ crystal, respectively.

The peak at 467 cm^{-1} is due to a second-order $2\times\text{LA(M)}$ scattering process. According to the literature, normal Raman peaks of MoS_2 appeared at about 380 and 408 cm^{-1} . The peak at 408 cm^{-1} is not observed in the spectra, and it may be due to the lower annealed temperature. If the laser power was very large and focused on the samples for a long time, the MoS_2 would be partially oxidized, and a peak of about 380 cm^{-1} might appear [64].

Raman peaks of both composites show that in 1:0.5, prominent peaks are of MoS_2 , which is double the amount. As the ratio of CuPc is increased up to 1:1, the peak intensity is decreased that appeared in the case of 1:0.5. In the case of 1:2, the prominent peaks of CuPc and MoS_2 peaks were diminished as CuPc is doubled to MoS_2 .

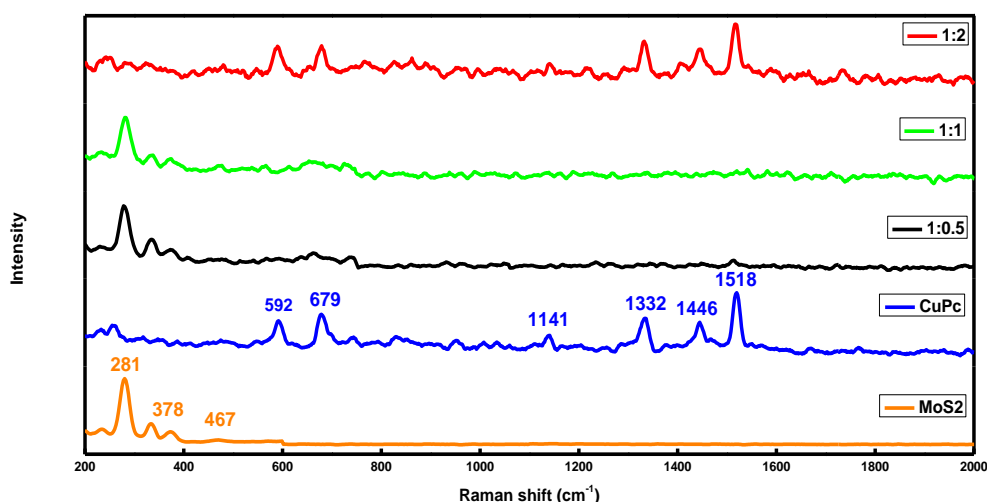


Figure 28: Raman analysis of CuPc, MoS_2 and composites.

4.1.3 FTIR analysis

FTIR (Figure 29) peaks of both the pristine and composites were shown in the graph. In the case of the CuPc band at 3435 cm^{-1} , it could be attributed to free group N-H stretching. The second prominent peak at 1620 cm^{-1} can be due to C=N stretching. The other peaks present at 1334 cm^{-1} could be by C-H bending and, at 3034 cm^{-1} , can be due to C-H stretching [61].

In the case of MoS₂, prominent peaks at 3424cm⁻¹ and 1631cm⁻¹ can be due to -OH functionalities absorbed on the surface of MoS₂. A characteristic vibrational mode at 455 cm⁻¹ is found and can be assigned to the Mo-S linkage of MoS₂. The other peaks at 595cm⁻¹, 907cm⁻¹ and 1401cm⁻¹ can assigned to the structure of MoS₂ [65].

In the comparative study of composites, in the ratio 1:0.5, MoS₂ is doubled to CuPc, and it contains more -OH functionalities attached to it, thus having more intense peaks than other composites. In a 1:2 composite, CuPc is doubled to MoS₂. As -OH functionalities decrease, peaks are less intense than 1:0.5. Moreover, -NH stretching peaks are less intense than -OH peaks. So, as the concentration of CuPc increases, the peaks belonging to CuPc become prominent, and peaks belonging to MoS₂ are diminished.

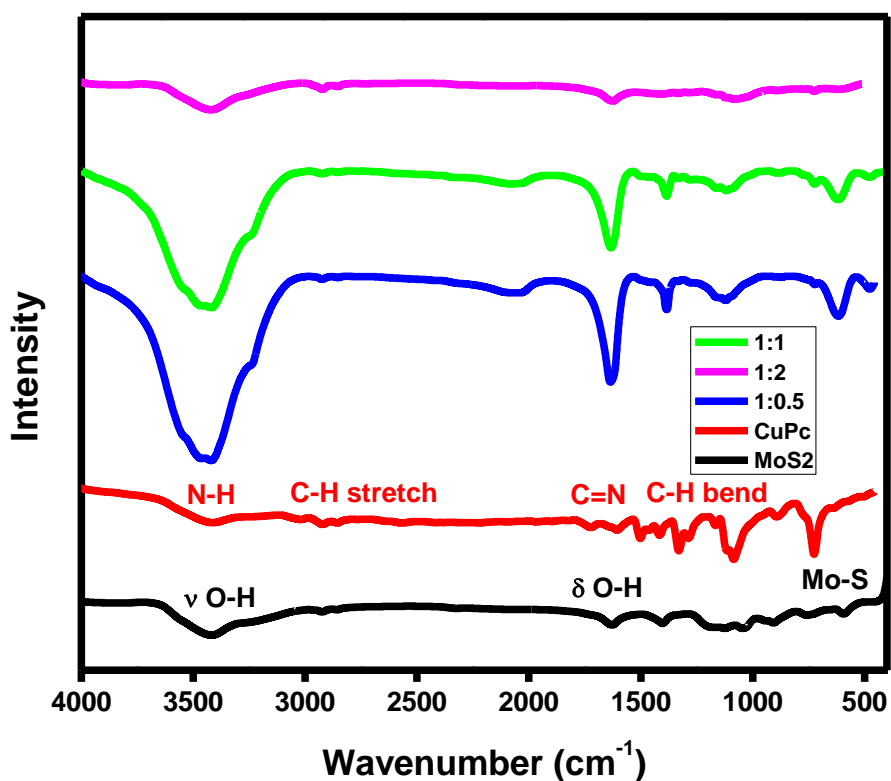


Figure 29: FTIR analysis of CuPc, MoS₂ and composites.

4.1.4 SEM-EDX

SEM images of both MoS₂, CuPc (Figure 30), and composites (Figure 31) are shown in the diagram below. MoS₂ shows a flower-like shape of the compound, and CuPc gives the structure like rods. The best composite ratio of 1:0.5 was further analyzed under SEM analysis as it was best selected for electrochemical studies. SEM images showed the successful synthesis of a composite with a structure like both of the pristine compounds, such as rod-like in the case of CuPc and flower-like MoS₂.

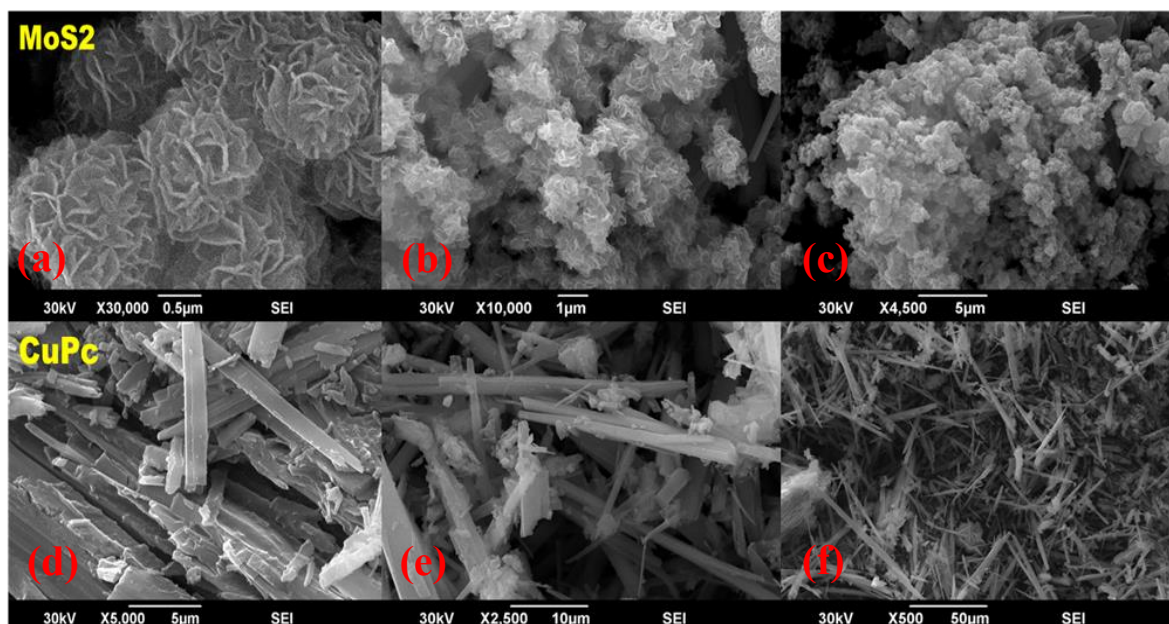


Figure 30: SEM images of MoS₂ and CuPc.

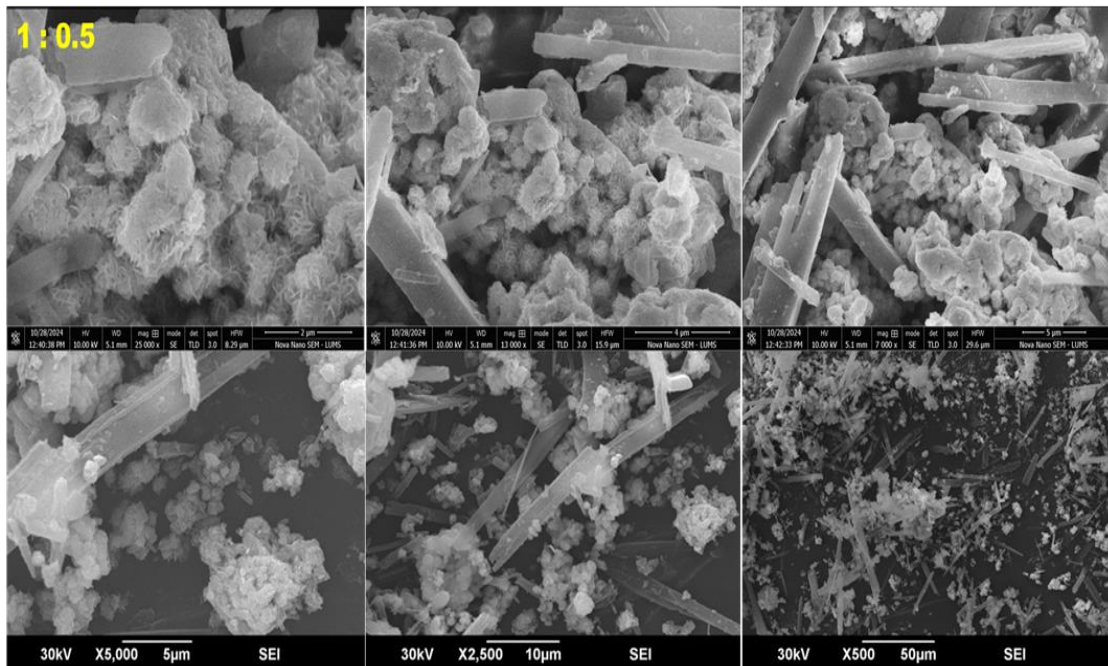


Figure 31: SEM images of composite of MoS₂/CuPc (1:0.5).

EDX (Figure 32) analysis of the best composite ratio 1:0.5 was also performed along with SEM. The % weight of different elements present in the composite are Carbon 61.01%, Mo 18.63%, Sulfur 8.78%, Copper 6.01%, and Nitrogen 5.57%.

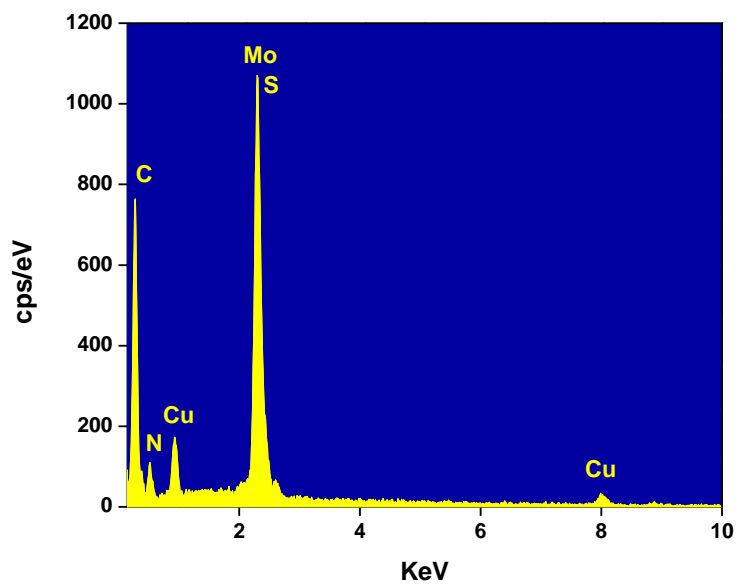


Figure 32: EDX analysis of composite of MoS₂/CuPc (1:0.5).

4.2 Electrochemical studies

4.2.1 Response towards $K_3Fe(CN)_6$

MoS₂ and CuPc were undergone in electrochemical response with electroanalytical techniques like cyclic voltammetry (CV) and electrochemical impedance spectroscopy (EIS). 5mM K₃Fe(CN)₆ with the addition of 0.1M KCl was used as a standard probe to check the electrochemical response of the pristine composites of different ratios at a 50 mv/s scan rate. The CV response shows that the best response towards electrochemical studies was given by the composite ratio 1:0.5, in which the MoS₂ is double the concentration of CuPc. The other ratios showed the reaction below the above said (can be seen in Figure 33). The Electrochemical active surface area (ECSA) was found with the help of the Randles-Sevcik equation as below:

$$I_p = 2.69e5 n^{3/2} A D^{1/2} C v^{1/2}$$

The ECSA for 1:0.5, 1:1, 1:2, MoS₂, CuPc and bare electrodes were as 0.089 cm², 0.084 cm², 0.048 cm², 0.078 cm², 0.072 cm² and 0.042 cm², respectively. The best composite ratio is 1:0.5, possessing the highest value of ECSA.

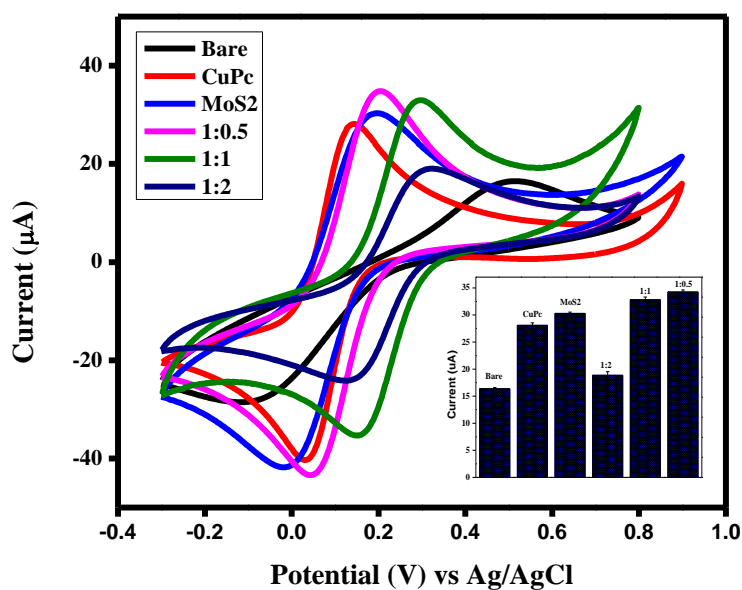


Figure 33: Electrochemical response with CV towards $K_3 Fe(CN)_6$.

EIS (Figure 34) gave the idea about the charge transfer resistance R_{ct} values for all the electrodes. The model circuit fitted was CPE with diffusion and then applied to all electrodes. The best response given in the CV by the 1:0.5 electrode also gave the R_{ct} value of 1.611 k Ω . The R_{ct} values for the 1:1, 1:2, CuPc, MoS₂, and bare ratio were 4.62k Ω , 7.31 k Ω , 12.23 k Ω , 5.17 k Ω and 49.77 k Ω , respectively. The values of R_{ct} showed that 1:0.5 is less resistive and more conductive towards electrochemical response.

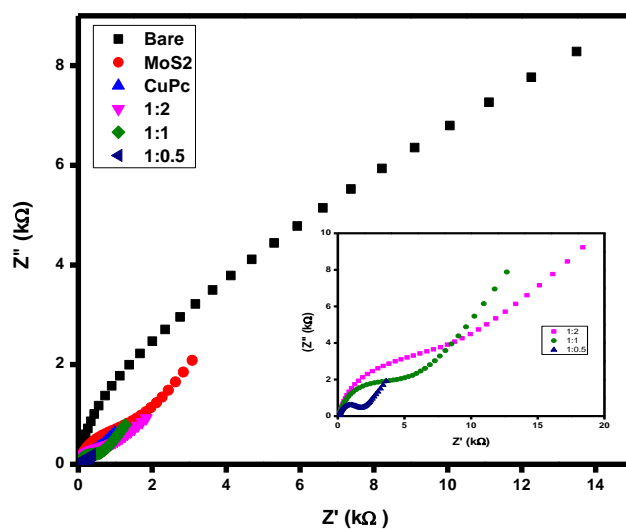


Figure 34: EIS response towards $K_3Fe(CN)_6$.

4.2.2 Optimization of pH

After selecting the best composite ratio, the best pH was chosen for further optimization and electrochemical studies. The results of cyclic voltammetry (CV) and differential pulse voltammetry (DPV) showed that the composite ratio of 1:0.5 gave electrochemical redox response at different pH values of 4,5,6, and 7 with 0.1 M Phosphate Buffer Solution. The analyte here is dopamine, which sets the molarity of the solution up to 0.5 mM for electrochemical response. The potential window was from -0.3 to 0.8 V with a scan rate of 50mv/s. The best results were shown at pH 5, both for CV and DPV. Thus, the pH5 was optimized for further electrochemical studies. The CV (Figure 35) and DPV (Figure 36) graphs, along with their linear graphs of current and voltage, are shown.

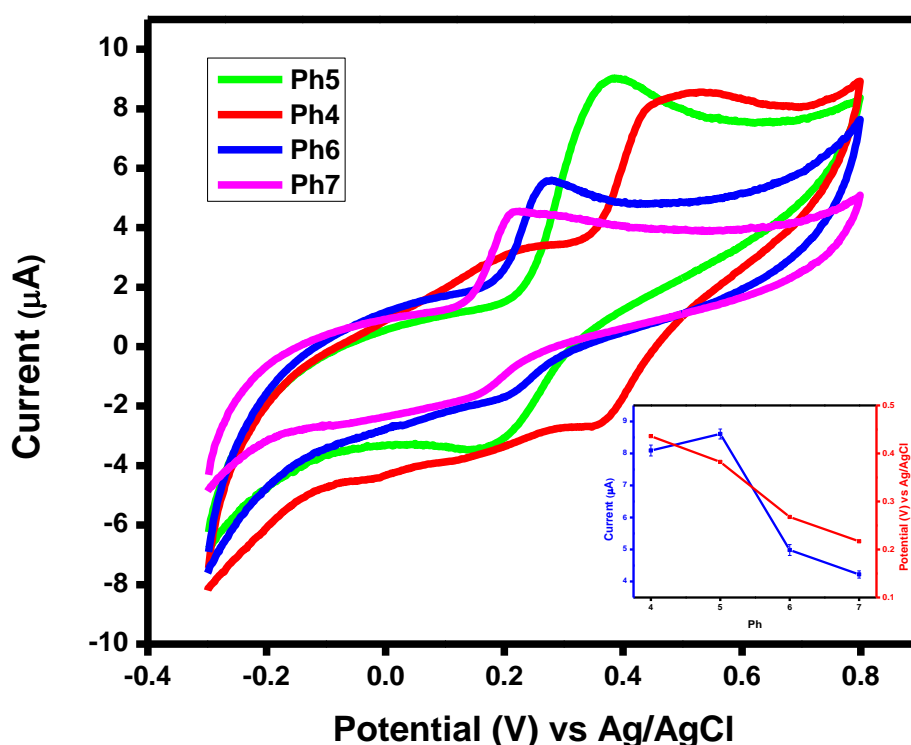


Figure 35: Different pH responses with composite MoS₂/CuPc (1:0.5) through CV.

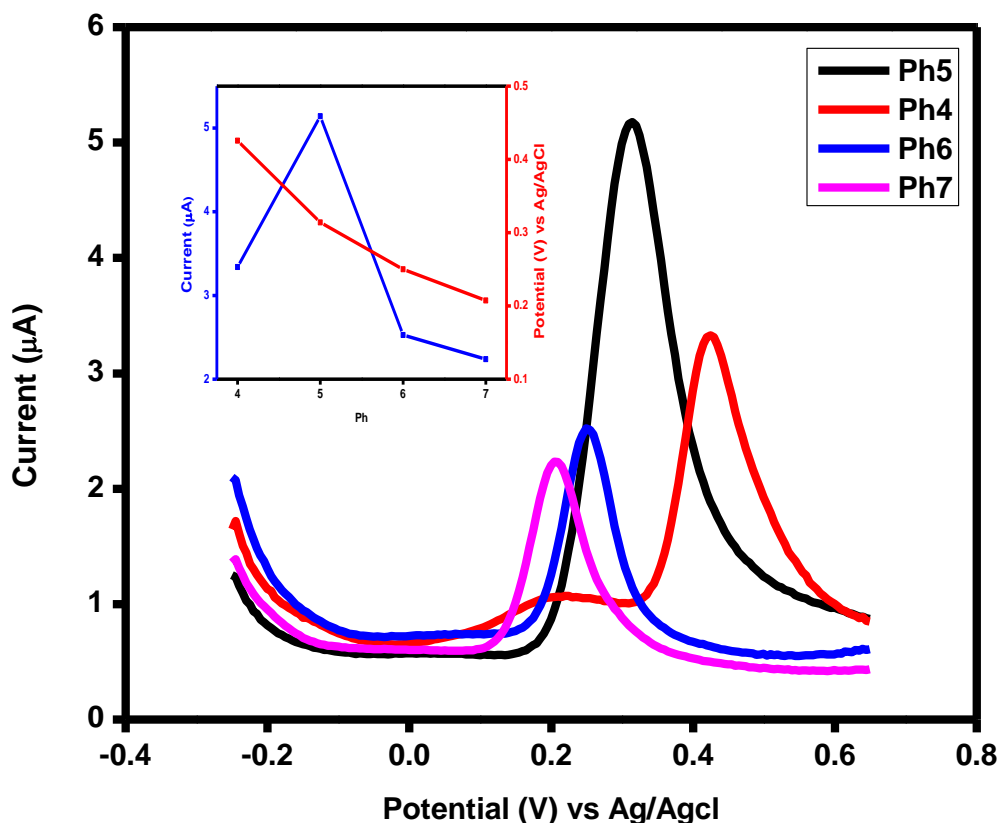


Figure 36: Different pH response for MoS₂/CuPc (1:0.5) with DPV.

4.2.3 Electrochemical response with dopamine

Under all the given conditions, 0.1 M Phosphate Buffer Solution at pH 5 with scan rate 50mv/s and dopamine concentration 0.5 mM, all the electrodes were studied for electrochemical studies. The response of CV (Figure 37) and DPV (Figure 38) were observed. We were studying the effect of receptor effect of CuPc towards MoS₂ and then further which composite is best for an electrochemical response, but accidentally, we found that the pristine MoS₂ is more favorable towards electrochemical response as compared to the best composite ratio of 1:0.5. The electrochemical studies of MoS₂ will be discussed after that.

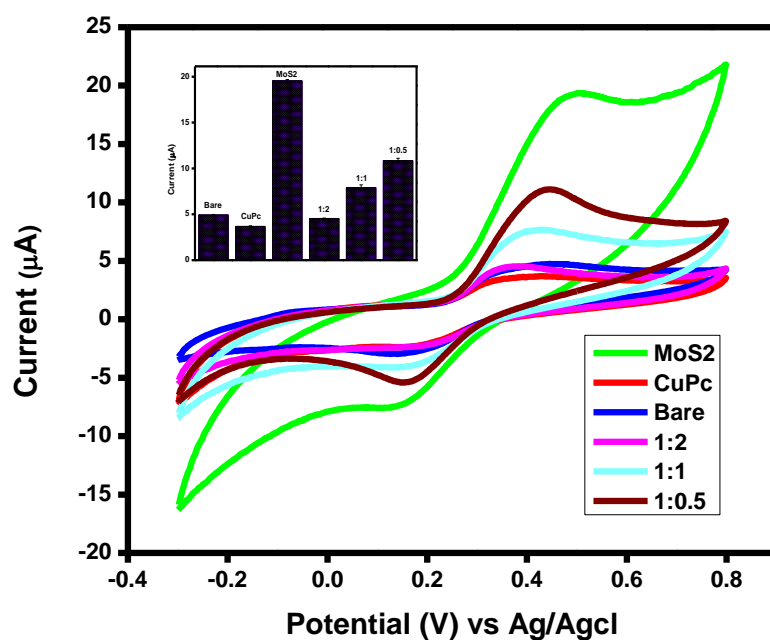


Figure 37: Electrochemical response with CV towards dopamine with all electrodes.

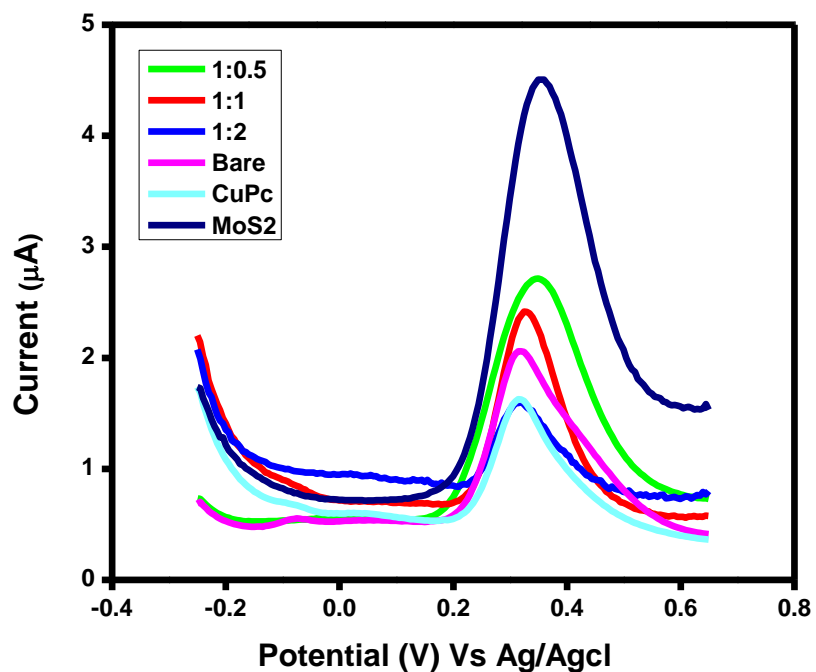


Figure 38: Electrochemical response with DPV towards dopamine with all electrodes.

4.2.4 Scan rate studies with MoS₂/CuPc (1:0.5)

The kinetic behavior of redox activity at the electrode interface was studied with the increase in scan rate (Figure 39). The anodic and cathodic current by the composite ratio 1:0.5 was investigated as the function of scan rate from 10-90 mv/s with 0.1M PBS at pH 5. Dopamine concentration was 0.5mM. By increasing the scan rate, it was observed that current is directly related to the scan rate. The linear graph with slope and regression values was also drawn. Line graphs were drawn using the current vs. square root of the scan rate to show the linear relation. In this way, we can predict that it is a diffusion-controlled process occurring here. The R² value for anodic current is 0.98, and for cathodic current is 0.99. Linear fitting of graph values close to 1 shows that it is a diffusion-controlled process.

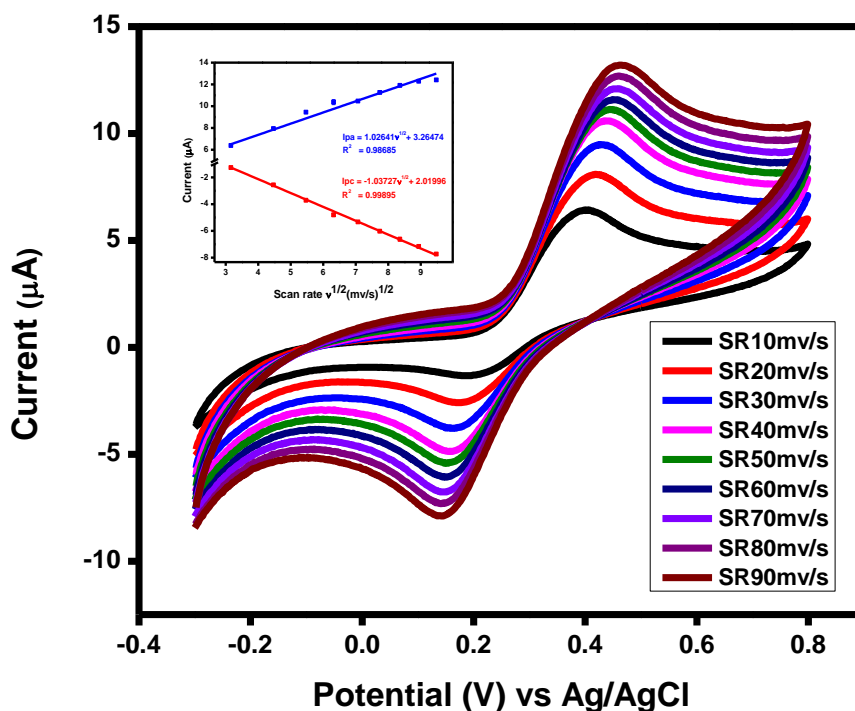


Figure 39: Effect of scan rate with CV for MoS₂/CuPc (1:0.5).

4.2.5 Concentration studies with MoS₂/CuPc (1:0.5)

The electrochemical behavior of composite material was checked against the increase of concentration with the help of CV (Figure 40) and DPV (Figure 42), as it was observed at a scan rate of 50 mV/s with pH 5 PBS. The anodic and cathodic current is enhanced with the increase in dopamine concentration. The concentration values for detecting dopamine were from 1-1000 μM and for DPV 1-800 μM . Linear ranges were obtained, and straight-line fitting gave slope values. Here, the linear range was divided into two halves. The respective values of LoD, LoQ, and sensitivity for the concentration studies with CV (Figure 41). for the linear range 1-300 μM is 4.70 μM , 15.68 μM and 0.21 $\mu\text{A } \mu\text{M}^{-1} \text{ cm}^{-2}$ and for the linear range 350-1000 μM is 11 μM , 36.6 μM and 0.091 $\mu\text{A } \mu\text{M}^{-1} \text{ cm}^{-2}$, respectively. For the DPV (Figure 43), the values of LoD, LoQ, and sensitivity with the linear range 1-200 μM is 8.21 μM , 27 μM and 0.06 $\mu\text{A } \mu\text{M}^{-1} \text{ cm}^{-2}$ and for linear range 200-800 μM is 3.13 μM , 10.45 μM and 0.19 $\mu\text{A } \mu\text{M}^{-1} \text{ cm}^{-2}$, respectively.

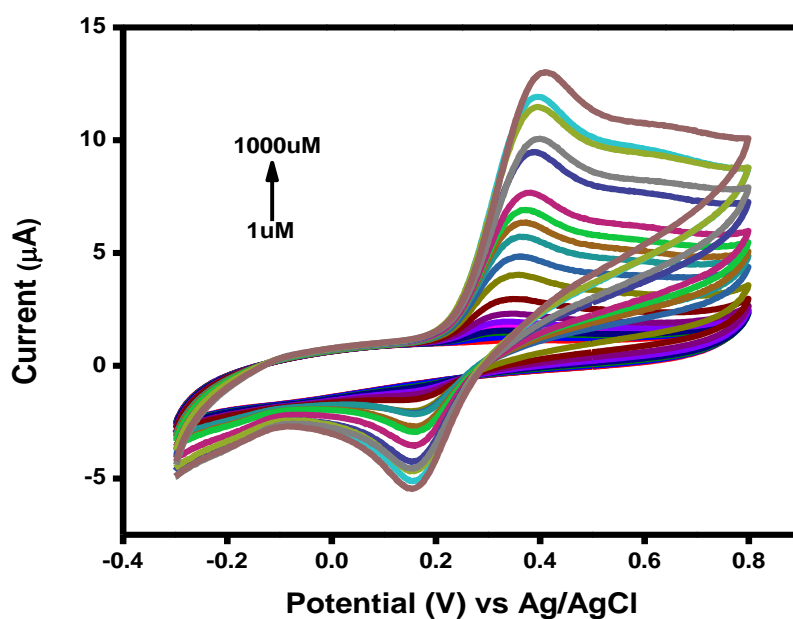


Figure 40: Effect of concentration with CV for MoS₂/CuPc (1:0.5).

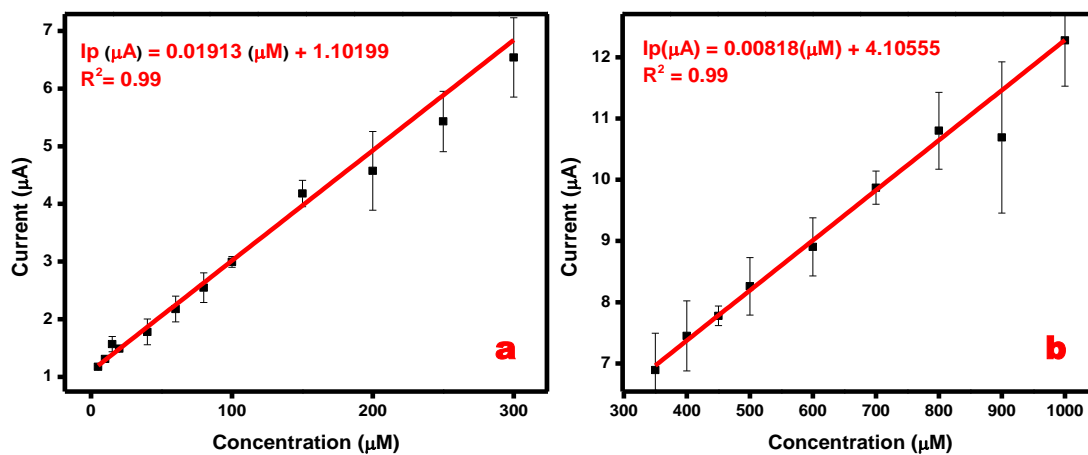


Figure 41: Linear regression curve graph through CV for MoS₂/CuPc (1:0.5) with linear range 1-300 μM (a) and 350-1000 μM (b).

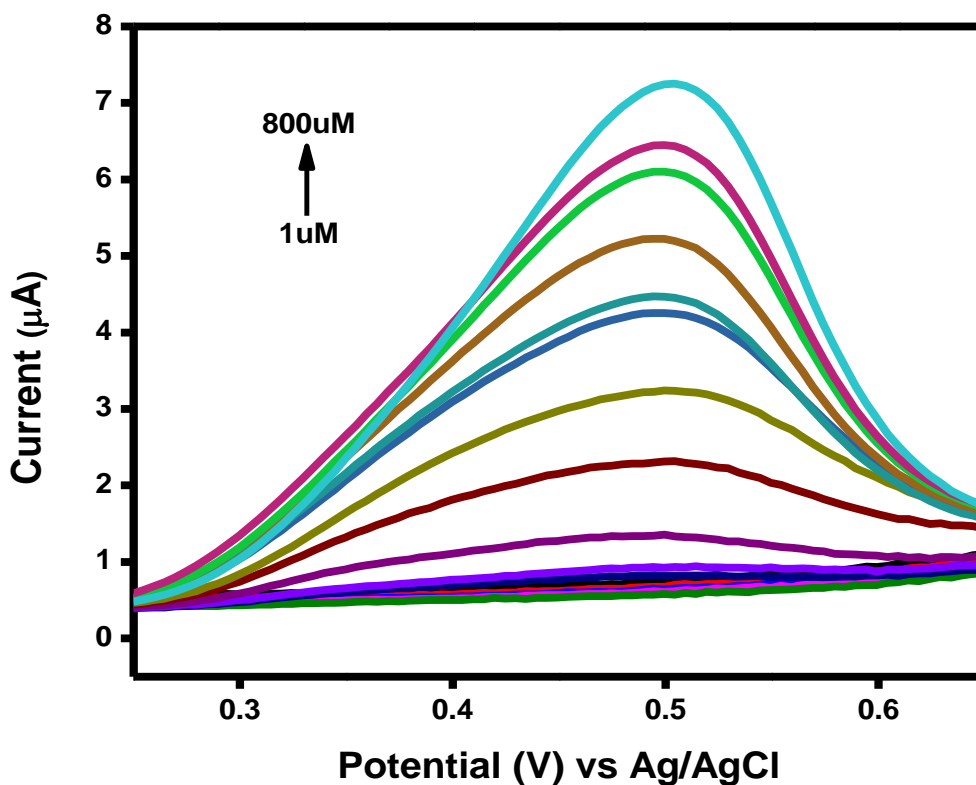


Figure 42: Effect of concentration with DPV for MoS₂/CuPc (1:0.5).

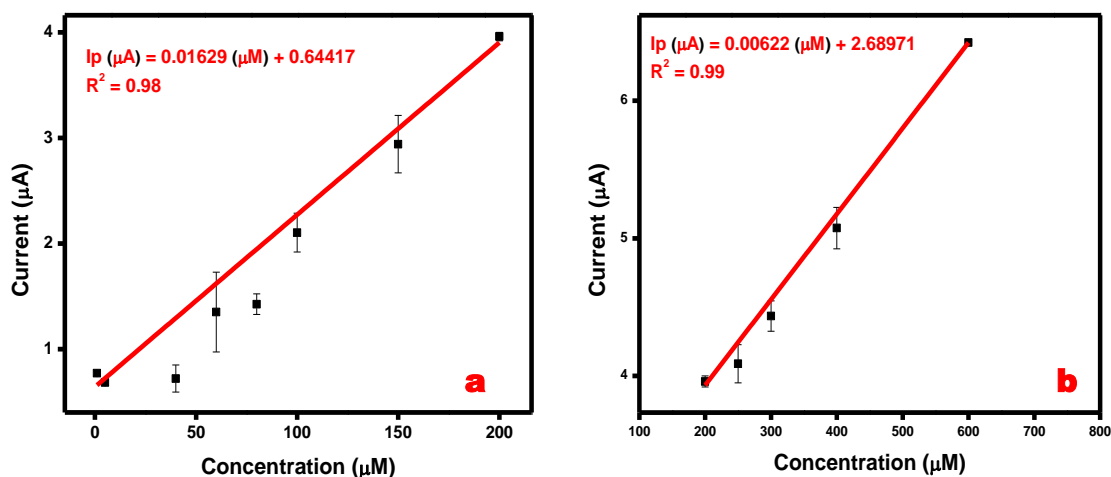


Figure 43: Linear regression curve through DPV for MoS₂/CuPc (1:0.5) with linear range 1-200 µM (a) and 200-600 µM (b).

4.2.6 Reproducibility in electrochemical response for MoS₂/CuPc (1:0.5)

Three different electrodes with the best ratio of the composite 1:0.5 were run at 50mv/s with 0.1 M PBS at pH 5 (as seen in Figure 44). The dopamine concentration was 0.5 mM, and the deposition amount was 8 µL for the best composite ratio. The electrochemical response with the CV was recorded for the three different electrodes, and it was depicted that the results obtained could be matched well. Relative standard deviation (RSD) was calculated by applying the formula. The value comes out to be 3.8 %, showing good dopamine sensing efficiency with our best composite ratio. The minor changes in response can be due to mass loading difference, evaporation time of solvent from the surface of GCE, film thickness, and electrode self-conductivity.

$$RSD = \text{Sum of standard deviation} / \text{sum of average} \times 100$$

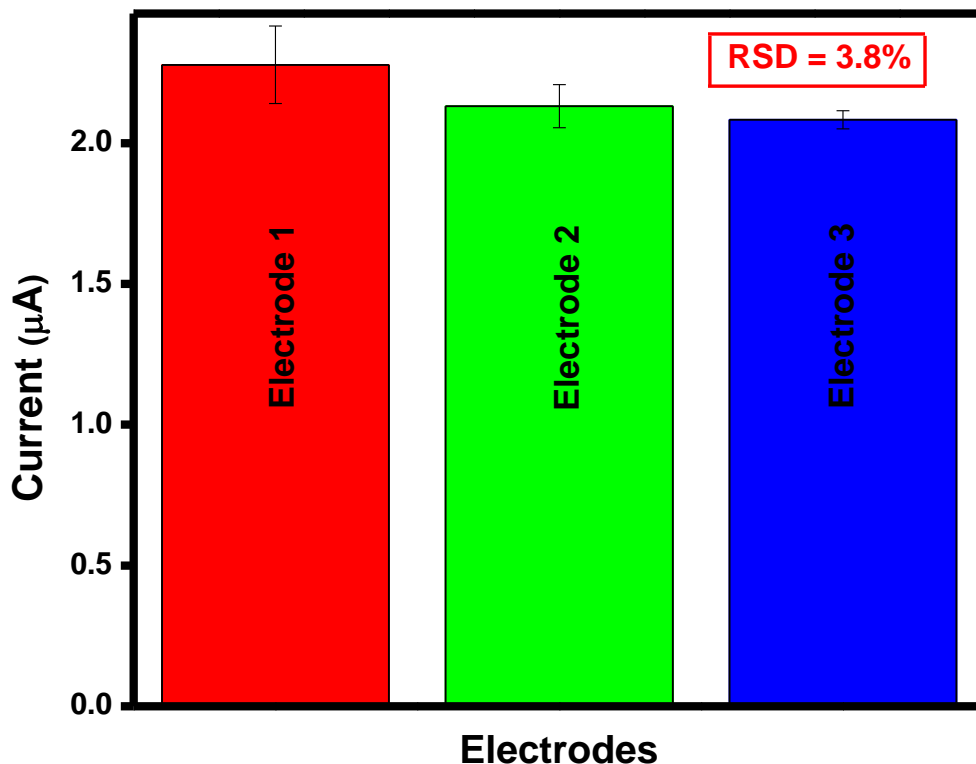


Figure 44: Electrochemical response for MoS₂/CuPc (1:0.5) with 3 different electrodes.

4.2.7 Stability studies of MoS₂/CuPc (1:0.5)

The stability of the best material chosen was checked with stability in 2 ways, either intraday or inter-day. 0.5 mM dopamine with a scan rate of 50 mv/s and 0.1 M PBS with pH 5 was checked (Figure 45). Firstly, DPV was repeated 10 times for the same material deposited, and the difference in electrochemical response was noted. The RSD value calculated was 5.35 %, which shows that the fabricated electrode can work efficiently for dopamine sensing.

The other way was to check the electrochemical response with DPV, which was performed at a difference of 4 days (Figure 46). All other conditions were the same, except the best electrode

was stored at 4° C in the refrigerator. The RSD value calculated was 5.23 %, showing an effective response toward dopamine sensing. The % loss in current was estimated as 33.1 %.

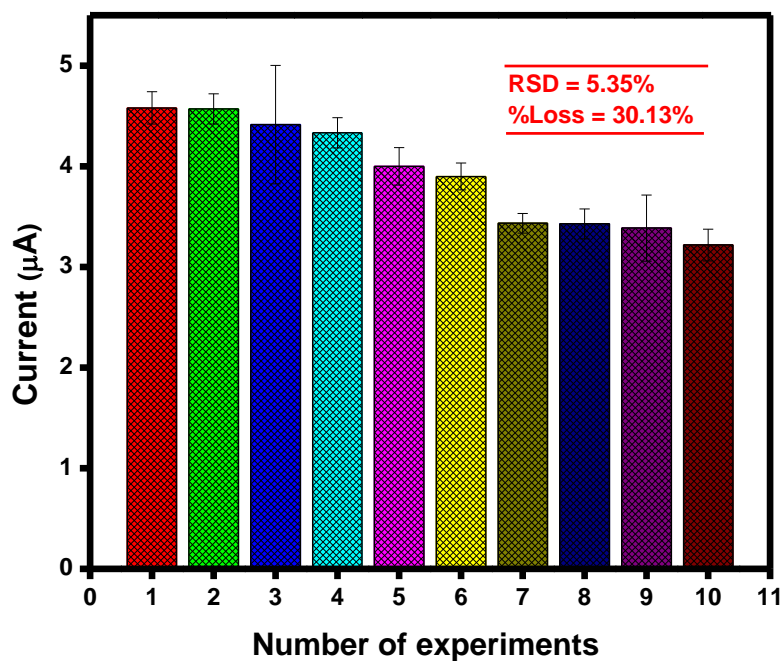


Figure 45: One day stability of MoS₂/CuPc (1:0.5) electrode.

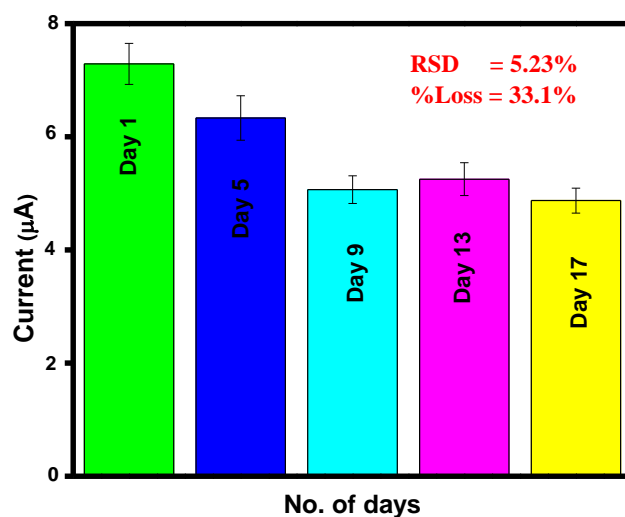


Figure 46: Different days stability with MoS₂/CuPc (1:0.5) electrode.

4.2.8 Effect of interferents with MoS₂/CuPc (1:0.5)

Different interferents were run to check if there was any effect of other compounds or ions present in the blood. In the following activity, double the amount of the interfering species was added, and the electrochemical response was checked under all other conditions. It was noted that interferent species have no such prominent effect in detecting dopamine. The reaction of dopamine was recorded at the exact position, and no extra peak was observed from the interferents (can be seen in Figure 47).

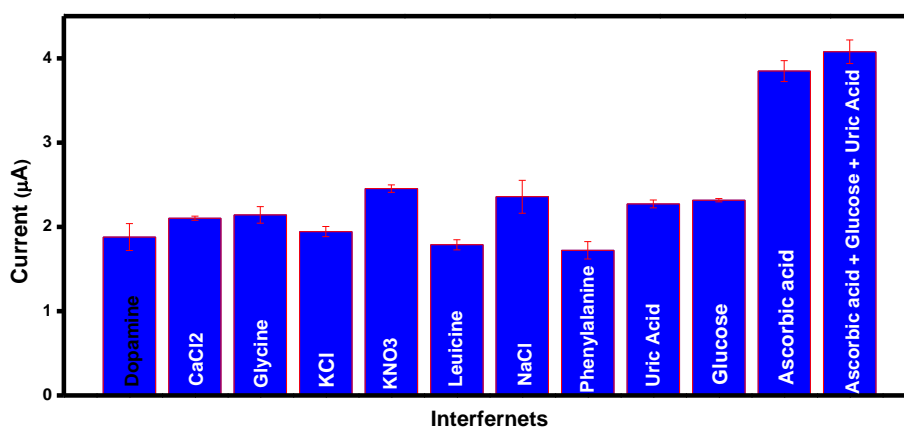


Figure 47: Effect of interferents on MoS₂/CuPc (1:0.5) electrode.

4.2.9 Scan rate studies with MoS₂

Under the given conditions, 0.5 mM dopamine was used with 0.1 M PBS solution at pH 5 and a scan rate of 50 mv/s; the effect of the scan rate was studied (Figure 48). As the scan rate increases, the current values and the response toward dopamine sensing are enhanced. The scan rate values chosen for electrochemical studies are from 10-90 mv/s. The linear graph with slope and regression values was also drawn. Line graphs were drawn using the current vs. square root of the scan rate to show the linear relation. In this way, we can predict that it is a diffusion-controlled process occurring here. The R² value for anodic current is 0.98, and for cathodic

current is 0.96. Linear fitting of graph values close to 1 shows that it is a diffusion-controlled process.

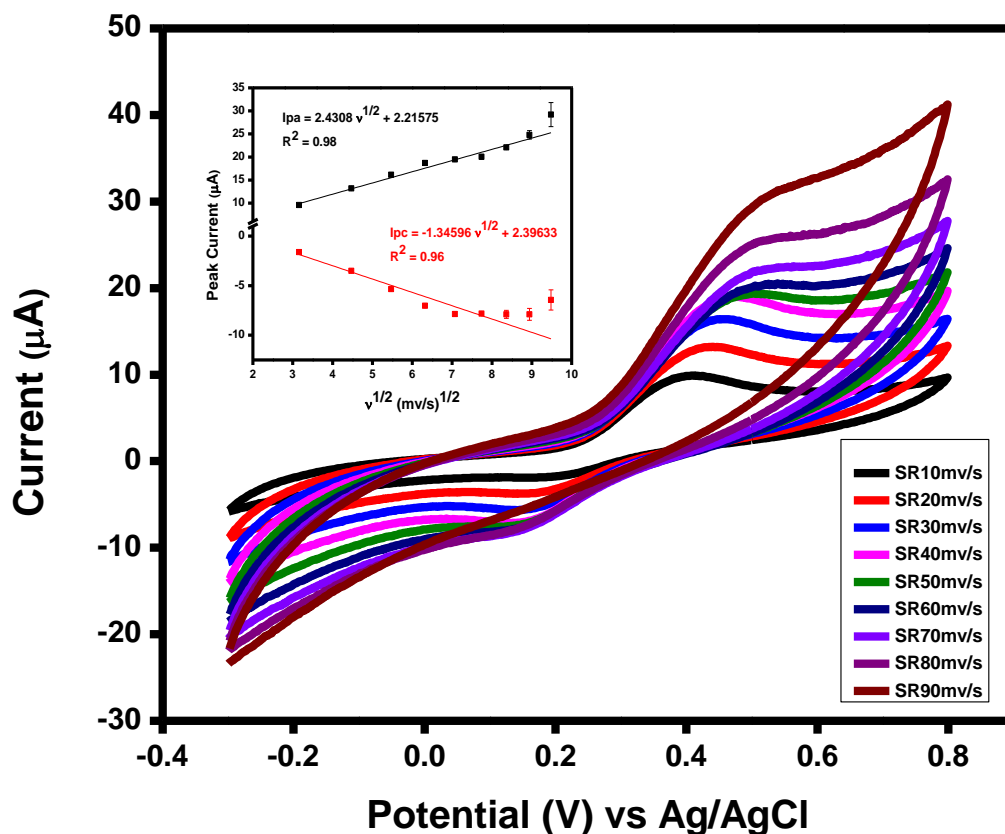


Figure 48: Effect of different scan rates through CV with MoS₂.

4.2.10 Concentration studies with MoS₂

For all the above conditions applied, the concentration studies were performed by CV (Figure 49) and DPV (Figure 51). The linear range of concentration chosen for CV and DPV was 1-1000 µM. It was noted that as the concentration of dopamine was increased, the current response towards electrochemical response was increased. The linear regression curve is also divided into 2 halves. In the first half with the linear range, 1-300 µM, the value of LoD, LoQ and sensitivity with CV (Figure 50) for MoS₂ is 22.1 µM, 73.8 µM and 0.12 µA µM⁻¹ cm⁻² and

for the linear range 500-1000 μM is 22.5 μM , 75 μM and 0.12 $\mu\text{A } \mu\text{M}^{-1} \text{ cm}^{-2}$, respectively and with DPV (Figure 52) and linear range 1-300 μM is 0.4 μM , 1.36 μM and 0.07 $\mu\text{A } \mu\text{M}^{-1} \text{ cm}^{-2}$ and for the linear range 500-1000 μM is 0.48 μM , 1.6 μM and 0.06 $\mu\text{A } \mu\text{M}^{-1} \text{ cm}^{-2}$, respectively.

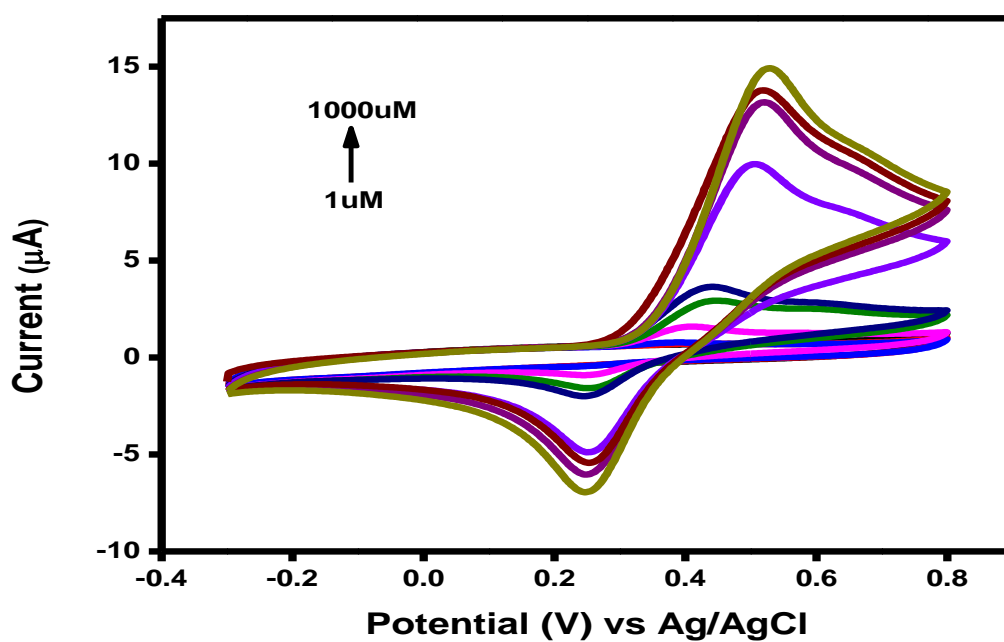


Figure 49: Effect of varying concentration with CV for MoS_2 .

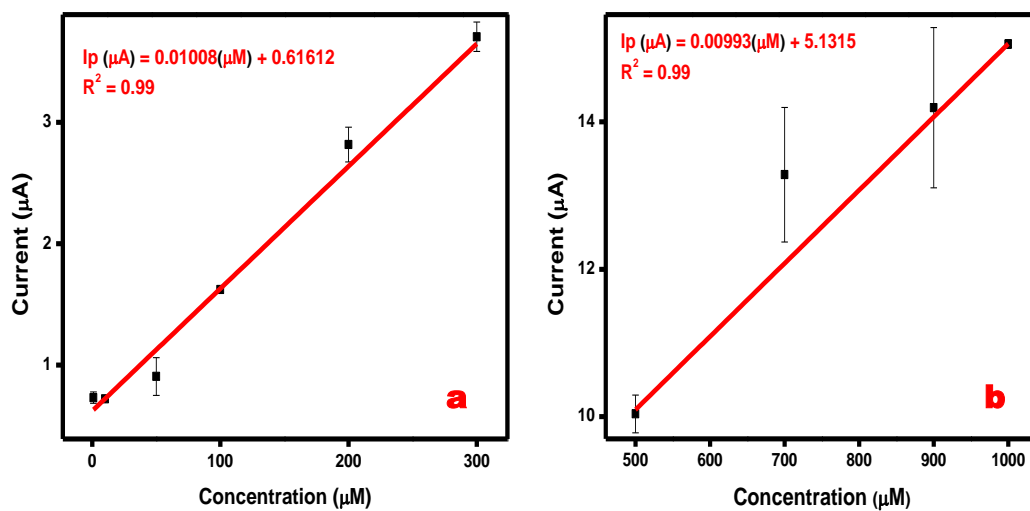


Figure 50: Linear regression curve through CV for MoS₂ with linear range 1-300 μM (a) and 500-1000 μM (b).

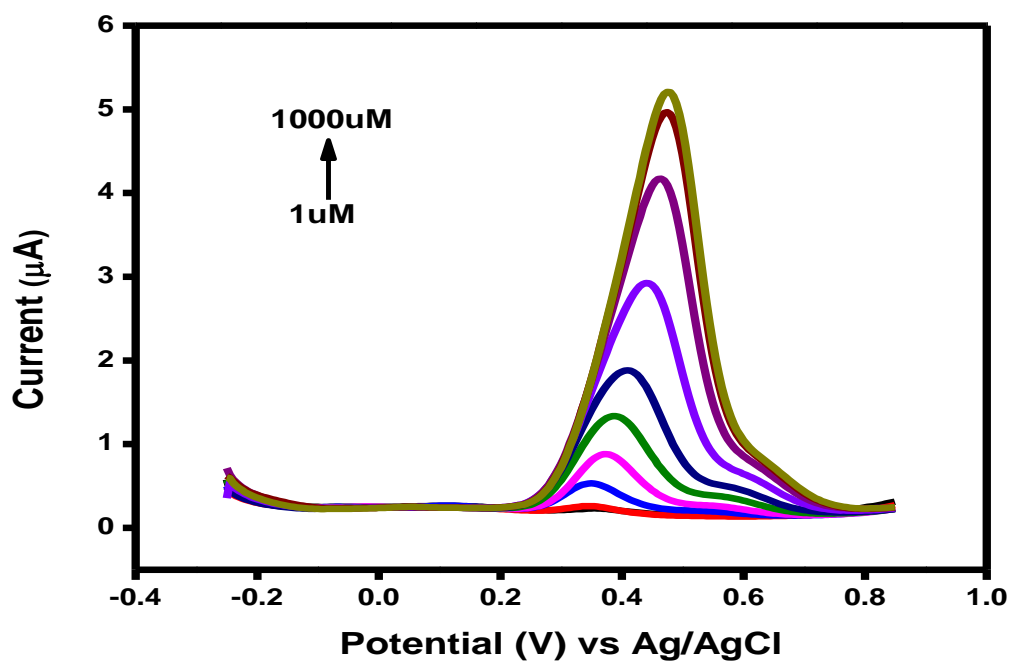


Figure 51: Effect of varying concentration with DPV for MoS₂.

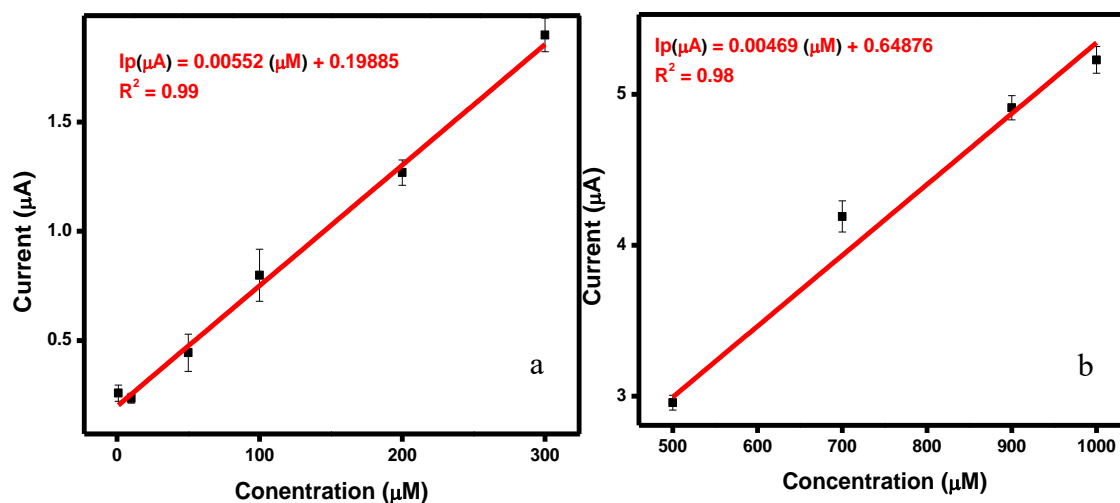


Figure 52: Linear regression curve through DPV for MoS₂ with linear range 1-300 µM (a) and 500-1000 µM (b).

4.2.11 Effect of Interferents on MoS₂

Different interferents were run with double the amount of dopamine, and their electrochemical response was recorded with DPV (Figure 53) with all the conditions the same as above. It was seen that there was no such different response with the interferents—results suggesting MoS₂ is more selective towards Dopamine sensing.

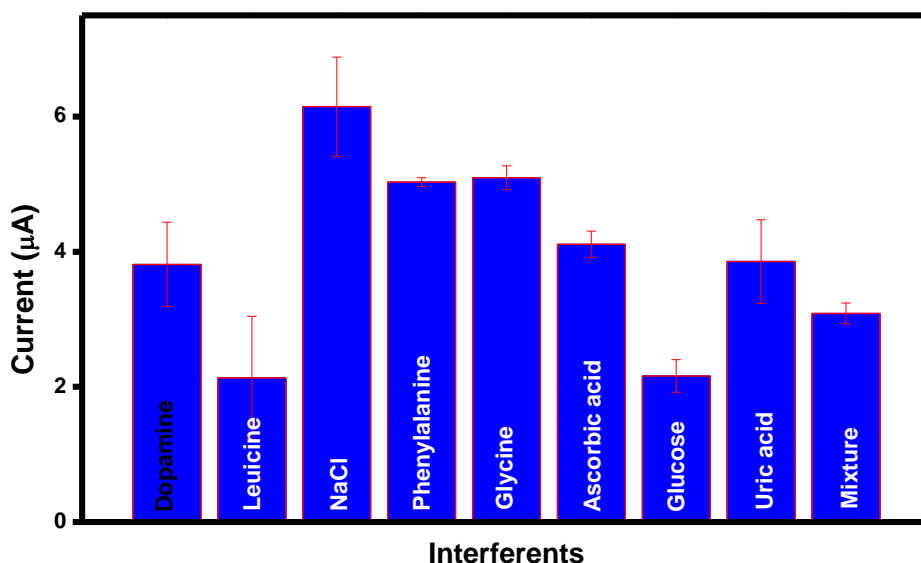


Figure 53: Effect of interferents with MoS₂.

4.2.12 Stability studies with MoS₂

Stability studies were performed with CV (Figure 54) and DPV (Figure 55) for MoS₂ under all the aforementioned conditions. CV and DPV response towards MoS₂ was noted for 6 days as it was stored in the refrigerator at 4° C overnight at pH 5. The RSD values for CV were 8.38 %, and the % loss was 84.5 %. The RSD values for DPV were 16.36 %, and the % loss was 67.1 %. Here, the point to be noted is that in acidic conditions, there can be a hindrance in the layer deposition of MoS₂ slurry on the surface of GCE, which is why the current loss value was observed more [66]. That is the possible reason for the significant % loss in the case of MoS₂ compared to the composite with CuPc. From this, we can conclude that composite 1:0.5 is the best choice for electrochemical sensing dopamine.

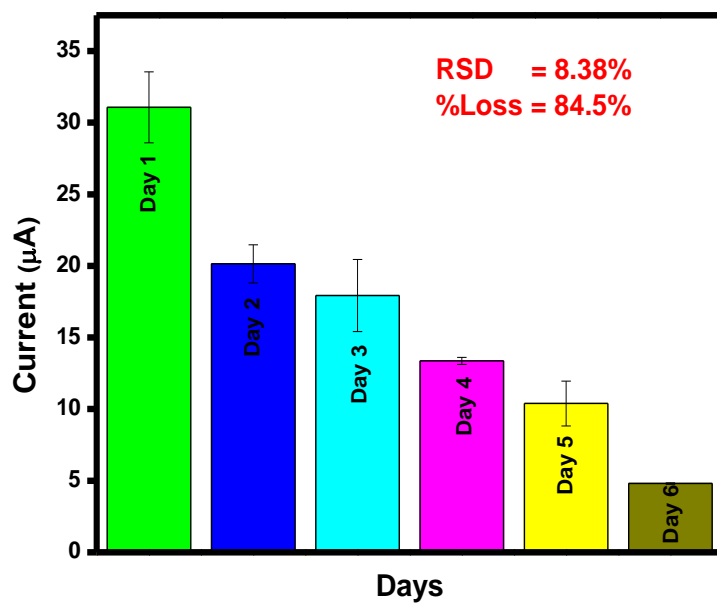


Figure 54: Stability studies for MoS₂ with CV.

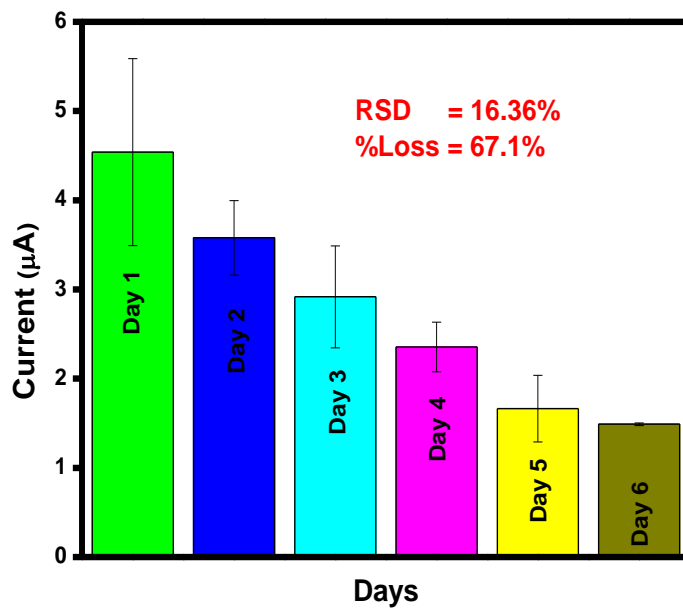


Figure 55: Stability studies for MoS₂ with DPV.

Chapter 5

5 Conclusion

For the electrochemical detection of dopamine, herein we synthesized a novel composite of MoS₂/CuPc with three different ratios, i.e., 1:0.5, 1:1, and 1:2. All the electrodes were used in the electrochemical detection of dopamine concentration 0.5 mM with scan rate 50 mV/s and pH5 with the help of electroanalytical techniques like cyclic voltammetry (CV), differential pulse voltammetry (DPV) and electrochemical impedance spectroscopy (EIS). In the initial stage of electrochemical studies, MoS₂ as a pristine compound was giving more electrochemical response towards the detection of dopamine as compared to MoS₂/CuPc composite ratio 1:0.5, but from the stability studies, we can confer that MoS₂ showed more % loss in the current value when its electrode was kept in acidic conditions as our optimized pH was acidic. The MoS₂/CuPc 1:0.5 composite showed more stability toward detecting dopamine under acidic conditions. So, from here, composite MoS₂/CuPc 1:0.5 can be best suited towards the detection of dopamine as compared to pristine MoS₂.

5.1 Future Recommendations

Different composites of MoS₂ and CuPc can be used for the electrochemical sensing of other neurotransmitters like acetylcholine, adrenaline (epinephrine), noradrenaline (norepinephrine), serotonin, and biomolecules like different enzymes, antibodies, DNA, gas sensing and detection of organophosphate pesticides like monocrotophos, ethoprophos, and profenofos.

Composites of phthalocyanines and 2-D materials like MoS₂ or WSe₂ can be used for other electrochemical applications, such as water splitting, battery development, and the fabrication of efficient energy storage devices.

6 References

- [1] D. Foundation. (1950, 12/12/2024). *Neurotransmission: Neurotransmitters*. Available: <https://dana.org/resources/neurotransmission-neurotransmitters/>
- [2] C. Clinic. (1921, 12/12/2024). *Neurotransmitters*. Available: <https://my.clevelandclinic.org/health/articles/22513-neurotransmitters>
- [3] A. A. Grace and B. S. Bunney, "Dopamine," *Neurotransmitter actions in the vertebrate nervous system*, pp. 285-319, 1985.
- [4] Healthline. (1999, 12/12/2024). *How Does Dopamine Affect the Body*. Available: <https://www.healthline.com/health/dopamine-effects>
- [5] C. Lee, X. Wei, J. W. Kysar, and J. Hone, "Measurement of the elastic properties and intrinsic strength of monolayer graphene," *science*, vol. 321, pp. 385-388, 2008.
- [6] J. Fan and M. Sun, "Transition metal dichalcogenides (tmcds) heterostructures: synthesis, excitons and photoelectric properties," *The Chemical Record*, vol. 22, p. e202100313, 2022.
- [7] A. Carvalho, M. Wang, X. Zhu, A. S. Rodin, H. Su, and A. H. Castro Neto, "Phosphorene: from theory to applications," *Nature Reviews Materials*, vol. 1, pp. 1-16, 2016.
- [8] Z. Huang, H. Liu, R. Hu, H. Qiao, H. Wang, Y. Liu, *et al.*, "Structures, properties and application of 2D monoelemental materials (Xenes) as graphene analogues under defect engineering," *Nano Today*, vol. 35, p. 100906, 2020.
- [9] E. Gao, S.-Z. Lin, Z. Qin, M. J. Buehler, X.-Q. Feng, and Z. Xu, "Mechanical exfoliation of two-dimensional materials," *Journal of the Mechanics and Physics of Solids*, vol. 115, pp. 248-262, 2018.
- [10] V. Nicolosi, M. Chhowalla, M. G. Kanatzidis, M. S. Strano, and J. N. Coleman, "Liquid exfoliation of layered materials," *Science*, vol. 340, p. 1226419, 2013.

- [11] J.-O. Carlsson and P. M. Martin, "Chemical vapor deposition," in *Handbook of Deposition Technologies for films and coatings*, ed: Elsevier, 2010, pp. 314-363.
- [12] J. Lai, W. Niu, R. Luque, and G. Xu, "Solvothermal synthesis of metal nanocrystals and their applications," *Nano Today*, vol. 10, pp. 240-267, 2015.
- [13] M. S. Stark, K. L. Kuntz, S. J. Martens, and S. C. Warren, "Intercalation of layered materials from bulk to 2D," *Advanced Materials*, vol. 31, p. 1808213, 2019.
- [14] S. Das, M. Kim, J.-w. Lee, and W. Choi, "Synthesis, properties, and applications of 2-D materials: A comprehensive review," *Critical Reviews in Solid State and Materials Sciences*, vol. 39, pp. 231-252, 2014.
- [15] N. R. Glavin, R. Rao, V. Varshney, E. Bianco, A. Apte, A. Roy, *et al.*, "Emerging applications of elemental 2D materials," *Advanced Materials*, vol. 32, p. 1904302, 2020.
- [16] U. Krishnan, M. Kaur, K. Singh, M. Kumar, and A. Kumar, "A synoptic review of MoS₂: Synthesis to applications," *Superlattices and Microstructures*, vol. 128, pp. 274-297, 2019.
- [17] K. S. Novoselov, D. Jiang, F. Schedin, T. Booth, V. Khotkevich, S. Morozov, *et al.*, "Two-dimensional atomic crystals," *Proceedings of the National Academy of Sciences*, vol. 102, pp. 10451-10453, 2005.
- [18] K. Gacem, M. Boukhicha, Z. Chen, and A. Shukla, "High quality 2D crystals made by anodic bonding: a general technique for layered materials," *Nanotechnology*, vol. 23, p. 505709, 2012.
- [19] P. Joensen, R. Frindt, and S. R. Morrison, "Single-layer MoS₂," *Materials research bulletin*, vol. 21, pp. 457-461, 1986.
- [20] E. Benavente and G. González, "Microwave activated lithium intercalation in transition metal sulfides," *Materials research bulletin*, vol. 32, pp. 709-717, 1997.

- [21] S. Balendhran, J. Z. Ou, M. Bhaskaran, S. Sriram, S. Ippolito, Z. Vasic, *et al.*, "Atomically thin layers of MoS₂ via a two step thermal evaporation–exfoliation method," *Nanoscale*, vol. 4, pp. 461-466, 2012.
- [22] K. F. Mak, C. Lee, J. Hone, J. Shan, and T. F. Heinz, "Atomically thin MoS₂: a new direct-gap semiconductor," *Physical review letters*, vol. 105, p. 136805, 2010.
- [23] T. Cao, G. Wang, W. Han, H. Ye, C. Zhu, J. Shi, *et al.*, "Valley-selective circular dichroism of monolayer molybdenum disulfide," *Nature communications*, vol. 3, p. 887, 2012.
- [24] S. Bertolazzi, J. Brivio, and A. Kis, "Stretching and breaking of ultrathin MoS₂," *ACS nano*, vol. 5, pp. 9703-9709, 2011.
- [25] V. An, Y. Irtegov, and C. De Izarra, "Study of tribological properties of nanolamellar WS₂ and MoS₂ as additives to lubricants," *Journal of Nanomaterials*, vol. 2014, p. 865839, 2014.
- [26] U. Krishnan, M. Kaur, K. Singh, G. Kaur, P. Singh, M. Kumar, *et al.*, "MoS₂/Ag nanocomposites for electrochemical sensing and photocatalytic degradation of textile pollutant," *Journal of Materials Science: Materials in Electronics*, vol. 30, pp. 3711-3721, 2019.
- [27] E. W. K. Koh, C. H. Chiu, Y. K. Lim, Y.-W. Zhang, and H. Pan, "Hydrogen adsorption on and diffusion through MoS₂ monolayer: First-principles study," *International journal of hydrogen energy*, vol. 37, pp. 14323-14328, 2012.
- [28] A. Ramadoss, T. Kim, G.-S. Kim, and S. J. Kim, "Enhanced activity of a hydrothermally synthesized mesoporous MoS₂ nanostructure for high performance supercapacitor applications," *New Journal of Chemistry*, vol. 38, pp. 2379-2385, 2014.
- [29] A. P. Lever, "The phthalocyanines," *Advances in Inorganic Chemistry and Radiochemistry*, vol. 7, pp. 27-114, 1965.

- [30] A. L. Thomas, *Phthalocyanine research and applications*: CRC Press, 2024.
- [31] J. Elvidge and A. Lever, "245. Metal chelates. Part II. Phthalocyanine–chromium complexes and perpendicular conjugation," *Journal of the Chemical Society (Resumed)*, pp. 1257-1265, 1961.
- [32] G. Loebbert, "Phthalocyanine compounds," *Kirk-Othmer Encyclopedia of Chemical Technology*, 2000.
- [33] S. Sandor, O. Prelipceanu, and I. Checiu, "Sulphonated phthalocyanine induced caudal malformative syndrome in the chick embryo," *Morphologie et embryologie*, vol. 31, pp. 173-181, 1985.
- [34] P. Gregory, "Industrial applications of phthalocyanines," *Journal of porphyrins and phthalocyanines*, 2012.
- [35] A. K. Tchekep, V. Suryanarayanan, and D. K. Pattanayak, "Alternative approach for highly sensitive and free-interference electrochemical dopamine sensing," *Carbon*, vol. 204, pp. 57-69, 2023.
- [36] M. Lakshmanakumar, N. Nesakumar, A. J. Kulandaisamy, and J. B. B. Rayappan, "Principles and recent developments in optical and electrochemical sensing of dopamine: A comprehensive review," *Measurement*, vol. 183, p. 109873, 2021.
- [37] H. Li, Y. Guo, S. Zeng, Q. Wei, P. Sharel, R. Zhu, *et al.*, "High-sensitivity, selective determination of dopamine using bimetallic nanoparticles modified boron-doped diamond electrode with anodic polarization treatment," *Journal of Materials Science*, vol. 56, pp. 4700-4715, 2021.
- [38] O. Koyun, H. Gursu, S. Gorduk, and Y. Sahin, "Highly sensitive electrochemical determination of dopamine with an overoxidized polypyrrole nanofiber pencil graphite electrode," *International Journal of Electrochemical Science*, vol. 12, pp. 6428-6444, 2017.

- [39] N. Hareesha and J. Manjunatha, "Fast and enhanced electrochemical sensing of dopamine at cost-effective poly (DL-phenylalanine) based graphite electrode," *Journal of Electroanalytical Chemistry*, vol. 878, p. 114533, 2020.
- [40] A. F. Khan, D. A. Brownson, E. P. Randviir, G. C. Smith, and C. E. Banks, "2D hexagonal boron nitride (2D-hBN) explored for the electrochemical sensing of dopamine," *Analytical chemistry*, vol. 88, pp. 9729-9737, 2016.
- [41] Q. Huang, X. Lin, L. Tong, and Q.-X. Tong, "Graphene quantum dots/multiwalled carbon nanotubes composite-based electrochemical sensor for detecting dopamine release from living cells," *ACS sustainable chemistry & engineering*, vol. 8, pp. 1644-1650, 2020.
- [42] Q. Liu, X. Zhu, Z. Huo, X. He, Y. Liang, and M. Xu, "Electrochemical detection of dopamine in the presence of ascorbic acid using PVP/graphene modified electrodes," *Talanta*, vol. 97, pp. 557-562, 2012.
- [43] A. Arroquia, I. Acosta, and M. P. G. Armada, "Self-assembled gold decorated polydopamine nanospheres as electrochemical sensor for simultaneous determination of ascorbic acid, dopamine, uric acid and tryptophan," *Materials Science and Engineering: C*, vol. 109, p. 110602, 2020.
- [44] E. Fazio, S. Spadaro, M. Bonsignore, N. Lavanya, C. Sekar, S. Leonardi, *et al.*, "Molybdenum oxide nanoparticles for the sensitive and selective detection of dopamine," *Journal of Electroanalytical Chemistry*, vol. 814, pp. 91-96, 2018.
- [45] E. Bahrami, R. Amini, and S. Vardak, "Electrochemical detection of dopamine via pencil graphite electrodes modified by Cu/Cu₂O nanoparticles," *Journal of Alloys and Compounds*, vol. 855, p. 157292, 2021.

- [46] Y. Li, C. Fan, and J. Zheng, "A high-efficiency electrochemical sensor of dopamine based on WS₂ nanosheets decorated with dandelion-like platinum–silver nanoparticles," *Journal of Materials Science: Materials in Electronics*, vol. 33, pp. 5061-5072, 2022.
- [47] W. Zhao, B. Ni, Q. Yuan, Y. Wang, Q. Zhang, and X. Wang, "Finely composition-tunable synthesis of ultrafine wavy PtRu nanowires as effective electrochemical sensors for dopamine detection," *Langmuir*, vol. 33, pp. 8070-8075, 2017.
- [48] B.-R. Li, Y.-J. Hsieh, Y.-X. Chen, Y.-T. Chung, C.-Y. Pan, and Y.-T. Chen, "An ultrasensitive nanowire-transistor biosensor for detecting dopamine release from living PC12 cells under hypoxic stimulation," *Journal of the American Chemical Society*, vol. 135, pp. 16034-16037, 2013.
- [49] S. A. Hira, M. Nallal, K. Rajendran, S. Song, S. Park, J.-M. Lee, *et al.*, "Ultrasensitive detection of hydrogen peroxide and dopamine using copolymer-grafted metal-organic framework based electrochemical sensor," *Analytica chimica acta*, vol. 1118, pp. 26-35, 2020.
- [50] V. N. C. da Silva, E. A. d. O. Farias, A. R. Araújo, F. E. X. Magalhães, J. R. N. Fernandes, J. M. T. Souza, *et al.*, "Rapid and selective detection of dopamine in human serum using an electrochemical sensor based on zinc oxide nanoparticles, nickel phthalocyanines, and carbon nanotubes," *Biosensors and Bioelectronics*, vol. 210, p. 114211, 2022.
- [51] Z. Huang, L. Zhang, P. Cao, N. Wang, and M. Lin, "Electrochemical sensing of dopamine using a Ni-based metal-organic framework modified electrode," *Ionics*, vol. 27, pp. 1339-1345, 2021.

- [52] K.-J. Huang, J.-Z. Zhang, Y.-J. Liu, and L.-L. Wang, "Novel electrochemical sensing platform based on molybdenum disulfide nanosheets-polyaniline composites and Au nanoparticles," *Sensors and Actuators B: Chemical*, vol. 194, pp. 303-310, 2014.
- [53] S. Ponnada, D. B. Gorle, M. S. Kiai, S. Rajagopal, R. K. Sharma, and A. Nowduri, "A facile, cost-effective, rapid, single-step synthesis of Ag–Cu decorated ZnO nanoflower-like composites (NFLCs) for electrochemical sensing of dopamine," *Materials Advances*, vol. 2, pp. 5986-5996, 2021.
- [54] A. M. Abdel-Aziz, H. H. Hassan, and I. H. Badr, "Activated glassy carbon electrode as an electrochemical sensing platform for the determination of 4-nitrophenol and dopamine in real samples," *ACS omega*, vol. 7, pp. 34127-34135, 2022.
- [55] A. Özcan, S. İlkbaş, and A. A. Özcan, "Development of a disposable and low-cost electrochemical sensor for dopamine detection based on poly (pyrrole-3-carboxylic acid)-modified electrochemically over-oxidized pencil graphite electrode," *Talanta*, vol. 165, pp. 489-495, 2017.
- [56] S. Palanisamy, S. Velmurugan, and T. C. Yang, "One-pot sonochemical synthesis of CuS nanoplates decorated partially reduced graphene oxide for biosensing of dopamine neurotransmitter," *Ultrasonics Sonochemistry*, vol. 64, p. 105043, 2020.
- [57] M. Hyder, G. R. K. Reddy, B. Naveen, and P. S. Kumar, "Copper-silver bimetallic nanoelectrocatalyst on pencil graphite substrate for highly selective amperometric dopamine sensor," *Chemical Physics Letters*, vol. 740, p. 137086, 2020.
- [58] P. Uppachai, S. Srijaranai, S. Poosittisak, I. Md Isa, and S. Mukdasai, "Supramolecular electrochemical sensor for dopamine detection based on self-assembled mixed surfactants on gold nanoparticles deposited graphene oxide," *Molecules*, vol. 25, p. 2528, 2020.

- [59] S. Balu, S. Palanisamy, V. Velusamy, T. C. Yang, and E.-S. I. El-Shafey, "Tin disulfide nanorod-graphene- β -cyclodextrin nanocomposites for sensing dopamine in rat brains and human blood serum," *Materials Science and Engineering: C*, vol. 108, p. 110367, 2020.
- [60] S. Sundar, G. Venkatachalam, and S. J. Kwon, "Biosynthesis of copper oxide (CuO) nanowires and their use for the electrochemical sensing of dopamine," *Nanomaterials*, vol. 8, p. 823, 2018.
- [61] Y.-M. Xia, W. Zhang, M.-Y. Li, M. Xia, L.-J. Zou, and W.-W. Gao, "Effective electrochemical determination of chloramphenicol and florfenicol based on graphene/copper phthalocyanine nanocomposites modified glassy carbon electrode," *Journal of the Electrochemical Society*, vol. 166, p. B654, 2019.
- [62] E. Sitara, H. Nasir, S. Iram, S. A. B. Bukhari, T. Akhtar, and S. Mumtaz, "Tailoring of ZnSe/GCN/MoS₂ ternary heterojunction with enhanced photoelectrochemical activity for water oxidation," *Surfaces and Interfaces*, vol. 37, p. 102632, 2023.
- [63] R. Prabakaran, R. Kesavamoorthy, G. Reddy, and F. P. Xavier, "Structural Investigation of Copper Phthalocyanine Thin Films Using X-Ray Diffraction, Raman Scattering and Optical Absorption Measurements," *physica status solidi (b)*, vol. 229, pp. 1175-1186, 2002.
- [64] X. Feng, Q. Tang, J. Zhou, J. Fang, P. Ding, L. Sun, *et al.*, "Novel mixed-solvothermal synthesis of MoS₂ nanosheets with controllable morphologies," *Crystal Research and Technology*, vol. 48, pp. 363-368, 2013.
- [65] A. T. Massey, R. Gusain, S. Kumari, and O. P. Khatri, "Hierarchical microspheres of MoS₂ nanosheets: efficient and regenerative adsorbent for removal of water-soluble dyes," *Industrial & Engineering Chemistry Research*, vol. 55, pp. 7124-7131, 2016.

- [66] Z. Zarach, A. P. Nowak, K. Trzciński, G. Gajowiec, G. Trykowski, M. Sawczak, *et al.*, "Influence of hydrochloric acid concentration and type of nitrogen source on the electrochemical performance of TiO₂/N-MoS₂ for energy storage applications," *Applied Surface Science*, vol. 608, p. 155187, 2023.